Investigation of charge migration/transfer in radical cations using Ehrenfest method with fully quantum nuclear motion

Thierry Tran

A dissertation submitted in partial fulfillment

of the requirements for the degree of

Doctor of Philosophy

of

University College London.

Chemistry Department

UCL

2022

I, Thierry Tran , confirm that the work presented in this thesis is my own. Where information has been derived from other sources, I confirm that this has been indicated in the work. Text taken from another source will be enclosed in quotation marks and a reference will be given.

Abstract

The main focus of this thesis is to investigate the effect of charge migration on molecular dynamics. Upon the creation of a superposition of cationic states by a short ionizing pulse in an attosecond pump-probe experiment, the electronic wavefunction is in a non-stationary state and the initial dynamics are purely electronic, driven by Charge Migration (CM) before the onset of any nuclear motions. The CM can be simulated using a frozen nuclear framework but its importance on long-term dynamics and competition with vibrationally mediated charge motion (i.e. Charge Transfer (CT)) remains unknown. Unravelling the mechanism behind CM and its importance on electron and nuclear coherence can help in designing an initial superposition of electronic states to steer nuclear motions toward a specific product. Further control of the photo-reactivity could be achieved with the use of probe/control laser pulses and open the door for more direct comparison with experimental results.

In order to investigate the dynamics upon photoionization with an attosecond pump-pulse, the coupled electron-nuclear dynamics of the system is simulated using nonadiabatic quantum dynamics techniques within the sudden approximation. A single-set approach is adopted for the expansion of the nuclear wavefunction using a linear combination of Gaussian Wavepackets (GWP). The calculation is done using the Quantum-Ehrenfest method (QuEh) and the time-dependent Potential Energy Surfaces (PES) are evaluated with the Complete Active Space Configuration Interatcion (CAS-CI) method. The resulting dynamics are analyzed with adiabatic/diabatic state populations, Normal Mode (NM) displacements and bond lengths averaged over the nuclear wavepacket using Gross Gaussian populations (GGP).

To reduce the cost of computation, the algorithm implemented in QUANTICS

is parallelized with a Message Passing Interface (MPI). Further, the section of code which interacts with the database that contains previously calculated points on the PES is rewritten using the Structured Query Language (SQL) and the SQLite engine.

For the purpose of unravelling the mechanism behind CM, the nonadiabatic dynamics of a model retinal Protonated Schiff Base (rPSB) and benzene are investigated by defining the initial electronic wavefunction in a systematic way. As demonstrated by the results on rPSB, the relaxation mechanism such as single and double bond length alternation and isomerization can controlled by varying the initial composition of electronic states. With the rich symmetry of benzene, the initial nuclear dynamics which are controlled by an initial gradient and electron dynamics can be analyzed using symmetry rules. The initial gradient is a combination of totally symmetric motion and non-symmetric components which correspond to the intra- (eigenstate) and inter-state (couplings) gradients, respectively. The electron dynamics and its associated nuclear motions can be examined by grouping together the localized holes where the CM occurs. With the initial gradient and CM, one can predict the initial nuclear relaxation and possibly control the photo-products formed by designing a specific superposition of electronic eigenstates.

To explore the effect of laser pulses on dynamics, an implementation within the dipole approximation using the dipole-electric field dot product is done in the GAUSSIAN program. The dynamics in the presence of an infrared probe pulse is simulated on model systems such as allene and the ethylene cation. The pulse is able to induce change in the electron and nuclear dynamics of the system and some of its effect can be explained using irreducible representations and the alignment of the electric fields.

The work presented in this thesis offers an insight into the photocontrol of

molecules and opens the door for further investigation of charge-directed dynamics.

Impact Statement

The advent of attosecond spectroscopy has opened the door to monitoring ultrafast phenomena occurring on the timescale of electronic motion. An ultrashort pulse in the ultraviolet (UV) to extreme ultraviolet (XUV) region will photoionize the molecule onto multiple cationic states at the same time. Thus, the resulting dynamics are heavily controlled by electronic coherence depicted as Charge Migration (CM) and the initial nuclear gradient. Understanding the reactivity of molecular systems upon photoionization to multiple electronic states with a broad energy laser requires us to employ nonadiabatic methods for the accurate simulation of coupled electron-nuclear dynamics.

The work presented in this thesis has an important impact on the field of nonadiabatic dynamics and attosecond spectroscopy where the quantum dynamics of molecular system is simulated with the Quantum-Ehrenfest (QuEh) method. The initial electronic wavefunction can be defined as a linear combination of electronic states and the resulting nuclear dynamics are coupled gaussian wavepackets following quantum trajectories on a time-dependent potential energy surface.

Moreover, the method has been succesfully employed for the investigation of nonadiabatic dynamics of model systems such as octa-3,5,6-trieniminium, benzene and ethylene cations. The high symmetry and already known relaxation mechanism allows us to easily rationalize the molecular dynamics and provide insight at the fundamental level. The works on octa-3,5,6-trieniminium and benzene cation have been submitted for publications and there is currently a manuscript in preparation for the research on the ethylene cation.

Finally, these findings improve our knowledge of CM and its effect on nuclear dynamics. Thus, it possible in the future to design initial superposition of states and steer the dynamics via means of a probe pulse to achieve control of the photo-

reactivity of molecules.

Acknowledgements

This has been an amazing journey for 3 years and a half full of discovery both in work and food. I just wish I did more sightseeing in London or around but it seems that my laziness is extremely difficult to beat when it doesn't involve work or cooking. Fortunately, I have been quite productive during my PhD despite spending 2 years under a worldwide epidemic working from home in Swizterland. However, that journey has been quite stressful and frustrating at some moments mostly when it is about figuring out if the data makes sense (and having back and forth with my second supervisor) or finishing the thesis on time. Overall, it has been a very enjoyable stay in United-Kingdom and very exciting projects to work on. Furthermore, my PhD have been full of support and help from people I would like to thank.

First of all, I would like to give my deepest appreciation to both of my supervisors Graham Worth and Mike Robb for their guidance and the opportunity I have received. Their feedback and comments help me improve a lot my way of working or writing and I would like to especially be thankful to them for their time and eagerness to answer all the questions I had whenever I was stuck (and the English corrections). I will never forget all of these skype meeting discussing very intensively about the results and manuscripts or the amazing figures I end up having in some papers.

One of the aspect I have enjoyed the most in my PhD was the interactions and ambiance in the Worth group. I would like to thank all the wonderful colleagues, Georgia, Alice, Sandra, Barry, Diptesh, Léon, Don and Luke (I know it is technically Bearpark group for both of you) that were part or are still part of the group for their willingness to help or collaborate on project and all the social events we had together. I probably drank more alcohol in the span of 1 year than during my

whole undergraduate life.

Of course, I wouldn't have had the opportunity to start the PhD if it wasn't for my family and their unconditional love and support. The 2 years under quarantine were quite challenging for keeping a good productivity, mostly when the connection through VPN from home didn't work or wasn't stable. Fortunately, I could enjoy my parents' food as much as I wanted during that time. Also, I would like to thank my little brother Eric for being as nerdy as me on video games and solving all my problems related to computer.

I would like also to thank Don De Dieu, Fabio, Aymeric, Xavier and Youhanidou for being amazing friends and flatmates. They would stop me whenever I was working non-stop at home. It was very enjoyable talking with them and sharing meals as well as being able to share our worries and help each other. I wish them good luck for their future. Finally, I would like to thank all the friends I made on video games that I did end up meeting for some of them. I had a lot of fun interacting with them and probably spend way too much time on these games. However, they did provide me a good reason to have a break in the evening no matter how busy I was.

Like any journey, it has come to and end and it is time to start a new chapter in my life with a bit of holidays in-between.

List of Publications

1. T. Tran, A. J. Jenkins, G.A. Worth, and M. A. Robb. The Quantum-Ehrenfest method with the inclusion of an IR pulse: Application to electron dynamics of the allene radical cation *J. Chem. Phys.*, (In Press), 153:031102, 2020. DOI: 10.1063/5.0015937.

2. G. Christopoulou, T. Tran, and G. A. Worth. Direct nonadiabatic quantum dynamics simulations of the photodissociation of phenol *Phys. Chem. Chem. Phys.*, (In Press), 23:23684-23695, 2021. DOI: 10.1039/D1CP01843D.

3. T. Tran, G.A. Worth, and M. A. Robb. Control of nuclear dynamics in the benzene cation by electronic wavepacket composition. *Commun. Chem.*, (In Press), 4:48, 2021. DOI: 10.1038/s42004-021-00485-3.

4. M. Olivucci, T. Tran, G. A. Worth, and M. A. Robb. Unlocking the Double Bond in Protonated Schiff Bases by Coherent Superposition of S_1 and S_2 *J. Phys. Chem. Lett.*, (In Press), 12:5639-5643, 2021. DOI: 10.1021/acs.jpclett.1c01379.

5. D. Danilov, T. Tran, M. J. Bearpark, J. P. Marangos, G. A. Worth and M. A. Robb. How electronic superpositions drive nuclear motion following the creation of a localized hole in the glycine radical cation *J. Chem. Phys.*, (Submitted).

6. T. Tran, D. Danilov, G.A. Worth, and M. A. Robb. Controlling the coupled electron-nuclear dynamic of ethylene cation with an IR pulse. (In Preparation).

Contents

List of Figures

List of Tables

Glossary

ab initio From the latin term meaning "from the beginning". It is derived from "ab" meaning "from" and "initio" being the singular form of "initium" meaning "beginning". In the context of computational Chemistry it is usually in reference to methods by which the Time-Independent Schrödinger equation is solved, without the use of experimental data. 57

AIMS Ab-Initio Multiple Spawning (method). 35

AO Atomic Orbital. 92

BLA Bond Length Alternation. 8, 109, 110, 112–114

BOA Born-Oppenheimer approximation. 148, 149

CAS-CI Complete Active Space Configuration Interaction (method). 1, 22, 54, 61, 62, 65, 66, 93, 111, 132, 142

CASPT2 Complete Active Space Perturbation Theory (2nd order). 56

CASSCF Complete Active Space Self-Consistent Field (method). 9, 11, 13, 22, 53–57, 60, 65, 68, 92, 105, 113, 121, 122, 132, 133, 142

CCS Coupled-Coherent States (method). 37

CEP Carrier Phase Envelope. 145

CI Configuration interaction. 48–56, 65

CISD Configuration Interaction Singles and Doubles. 51

CISDT Configuration Interaction Singles, Doubles and Triples. 51

CM Charge Migration. 1, 2, 20, 21, 23, 29–31, 95, 102, 103, 120, 132, 134, 139, 141, 143

CoIn Conical Intersection. 8, 9, 22, 34, 48, 95, 97, 98, 101, 103, 108–110, 113, 115–118, 120, 123–125, 128, 131, 132, 139, 143, 145

CSF Configuration State Function. 44, 48–50, 56, 61, 65, 119

CT Charge Transfer. 1, 21, 29, 109

CT-MQC Coupled-Trajectory Mixed Quantum-Classical (method). 36, 38

DD-vMCG Direct-Dynamics Variational Multi-Configurational Gaussian (method). An on-the-fly quantum dynamics method based on vMCG. 6, 13, 18, 22, 34–38, 40, 41, 57, 59, 60, 62–64, 66–78, 81–86, 88, 90, 91, 105, 141, 142, 154

DFT Density Functional Theory. 47, 48

EOM Equation(s)-Of-Motion. 22, 33–36, 57–61, 69, 127, 141

FC Franck-Condon. 11, 13, 109, 111–116, 121–124, 133, 134

FCI Full Configuration Interaction. 50, 51, 53

FEL Free-Electron Laser. 5, 26–28

FMS Full Multiple Spawning (method). 35

GFP Green Fluorescent Protein. 107

GGP Gross Gaussian Population. 1, 9–11, 63, 66, 96, 119, 124, 129, 138

GUGA Generalized Unitary Graphical Approach. 53

GWP Gaussian Wavepacket(s). 1, 5, 7, 8, 10, 11, 13, 18, 32–37, 41, 57, 59–63, 66, 69, 70, 73, 77, 82–85, 89, 93, 95–99, 101–105, 111, 119, 121, 129, 133, 138, 140, 141, 144, 152

HF Hartree-Fock. 45, 46, 50, 51, 54

HHG High Harmonic Generation. 26, 27, 116, 130, 131

IR Infrared. 23, 29, 30, 130–132, 134, 137, 143

LCAO Linear combination of atomic orbitals, sometimes extended to LCAO-MO (see MO glossary entry below). 43

LHA Local Harmonic Approximation. 59–61, 66, 69, 133

MCE Multi-Configurational Ehrenfest (method). 37, 39

MCSCF MultiConfiguration Self-Consistent Field (theory). 51–53, 55, 92

MCTDH Multi Configuration Time Dependent Hartree (method). 19, 31, 70, 91, 116

MO Molecular-Orbital (theory). 9, 43, 50, 51, 53–56, 62, 73, 81, 92, 93, 122, 132

MPI Message Passing Interface. 2, 6, 22, 68–77, 79–84, 88, 90, 104, 105, 142, 143, 153, 154

NIR Near-infrared. 116

NM Normal Mode (displacement). Set of nuclear coordinates obtained from a frequency calculation and the displacement is set with respect to an initial geometry. 1, 7, 9–11, 13, 64, 82, 85, 86, 93, 95, 96, 99–104, 112, 118–121, 123–128, 134–139

on-the-fly "As needed." Usually referring to a dynamics method that does not require precomputed potential energy surfaces and hence the surfaces are calculated as needed. 16, 18, 31–33, 57, 85

OpenMP Open Multi-Processing Interface. 13, 67–73, 77, 78, 86, 87, 90, 104, 142, 152

PES Potential energy surface. 1, 2, 5, 9, 11, 18, 21, 22, 31, 33, 34, 36–38, 40, 41, 57, 59–61, 64, 66–70, 72, 77, 81, 83–86, 90–92, 105, 114, 117, 131, 141, 142, 144, 149, 150

QM/MM Quantum Mechanic/Molecular Mechanic. 113

QuEh Quantum-Ehrenfest (method). An on-the-fly quantum dynamics method based on the single-set DD-vMCG where GWP are propagated on a time-dependent PES. 1, 10, 21, 22, 37, 39–42, 57, 61, 62, 64, 66–68, 82–84, 91–93, 95, 104–107, 111, 121, 123, 126, 128, 129, 132, 139, 141–145

RASSCF Restricted Active Space Self-Consistent Field (method). 56, 57

rPSB retinal Protonated Schiff Base. 2, 8, 13, 22, 107–113, 115, 139, 143

rPSBAT all-trans retinal Protonated Schiff Base. 8, 108

SA State-Average. 55

SCF Self-consistent field (method). 47, 51, 54

SD Slater determinant. 42–46, 48, 49

SPF Single-Particle Function(s). 19

SQL Structured Query Language. 2, 22, 68, 87–90, 105, 142, 143

TD-DFT Time-Dependent Density Functional Theory. 48

TDSE Time-Dependent Schrödinger Equation. 20, 57, 58, 141, 146, 149, 150

TISE Time-Independent Schrödinger Equation. 20, 42, 46, 146

UV Ultraviolet. 1, 25–27

VIS Visible. 25, 26, 116

vMCG Variational Multi-Configurational Gaussian (method) where all SPFs of the MCTDH method are replaced with Gaussian functions. 16, 39, 57, 63, 152

XUV Extreme Ultraviolet. 1, 26, 29, 30, 116, 118, 129, 130, 132

Chapter 1

Introduction

A chemical reaction is a rearrangement of atoms involving formation and breaking of bonds from a reactant to a product. Observing chemical reactivity with a laser is one goal of spectroscopy. There are various techniques and schemes to study ultrafast molecular processes using laser pulses. Events happening at the timescale of nuclear dynamics such as molecular relaxation are monitored with femtosecond pulses and the door for probing electron dynamics which occur in the attosecond timescale has been opened thanks to the recent advance in attosecond technology. Upon photoionization with an attosecond pulse, a localized hole (i.e. removal of an electron) is created followed by a fast charge-directed motion (i.e. hole migration) and this fast motion have been labelled as Charge Migration (CM).

However, experimental data provided in the form of spectra are not always easy to interpret and only give indirect information on the dynamics of the molecule. With the help of computer simulations, it is possible to assign a mechanism to the experimental results by computing the time evolution of the system. Due to the intrinsic quantum nature of molecules, a wavefunction approach is required for the representation of the system which implies solving the time-dependent Schrödinger equation (TDSE). By using a basis of electronic eigenstates which are the solutions of the time-independent Schrödinger equation (TISE) for the electronic Hamiltonian, it is possible to represent a localized hole as a linear combination of these

states and the non-stationary nature of the electronic wavefunction (i.e. not an eigenstate) leads to electron dynamics. Thus, the CM is a direct consequence of the superposition of electronic states.

To provide insight from a theoretical point of view, an appropriate level of theory is required to properly model the molecular wavefunction. The time evolution of a system on multiple electronic states is computed using nonadiabatic methods and they can be categorized based on the expansion of the full wavefunction.

In this thesis, the simulation of CM in molecular systems as well as the competition with other form of electron dynamics such as Charge Transfer (CT) which is a vibrationally-mediated charge motion (i.e. coupled with nuclear dynamics). The nonadiabatic dynamics are simulated with the Quantum-Ehrenfest (QuEh) method. The work presented will demonstrate that starting from a superposition of electronic eigenstates leads to fast and periodic electron dynamics as well as a specific initial gradient that can be tuned by changing the relative phase between states. Both of these effects can have strong influences on the subsequent nuclear dynamics. Furthermore, the coupled electron-nuclear dynamics will be rationalized using symmetry rules. Thus, the charge-directed motion could be controlled and predicted (with symmetry) by carefully choosing the initial superposition and the dynamics can be further tweaked by the use of a probe/control laser.

The structure of the thesis is organized as follows. Chapter 2 provides a literature review on experimental works focusing on spectroscopy with the possible methods for generation of attosecond pulses and a brief discussion on the effect of photoionization with ultrashort laser pulse. A comparative review of nonadiabatic methods is also presented in this chapter with a discussion on how external electric field interactions are commonly implemented for single-set approaches. The focus of this thesis is on the usage of a full quantum method with an Ehrenfest approach for the Potential Energy Surface (PES) for the simulation of nonadiabatic dynam-

ics induced by broad energy pulse photoionization. Chapter 3 introduces the main variational approaches for electronic structure methods and a derivation of the main Equations-Of-Motion (EOM) used in the the Direct Dynamics variational Multi-Configurational Gaussian method (DD-vMCG) and QuEh which are both implemented in the QUANTICS package. One particular aspect of DD-vMCG compared to QuEh is the use of a database which contains previously calculated points of the PES and thus, running expensive electronic calculations can be minimized through an interpolation using the points in the database. For the representation of the PES, a multiconfigurational approach is taken using the Complete Active Space Configuration Interaction method (CAS-CI) which is based on the Complete Active Space Self-Consistent Field method (CASSCF). A section is dedicated to the data analysis to show how the data from a quantum simulation can be represented and how the expectation values (i.e. averages) are evaluated. Chapter 4 shows the development done in the QUANTICS package for the DD-vMCG and QuEh methods to circumvent the current limitations of the algorithm and expand its execution to heavily parallel computing architecture system by further parallelizing the program with a Message Passing Interface (MPI). The restriction on the use of database with that specific parallel interface is solved by using the Structured Query Language (SQL) for the handling of the database. Development work is also done in the GAUSSIAN program on the CASSCF code to include the effects of external electric field in QuEh simulations. In chapter 5, the data from QuEh simulations on retinal Protonated Schiff Base (rPSB) and the benzene and ethylene cations are presented. The dynamics induced by superposition of eigenstates is rationalized in three steps. The first step is by unravelling the effect of changing the composition of two cationic states on a rPSB model system. The second step is the link between symmetry which can be employed to predict the location of conical intersections (CoIn) between electronic states and the dynamics

initiated on a coherent superposition of states. Thus, the work on benzene cation rationalizes the dynamics using symmetry arguments. Finally, the photocontrol of ethylene cation is attempted by using a control/probe infrared (IR) laser pulse and the effects explained using symmetry rules.

By investigating the importance of CM on nuclear wavepackets dynamics, it provides an insight into the coupled electron-nuclear dynamics observed indirectly in attosecond spectroscopy experiments and that using a coherent superposition of electronic states is required to be able to reproduce qualitatively the molecular dynamics upon photionization with an attosecond pump-pulse. Furthermore, being able to predict the change in the geometry of the molecule allows us to create initial superposition of electronic states in an attempt to guide the photo-reactivity of the system. Finally, the investigation on the effect of a probe-pulse in dynamics brings forth more options for photocontrol of the molecular wavefunction.

Chapter 2

Theory

2.1 Introduction

The key concept explored here is electron correlation and its importance on the nuclear dynamics. From a classical point of view, the interaction of an electron with its environment is purely electrostatic. By treating the electron quantum mechanically, electronic correlation comes into picture, an important concept in chemistry as well as molecular and atomic physics.[1–3] It can be described as the interaction between electrons where the motion of an electron is influenced by the presence of other electrons. An accurate treatment of this interaction is required in order to properly describe many molecular properties such as bond lengths, dissociation energies and ionization potentials. A more thorough discussion on the treatment of the electron from a computational point of view is given in chapter 3. Theoretically, it has been shown that dynamics purely driven by electron correlation is possible by creating a superposition of eigenstates.[4,5] Moreover, the dynamics induced by this superposition has been shown to occur on the femtosecond to subfemtosecond timescales. Thus, it will require attosecond pulse technology which have the sufficient time resolution to monitor these events.

The recent advance in attosecond spectroscopy has made possible the monitoring of molecular phenomena which are faster than nuclear motions.[6–9] The study of a molecular system upon absorption of photons from an attosecond laser pulse

requires a fundamental understanding of the nature of the pulse used in the experiment. An interpretation of these results can be achieved through computer simulations with an understanding of the mathematical models employed and their limitations.

In this chapter, a short introduction on attosecond spectroscopy will be presented as well as the current technology employed to generate sub-femtosecond laser pulses. An outlook is provided from theory by reviewing nonadiabatic dynamics methods and classifying them based on the expansion and parametrization of the molecular wavefunction into either a single-set or multi-set formalism. In the last Section, different approaches for the inclusion of a pulse in dynamic simulations are introduced for the single-set approach.

2.2 Attosecond Spectroscopy

To put perspective into the molecular timescale, it is known that nuclear motions such as vibrations, rotations and translations occur normally in the femtosecond range, whereas, electronic motion happens at an attosecond timescale (10^{-18} s).[10,11] Femtosecond spectroscopy, which uses laser pulses in the visible (VIS) to ultraviolet (UV) range, provides information about nuclear motion in molecules.[12] Our understanding of intramolecular processes as well as the the dynamics of bond breaking and bond formation has thus progressed thanks to this technique.

Using attosecond pulses for pump-probe experiments, it becomes feasible to monitor electron dynamics, opening the possibility of exploring the effect of early dynamics purely driven by electronic effects on the subsequent molecular motions.[7,8,13,14] It is theoretically possible to generate attosecond pulse down to a single cycle of oscillation of the electric field (i.e. with an oscillation period below 1 fs) which would correspond to a photon energy in the visible region at the minimum. With the current technology for the generation of stable attosecond

pulses, spectroscopy experiments with these laser involve photon energies in the range of UV to X-ray. The main difference between the two types of spectroscopy, other than the pulse duration, is the type of molecular species monitored. With UV/VIS photons, the main product is photo-excited molecules whereas higher energy photons (UV to X-ray) create (core) ionized species.

Applications other than pump-probe experiments are well documented in the literature for attosecond science such as molecular imaging.[9]

2.2.1 Laser Sources

Ultrashort laser pulses can be created by either of the following technologies: High-Harmonic Generation (HHG)[9,15] or Free-Electron Laser (FEL).[9,16] The former technology creates highly coherent photons in the UV to soft X-ray spectrum while the latter generates photons in the extreme ultraviolet (XUV) to X-ray regime.

The process to generate attosecond pulse using HHG can be explained using the semi-classical three step model.[9,17] The first step involves the removal of an electron from an atom in the gas phase through tunnel ionization. The ionization happens using a laser (the driving laser) producing photons in the UV range. After the ionization process, the electron moves freely away from the atom in the continuum of state and is then accelerated back by the oscillating electric field of the laser pulse reversing direction. The last step is the recombination of the accelerated electron with the parent ion reforming the initial atom with an emission of a short pulse. The whole process happens in the span of a full cycle of the oscillating electric field from the driving laser. Thus, using a (sub-)femtosecond laser (from an UV source), the process happening at the attoscecond timescale releases burst of photons at different harmonic and it happens for every cycle of the electric field leading to the formation of a train of attosecond pulses. An illustrative representation of the three step model can be found in Fig. 2.1. The physical mechanism behind it is that by focusing an intense short laser pulse into a gas medium, a nonlinear

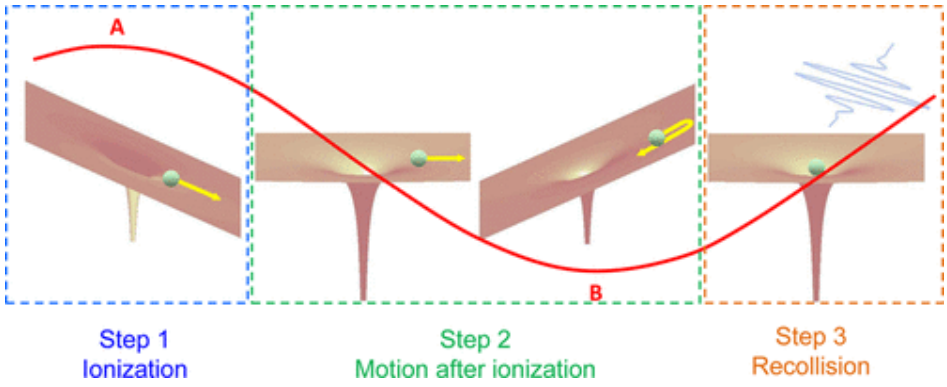

Fig. 2.1: Schematic of the three step model with (1) ionization, (2) motion and acceleration followed by (3) recollision. Reproduced with permission from Ref. 9. Copyright 2017 American Chemical Society.

effect is observed on the electrical response and thus, high-order harmonics of the frequency driving laser are generated. The generation of isolated attosecond pulses can be done using gating techniques.[9,18–20] Only odd harmonics are generated and from the review of Nisoli et al.,[9] this has been explained in terms of a symmetric response of the reversal of the driving field which cause a reversal of the nonlinear polarization.

The HHG technique allows the generation of highly coherent pulses for the purpose of pump-probe experiments. In the emission spectrum produced by HHG, only the three first harmonics show a relative important intensity followed by a plateau and a cut-off region. Thus, experiments involving pulse from higher harmonics rely on a low pulse intensity (i.e. low photon counts). The type of noble gas employed can affect up to which harmonic can be measured.

An different alternative to generate high energy photons (UV to X-ray range) is through a FEL where the medium is a beam of free electrons rather than noble gas. The electrons are propagated at a relativistic velocity in an undulator region consisting of a periodic arrangement of magnets where the electrons undergo transverse oscillation and release photons in the forward direction of propagation. A schematic of the mechanism in the undulator is shown in Fig. 2.2. As high-

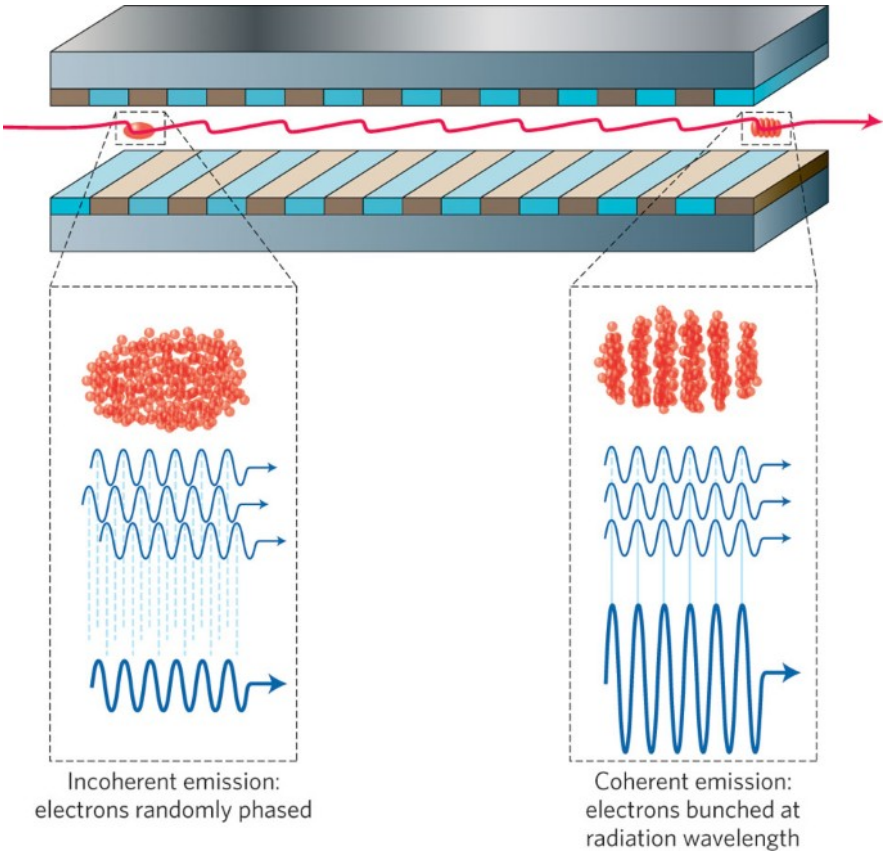

Fig. 2.2: Schematic of the FEL operating principle with the path of the electrons in red and the initial part (i.e. entrance) generating incoherent radiation and at later stage (on the right) an in-phase oscillation and radiation until saturation. Reproduced with permission from Ref. 16. Copyright 2010 Macmillan Publishers Limited.

lighted in the review of Nisoli et al.[9] and the work of McNeil and Thompson,[16] the drawback is that the electrons oscillate with random phases in the entrance of the undulator and thus, it generates highly incoherent radiation. As the group of electrons interact with each other due to the collective radiations, the electrons start to oscillate in phase at resonant wavelength until saturation of the process. In this last regime known as self-amplified spontaneous emissions, a burst of photons is released with some drawbacks such as stochastic temporal structure and an intrinsic time jitter due to electron propagating at relativistic speed and measurement done in a lab frame.[9,21–23] By isolating the emissions generated in that special regime, isolated attosecond pulse has been successfully generated from FEL.[24]

The two sources of lasers have been succesfully employed for attosecond science and it was achieved by using isolated attosecond pulses for pump-probe scheme experiment where a XUV is used for the pump process. The subsequent probe pulse can be either another XUV pulse from the same source or a synchronized infrared (IR) pulse.

2.2.2 Charge Migration

The actions responsible for the change (i.e. movement) of the electronic density are commonly separated into either Charge Migration (CM) or Charge Transfer (CT).[25–27] The former case corresponds to fast motion of an electron (or hole) happening on the femtosecond to sub-femtosecond timescale which takes place over a static nuclear framework (i.e. almost no nuclear motion over the time frame of electron dynamics).[4,5,28,29] The second situation corresponds to a formal motion of the charge from one part of the molecule to another and is mediated by a change in nuclear arrangement. However, the competition between the two phenomena and the nature/timescale of the transition between the two types of regime still remain as open questions.[25]

For the description of electronic states, the term CT is also used for the characterization of excited states involving a promotion of electrons between spatially separated sites. In this work, such electronic states will be referred as CT-state whereas CT will correspond to the vibrationally mediated charge dynamics.

From the experimental works of Weinkauf et al.,[30,31] it has been shown that for oligopeptide radical ions (after photoionization) a fast dissociation as well as a selective bond-breaking are observed. In their experiments, the photodissociation could be altered by using specific sequences of amino acids or with laser control. The 'photocontrol' is achieved by fine-tuning the local ionization energy (i.e. by amino acid sequence engineering) and resonant laser ionization (i.e. targeted hole formation). Thus, there is experimental evidence of fast electron dynamics and

charge-driven dynamics.

Cederbaum and Zobeley showed that fast electron dynamics is a purely electronic correlation driven effect.[4] In the creation of a localized hole, the system is on a superposition of ionic eigenstates (i.e. non-stationary state) and the subsequent hole dynamic is driven by the electronic correlation. Moreover, the CM happens within a few femtoseconds and in that timescale, the nuclei would show very little motion.

In the context of attosecond science, observations of phenomena driven by electron dynamics in cations have been experimentally reported such as in the works of Sansone et al.[32] and Jiang et al.[33,34] In these works, an XUV/(IR or XUV) pump-probe scheme has been employed to monitor the photodissociation of dihydrogen upon photoionization. The pulse induced a coherent superposition cationic states which leads to electron dynamics resulting in electron ejection with asymmetric angular distribution and localization of the remaining electron. Furthermore, the magnitude and direction of these two events are influenced by the pump-probe delay.

2.3 Nonadiabatic dynamics

As shown by the experimental findings and highlighted by the review of Nisoli et al.,[9] electron dynamics with observed asymmetry are taking place, and thus it has been hypothesized that the effect of the attosecond pulse is to generate a non-stationary electronic wavepacket corresponding to a superposition of cationic states. By using the uncertainty principle of Heisenberg on the relationship between energy and time, it can be rationalized that a very short pulse (in the attosecond regime) must have a very broad energy range. Thus, the ionization step can hit multiple cationic eigenstates and it has been shown from theoretical simulations and experimental ionization cross-sections that the isolated attosecond

pulses can indeed ionize to multiple states which would leads to CM due superposition of electronic states and the cationic eigenstates being coupled by electron correlation.

In the current work, the focus is on the CM taking place upon creation of a coherent superposition of states and the ionization step is not explicitely taken into account. Thus, all simulations and theoretical frameworks will be done in the sudden approximation and the interaction between the leaving electronic wavepacket and molecular ion wavefunction happening during the ionization step is not considered. A review of methods to theoretically model the ionization process can be found in Ref. 9 and the relevant finding for the current work is that even theoretical simulations show that the ionization involves the creation of a coherent superposition of electronic states.

To simulate the event after photoionization, the method employed should be able to treat dynamics on multiple electronic states or in a way of representating the electronic wavepacket in a non-eigenstate of the electronic Hamiltonian. Such methods are called nonadiabatic dynamics. A theoretical background on the definition of electronic state (eigenstate), Potential Energy Surface (PES), adiabatic/diabatic representation are briefly presented in Appendix A starting from the full molecular Hamiltonian for the non-relativistic case (i.e. no heavy atoms and electron motion at relativistic speed). The current work focuses on an on-the-fly approach for the dynamics thanks to the ability to explore the PES of system with many degrees of freedom. The drawback of the on-the-fly methods is the poor description of the nuclear wavepacket compared to highly accurate nuclear wavepacket dynamics methods such Multi Configuration Time Dependent Hartree (MCTDH)[35–37] which uses a grid-based approach for the treatment of the nuclear wavefunction and mapping of the PES as function of nuclear coordinate. The main limitations of the method are the need of pre-fitted PES, with its own set of

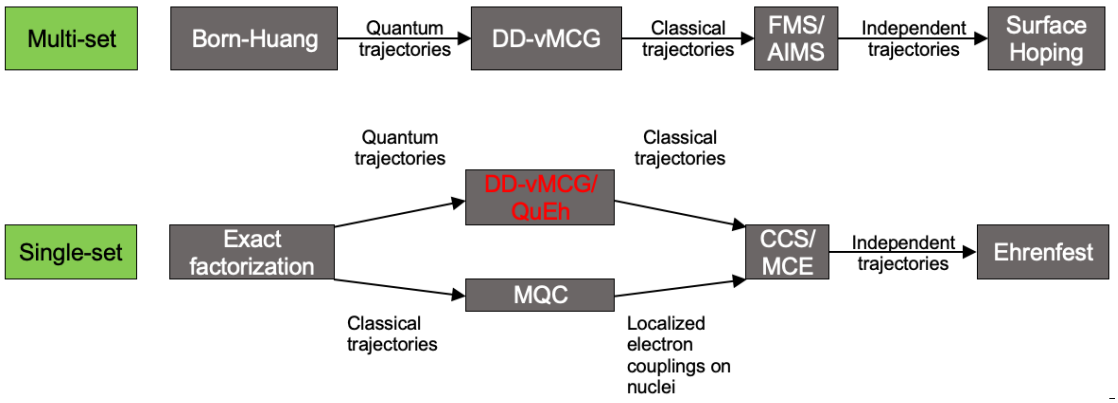

Fig. 2.3: Schematic representation of relationship between different nonadiabatic dynamics methods discussed in this work, based on the scheme of Vacher et al. in Ref. 38. The methods of interest in this thesis are higlighted in red and are elaborated in details in chapter 3

challenges compared to an on-the-fly approach, and simulations on systems with small number of degrees of freedom due to the cost of computation. A short review on nonadiabatic dynamics methods is presented here based on the classification and relationship given by Vacher et al.[38] as shown in Fig. 2.3.

In the list of methods presented by the authors, the electrons are all treated quantum mechanically with the help of electronic structure programs. The major differences are the treatment of the nuclear wavefunction and the approximations included. The methods can be categorized into two sets of approach. In the multi-set formalism, a set of basis functions is used for each electronic state and thus, the individual basis function only perceives the gradient of a single adiabatic/diabatic state. In the single-set approach, the nuclear motions are represented by one set of fully coherent basis functions feeling the gradient of a linear combination of electronic states (i.e. 'single' time-dependent state). That single effective state is often referred to as an Ehrenfest state. That categorization can also be linked to the perspective works of Agostini and Curchod[39,40] where the two formalisms can be related to a different initial ansatz. A schematic representation of how a single Gaussian wavepacket (GWP) evolves in the two formalisms is shown on Fig. 2.4.

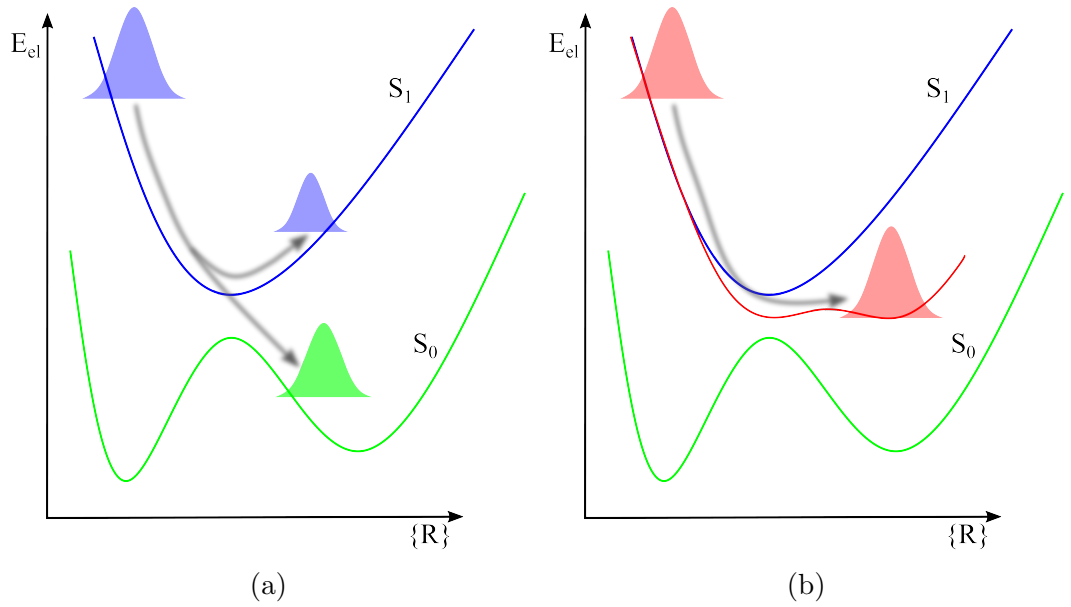

Fig. 2.4: Schematic representation of the propagation of a single GWP in the multi-set formalism (left) moving on a set of adiabatic states and in the single-set formalism (right) moving on a single time-dependent PES (in red).

The categorization of the methods is done on the interpretation of the nuclear dynamics and the gradient felt by the trajectories. Thus, the relational links between methods are purely on a conceptual view of the approximations and we do not go into the exact nature of the derivation of the Equations-Of-Motion (EOM), integrators and the numerical challenges. As for the cost of computation, one can easily guess, the more approximations are introduced, the simpler the EOM and thus, a reduced cost of computation. The main nature of most of the approximations in nonadiabatic dynamics are the representation of the nuclear wavefunction with a discretized basis and the motion of the basis to reproduce as closely as possible the 'ideal' nuclear wavepacket motion. In the different methods briefly reviewed here, only the main characteristics for comparison purpose are listed.

For on-the-fly nonadiabatic dynamic methods, the accuracy of the representation of the electronic wavefunction and PES is down to the choice of electronic structure method where one has to balance the cost of the computation and accura-

cy/stability of the method. The other factor to take into account is the treatment of the nonadiabatic effects and the diabatization of the PES which introduced further approximation in the representation of the electronic wavefunction.

2.3.1 Multi-set

The multi-set approach can be started using the Born-Huang ansatz to expand the molecular wavefunction Ψ.[39,41] The important part is that the electronic wavefunction ψ is discretized as a linear combination of time-independent states s and that a set of nuclear basis functions χ is defined for each state.

$$\Psi\left(\boldsymbol{R},\boldsymbol{r},t\right)=\sum_{s}A_{s}\left(t\right)\chi_{s}\left(\boldsymbol{R},t\right)\psi_{s}\left(\boldsymbol{r};\boldsymbol{R}\right) \tag{2.1}$$

The time dependency t is all put into the nuclear basis and the expansion coefficient A_s that is related to the population of the electronic state. In that representation, it gives rise to a picture of time-independent PES with CoIn in region of state crossing and the resulting nuclear dynamics in that representation corresponds to nuclear wavepackets moving on individual surfaces along nuclear coordinate $\boldsymbol{R}$. The time-independent electronic wavefunction is a function of the electron coordinates $\boldsymbol{r}$ and shows a parametrical dependence on the nuclei positions $\boldsymbol{R}$.

The Direct Dynamics variational Multi-Configurational Gaussian method (DD-vMCG) of Worth et al.[42–46] expand the nuclear wavefunction using a linear combination of Gaussian Wavepacket (GWP) and approximating the effect of the electron on the nuclei by a local expansion of the diabatic PES. By taking a variational approach for the derivation of the EOM, the simulation yields a dynamics with a set of coupled quantum trajectories. The quantum motion is due to the optimal propagation of the basis set to reproduce as closely as possible the ideal exact nuclear wavefunction spreading. The main approximation in the nuclear description is the truncation of the basis set which is set from the beginning of the dynamics. Another restriction applied to the basis set for numerical stability

is the use of frozen width GWP. The DD-vMCG dynamics can be done in the multi-set or single-set formalism and in both case, the nuclear wavefunction χ is expanded using a linear combination of GWP g. In the former approach, a set of GWP is defined for each diabatic state s (see eq. 2.2) and only the gradient and curvature of a single time-independent state is applied to the dynamics of the basis functions.

$$\chi_s(\boldsymbol{R}, t) = \sum_j A_j^{(s)}(t)\, g_j(\boldsymbol{R}, t) \tag{2.2}$$

By introducing a classical approach for the EOM of the basis functions in the multi-set approach leads to the Full Multiple Spawning (FMS) and Ab Initio Multiple Spawning (AIMS) method of Martínez et al.[47,48] The important feature of the AIMS method is the adaptive expansion of the basis set in region of strong nonadiabatic couplings. The advantage of that approach is the efficient description of the bifurcation in region of state crossings.

By further uncoupling the trajectories and using an independent trajectory approach leads to the Surface Hopping method.[49] The trajectories feel the gradient of a single electronic state and jump from one state to another (i.e. hop) based on a hopping probability. That quantity is computed using nonadiabatic couplings and the hopping event occurs based on random number generator (stochastic algorithm). The advantage of the method is that classical EOM can be integrated easily using very accurate numerical methods due to the straightforward description of the couplings and electronic states. However, semi-classical approaches with uncoupled trajectories are known to suffer from slow convergence and thus, a large number of trajectories is needed along a careful approach for the initial condition samplings.

2.3.2 Single-set

The methods that fall in the single-set formalism starts from the exact factorization ansatz[39,50] where the molecular wavefunction Ψ is written as a product of nuclear χ and electronic wavefunction ψ.

$$\Psi(\boldsymbol{R}, \boldsymbol{r}, t) = \chi(\boldsymbol{R}, t)\, \psi(\boldsymbol{r}, t; \boldsymbol{R}) \tag{2.3}$$

The electronic wavefunction is a function of the electrons position $\boldsymbol{r}$ and shows a parametrical dependence on the nuclear position $\boldsymbol{R}$. In the exact factorization representation, the nuclear wavepacket spreads on a single time-dependent PES.[40]

The time-dependent electronic wavefunction can be projected at any time t at a specific parametrization $\boldsymbol{R}$ (i.e. geometry) onto a set of adiabatic/diabatic states and the main challenge is the overall definition (over the whole configuration space $\boldsymbol{R}$) of ψ. To be able to compute the dynamics using the exact factorization ansatz, various approximations and nuclear/electronic ansatz are further introduced. The localized time-dependent electronic state (at a given $\boldsymbol{R}$) is known as the Ehrenfest state which is generally defined as a superposition of electronic adiabatic/diabatic states.

By introducing the classical limit to the nuclear motion leads to the Coupled-Trajectory Mixed Quantum-Classical (CT-MQC) method of Agostini et al.[51–55] where the coupling of the electrons on the nuclei is done through a vector potential term. Thus the natural decoherence effect is captured by the quantum momentum term included in the EOM. The nuclear density is constructed using a sum of frozen width GWP.

The DD-vMCG method introduced before can also be run in the single-set formalism where one set of j GWP g is defined for the nuclear wavefunction χ (see eq. 2.4). The basis functions feel the shape of a time-dependent PES built on a linear combination of time-independent states $|s\rangle$ which yields an Ehrenfest-like state. The coefficients for the electronic state s are contracted within the expansion

coefficient $A_{j,s}$. A further push toward the Ehrenfest treatment is done with the Quantum-Ehrenfest method (QuEh, see eq. 2.5a and 2.5b).[38,56,57] In this approach, the Ehrenfest part of the electron dynamics is done within the electronic structure by multiconfigurational treatment for it. Thus, the nuclear dynamics is done with the same framework as DD-vMCG with GWP running on a single Ehrenfest PES expanded locally up to second order.

$$\chi\left(\boldsymbol{R},t\right)=\sum_{j}\sum_{s}A_{j,s}\left(t\right)g_{j}\left(\boldsymbol{R},t\right)\left|s\right\rangle \tag{2.4}$$

$$\chi\left(\boldsymbol{R},t\right)=\sum_{j}A_{j}\left(t\right)g_{j}\left(\boldsymbol{R},t\right)\left|j\right\rangle \tag{2.5a}$$

$$\left|j\right\rangle=\sum_{s}c_{j,s}\left|s\right\rangle \tag{2.5b}$$

In the semi-classical approach adpoted by Shalashilin et al.[58–61] in the Coupled-Coherent States (CCS) and Multi-Configurational Ehrenfest (MCE), a set of coupled classical trajectories evolves on a time-dependent PES built on Ehrenfest trajectories. In these two methods, the general feature is that both employed a basis of GWP in addition to the classical trajectories.

The Ehrenfest method[62–66] takes the full classical localized approach for trajectories by uncoupling them. In this method, the individual trajectory evolve classically on a set of time-dependent Ehrenfest state. The trajectories evolve all independently (no coupled motion) and they all start with a defined amplitude (i.e. nuclear population) frozen throughout the propagation. Thus, a great emphasis is put on sampling for the initial condition in semi-classical method using fully uncoupled trajectory like the Ehrenfest method or the multi-set equivalent, the Tully Surface Hopping algorithm.[67]

2.3.3 Simulation of pulse effects in dynamics

The current review only cover the inclusion of a pulse in the single-set formalism method since the focus of the project is the simulation of control/probe pulse following attosecond pulse photoionization. Due to the nature of the electronic state being a superposition of cationic state, the single-set formalism seems to be more straightforward to simulate fast electronic effect due to a non-stationary state. Various approaches and approximations can be employed to simulate the effect of a theoretical pulse in dynamics.

For the single-set method, throughout the literature, two main approaches seems to be adopted for the inclusion of an external electric field in the dynamics.

The first one is through the use of a Floquet Hamiltonian formalism (i.e. time-dependent electronic Hamiltonian) in the case of a periodic electric field.[68,69] In this approach, the time-dependent process is treated by extracting the eigenstate (i.e. Floquet state) of the electronic Hamiltonian with the time-periodic term in it. The physical interpretation of these states is that they do not correspond to a real eigenstate of the time-independent electronic Hamiltonian but a state where the PES has been 'dressed' with the field. This is the approach employed by Agostini et al.[70] for the CT-MQC methods.

In the second method, the interaction is added through an electric field term interaction within the dipole approximation and can be employed for any arbitrary external electric field (no condition on being periodic). For Ehrenfest-based methods, it is the most popular approach as the electronic state is a single effective time-dependent state and thus, the pulse interaction has to be included at the electronic level. This is the approach also employed by the DD-vMCG method. The particularity in that method is that the individual electronic state are still visible from an algorithmic perspective and thus, the extra term can be included by adding a new operator in the nuclear Hamiltonian. Multiple overlapping external

pulses can be defined explicitly and can be added as an intra- or inter-electronic state effect by taking an electric field and dipole dot product. The dipole included in question can be the transition dipole moment for excitation or the state dipole for purely pulse-driven nuclear effect. This was done for the vMCG method in the work of Penfold et al.[71] and thus, a propagation with the presence of an external pulse is possible for the direct dynamics version. In the QuEh method, only one apparent effective state is seen from the perspective of the nuclear basis function and thus, any electron-pulse interaction cannot be treated currently. In the MCE method, the same approach has been used and some work has been done toward simulating non-linear response with respect to field using a dipole-electric field operator.[72] Similar studies with a pulse effect using the same formalism can be found using the classical Ehrenfest method.[73]

2.4 Summary

The progress in attosecond science has allowed the exploration of dynamics at the electronic timescale. Due to the nature of the pulse, a large number of cationic state are reached upon photoionization and events happening at the sub-femtosecond timescale lead to asymmetry in the molecular dynamics. The use of a subsequent probe pulse can push the molecular dynamics in a different direction (e.g. different photo-products).

One can find an extensive list of available of methods for simulating the nonadiabatic dynamics of molecular system for the purpose of rationalizing spectroscopic results. The current review took an approach by classifying the method based on the expansion of the electronic wavefunction and the definition of nuclear basis function for the given expansion (i.e. single-set vs multi-set). The current work is focused on the single-set formalism for a more straightforward approach to dynamics involving electron dynamics built on a superposition states.

For this work, an approach with quantum trajectories is taken due to the advantage of faster convergence with respect to the nuclear wavefunction representation and the ability to treat coherence and quantum nuclear effect without *ad hoc* correction scheme. Thus, the development and research are done for DD-vMCG and its QuEh variant. However, some approximations are taken in these methods to make the simulations computationally affordable and numerically stable such as truncated (i.e. fixed) nuclear basis set, local definition of the PES, etc.

The emphasis is on the QuEh method where the full time-dependent treatment of the electronic wavefunction is done within the electronic structure method. To investigate the effect of an external pulse on the dynamics, a first simple implementation of it is done for this work and the algorithm and results are presented in the Development chapter 4.

Chapter 3

Methodology

3.1 Introduction

The interpretation of results from an attosecond spectroscopy experiments can be achieved through the use of computer simulations to develop an understanding at the molecular level. Due to the high complexity of the phenomena observed (e.g. multiple electronic states, coherence, high energy photons, coupled nuclear-electron dynamics), an appropriate level of theory should be employed to model the dynamics of the molecular system. An application of the theory outlined in chapter 2 is done with an accurate description of the electrons and nuclei at the quantum level using a single-set approach. This chapter is focused on the methods employed for the computation and the relevant data analysis.

Using electronic structure methods, different molecular properties can be computed such as the energies, dipole moments, gradients, Hessians and nonadiabatic couplings. The gradients and Hessians are the first and second derivatives of the Potential Energy Suraces (PES) with respect to the nuclear coordinates. These quantities are needed by the nuclear dynamics driver program in order to propagate the nuclear wavefunction in time as in both the Direct Dynamics variational Multi-Configuration Gaussian (DD-vMCG) and Quantum-Ehrenfest (QuEh) methods, the information of the PES is expanded up to second order around the centre of the Gaussian Wavepackets (GWP). The main consideration in the choice of the

electronic structure method is to balance accuracy and cost of computation. In this section, various variational methods are introduced with a particular emphasis on multi-configuration approaches which would allow a balanced description of the electronic states with analytical derivatives readily available for these methods.

The electronic structure methods that are used specifically for the QuEh algorithm is presented in section 3.2. The nonadiabatic dynamics method used is detailed in section 3.3. The data analysis protocol for the results presented in chapter 4 and 5 are introduced in section 3.4.

3.2 Electronic Structure

The aim of electronic structure methods is to solve the time-independent Schrödinger Equation (TISE) of the electronic Hamiltonian (see eq. A.11 in appendix). The ansatz to solve that equation is by using a product of N one-electron functions ψ_i for the representation of the full electronic wavefunction ψ_{el} containing N electrons.

$$\psi_{el}(r_1, \ldots, r_N) = \psi_1(r_1)\psi_2(r_2)\ldots\psi_N(r_N) \tag{3.1}$$

The equation shown in eq. 3.1 is called a Hartree product and doesn't account for interacting electrons. Moreover, it doesn't include the fermionic nature of the electron which leads to the Pauli exclusion principle (i.e. two fermions cannot have the same exact quantum state) and the anti-symmetric nature of the fermionic wavefunction when exchanging two indistinguishable electrons.

A way to account for the antisymmetric nature of the electronic wavefunction as well as satisfy the Pauli exclusion principle is to write ψ_{el} using a Slater determinant (SD)[74,75]

$$\left|\phi_1(r_1)\phi_2(r_1)\dots\phi_N(r_1)\right| = \frac{1}{\sqrt{N!}}\begin{vmatrix} \phi_1(r_1) & \phi_2(r_1) & \dots & \phi_N(r_1) \\ \phi_1(r_2) & \phi_2(r_2) & \dots & \phi_N(r_2) \\ \vdots & \vdots & \ddots & \vdots \\ \phi_1(r_N) & \phi_2(r_N) & \dots & \phi_N(r_N) \end{vmatrix} \tag{3.2}$$

where $\phi_i(r_i)$ are the one-electron Molecular Orbitals (MO) at coordinate r_i. A procedure to obtain the MO is by using a Linear Combination of k Atomic Orbitals (LCAO)[76–78]

$$\phi_i = \sum_{k=1}^{k_N} d_{ki}\theta_k \tag{3.3}$$

where d_{ki} is the atomic orbital coefficients and θ_k is the atomic orbitals. In electronic structure methods, the most common basis function is the gaussian function for the construction of atomic orbitals due to better computational efficiency compared to slater type functions.[79–81]

The exact electronic wavefunction is an eigenfunction of total spin and projected spin. However, the SD are only eigenfunctions of the projected spin. For simplicity, it is advantageous to work with a basis of spin eigenfunctions which are simultaneously eigenfunctions of one electron effective Hamiltonian and the total/projected spin.[82,83] Mathematically, this means that the commutator is zero between the occupation $\hat{N}$ operator

$$\hat{N}_p = \hat{N}_{p\alpha} + \hat{N}_{p\beta} \tag{3.4}$$

which is an operator that counts the number of α and β electrons in an orbital p and the spin operator (either projected $\hat{S}_z$ or total spin $\hat{S}^2$, see eq. 3.5a and 3.5b, respectively).

$$\left[\hat{N}_p, \hat{S}_z\right] = 0 \tag{3.5a}$$

$$\left[\hat{N}_p, \hat{S}^2\right] = 0 \tag{3.5b}$$

This set of spin adapted basis functions are denoted as Configuration State Functions (CSF). The CSF are built as linear combinations of degenerate SD of the same orbital configuration. The number of SD for a given value of projected spin M_S and the number of CSF for a total spin of value S can be calculated with the following equations

$$n_{SD} = \binom{M}{\frac{N}{2} + M_S}\binom{M}{\frac{N}{2} - M_S} \tag{3.6a}$$

$$n_{CSF} = \frac{2S+1}{M+1}\binom{M+1}{\frac{N}{2} - S}\binom{M+1}{M - \frac{N}{2} - S} \tag{3.6b}$$

where M is the number of orbitals and N the number of electrons.

One can obtain the electronic energy E_{el} for a specific form (i.e. specific value of the coefficient and basis parameters) of the wavefunction with the following equation for the expectation value of the electronic Hamiltonian $\hat{H}_{el}$ (see eq. A.12 in appendix for definition of $\hat{H}_{el}$)

$$E_{el} = \langle \psi_{el} | \, \hat{H}_{el} \, | \psi_{el} \rangle \, . \tag{3.7}$$

The ground state solution can be obtained by minimizing the expectation value of the energy with respect to a variational parameter V

$$\frac{\partial}{\partial V} \frac{\langle \psi_{el} | \, \hat{H}_{el} \, | \psi_{el} \rangle}{\langle \psi_{el} | \psi_{el} \rangle} = 0 \tag{3.8}$$

where any trial electronic wavefunction ψ_{el}, which is dependent on V, satisfies the following inequality

$$E_{el} \leq \frac{\langle \psi_{el} | \, \hat{H}_{el} \, | \psi_{el} \rangle}{\langle \psi_{el} | \psi_{el} \rangle}. \tag{3.9}$$

An electronic structure method is called variational if the wavefunction parameters are optimized by minimizing the energy. For the optimization process, an energy equation is defined for each method as a function of the variational parameters and there is various way to find the stationary point (i.e. minimum

energy). If the energy displays a linear dependency on the variable, a diagonalization method can be employed to get the solutions. In the general case, the solution is obtained by solving a set of linear equations using a quadratic model of the energy (as function of the variational parameter) where the mathematical expression is expanded up to second order as Taylor series. The first and second order term are respectively the electronic gradients and Hessians. The optimization here is done through an iterative process where the parameters are varied by a step size using method such as Newton(-Raphson).[82,83] The electronic gradient is set to zero as a condition of convergence of the iterative process together with the energy variation between two subsequent iterations.

The different methods introduced in this section will be written in the second quantization formalism using annhilation and creation operators.

3.2.1 Hartree-Fock

In the Hartree-Fock (HF) method,[84,85] the electronic wavefunction is parametrized in the following way

$$|HF\rangle = e^{-\hat{K}} |0\rangle \tag{3.10}$$

where $|0\rangle$ is a single configuration (i.e. a SD) and $e^{-\hat{K}}$ is the operator that performs a unitary transformation among the molecular orbitals. The matrix $\hat{K}$ is an anti-Hermitian matrix and the general form is written as

$$\hat{K} = \sum_{pq} k_{pq} \left(\hat{E}_{pq} - \hat{E}_{qp} \right) = \sum_{pq} k_{pq} \hat{E}^{-}_{pq} \tag{3.11}$$

where $\hat{E}_{pq}$ is the one-electron excitation operator written in second quantization as a product of creation and annihilation operator and k_{pq} is the element of the anti-Hermitian matrix.[82] The non-zero elements in the orbital-rotation matrix can be separated into two categories, the redundant and non-redundant parameters. The redundant parameters do not affect the description of the wavefunction for

any order of $\hat{K}$ and a parameter is said to be redundant if it satisfies the following condition

$$\hat{E}^{-}_{pq} |0\rangle = 0. \tag{3.12}$$

By applying the excitation operator $\hat{E}^{-}_{pq}$ to the ground state configuration $|0\rangle$, one can identify the occupied-occupied and virtual-virtual orbital rotations as being redundant and only the occupied-virtual rotation gives non-vanishing results. Thus, only the elements mixing the occupied and virtual space are non-redundant.

The ground state HF solution is obtained by applying the variational principle to the wavefunction in eq. 3.10 and it is done by minimizing the energy with respect to the orbital-rotation parameter. Convergence is reached once the orbital basis obtained yields a matrix $\hat{K}$ of zero.

In the HF method, the solution obtained is for a set of non-interacting electrons within a mean-field approach. The solution fulfills the Pauli exclusion principle and the anti-symmetric nature of the wavefunction via the means of SD. Thus, the solution can be found by solving a set of effective one-electron TISE called Hartree-Fock equations with an associated Fock operator

$$\hat{f} = \sum_{pq} f_{pq} \hat{E}_{pq}. \tag{3.13}$$

For a closed-shell system, the matrix elements of the Fock operator are given by the following equation

$$f_{pq} = h_{pq} + \sum_{i} (2g_{pqii} - g_{piiq}) \tag{3.14}$$

where h and g are the matrix elements of the one- and two-electron operators, respectively.

These equations are solved by diagonalizing the Fock matrix where the solutions (i.e. eigenvectors) are the canonical spin orbitals of the molecular system and the associated eigenvalues are the orbitals energies. The total HF energy is given by

evaluating the expectation value of the energy

$$E = \langle HF| \hat{H} |HF\rangle = 2\sum_{i} h_{ii} + \sum_{ij} (2g_{iijj} - g_{ijji}) + h_{nuc} \tag{3.15}$$

where h_{nuc} is the nuclei-nuclei repulsion term (treated as a constant for a given system and geometry). By expanding the energy up to second order, a step size can be estimated to vary the orbital-rotation parameters. The energy is optimized through an iterative process, called the Self-Consistent Field (SCF) method where the Fock matrix is diagonalized and reconstructed at each step of the orbital optimization until the electronic gradient reaches zero.

Two of the major challenges for electronic structure methods are the treatment of electron correlation[3,86] and the characterization of excited states.[87] Electron correlation is defined as the difference between the exact solution and the HF solution for a given basis set. The electron correlation is separated into static and dynamic contributions.[3,86] The dynamic correlation arises from the coupling of electronic motion, while the static correlation comes from the need to use multiple (quasi)-degenerate electronic configurations to describe a specific electronic state. The effect of electron correlation on the energy is geometry and state dependent and the molecular properties are influenced by the accuracy of its description. There are two major approaches for the inclusion of electron correlation: one based on the electron density known as Density Functional Theory (DFT)[1,2] and one based on the wavefunction known as Post-HF methods.

An accurate and balanced description of the excited states can be achieved with partial inclusion of the electronic correlation if a correct ordering of electronic states (with the correct character such as nπ or $\pi\pi$ states) is obtained with an accurate gap between energy levels. The energy difference for the individual states due to electronic correlation can be categorized as differential and external contributions.[88] In the former, the inclusion of correlation changes the relative energy between electronic states and in the latter case, its effect is to shift (up

or down) the energy of the individual state by the same value. Thus, a balanced treatment can be achieved if the methods employed manage to capture most of the differential contribution.

While DFT offers the possibility of exploring the nonadiabatic dynamics of relatively large systems due to its low cost of computation, the treatment of excited states with the Time-Dependent Density Functional Theory (TD-DFT)[89] approach can lead to instability or incorrect description of states (i.e. energy gap and state ordering) near a region of degeneracy. Moreover, the ground state is treated at a different level of theory (DFT) while the excited state are computed using a linear response formalism using the reference ground state density. Response method approaches are known to perform poorly in case of a degeneracy involving the ground state as well as giving a poor description of the topology of the CoIn.[87,90]

In the current work, the initial condition of the electronic wavefunction involves creating a superposition of multiple adiabatic/diabatic states including the ground state in some cases. Thus, all electronic states should be treated at the same level of theory and the proper topology of Conical Intersections (CoIn) is of utmost importance to be able to qualitatively provide insight into the dynamics of a molecule upon photoexcitation/ionization. This work thus focuses on the usage of wavefunction approaches for the treatment of electrons.

3.2.2 Configuration Interaction

One approach to add the missing electronic correlation is by including more configurations (CSF or SD) in the description of the wavefunction.

In the Configuration Interaction (CI) method,[91,92] the electronic wavefunction $|C\rangle$ is expanded as a linear combination of configurations $|i\rangle$

$$|\boldsymbol{C}\rangle = \sum_i C_i \, |i\rangle \tag{3.16}$$

The two components of electron correlation can be captured up to a certain de-

gree with the CI method. The static correlation arises from the multi-configuration nature of the electronic states and thus, it can be recovered by including the dominant configurations and the nearly degenerate configurations. This set of SD/CSF are referred as the reference configuration and the dynamic correlation is obtained by adding configurations that are generated by excitations of electrons in the reference space.

The solution is obtained by variationally optimizing the wavefunction with respect to the C_i coefficients

$$\sum_i (C_i)^2 = 1. \tag{3.17}$$

and because the CI ansatz is a linear expansion of the wavefunction, it is equivalent to solving an eigenvalue problems of the form

$$\hat{H} \left|\boldsymbol{C}\right\rangle = E \left|\boldsymbol{C}\right\rangle . \tag{3.18}$$

The construction of the CI wavefunction is done by diagonalizing the electronic Hamiltonian matrix in the basis of the configurations $|i\rangle$.

In order to derive the CI energy expression for a variational optimization of the electronic energy, it is more convenient to expand around a zero reference state (i.e. solution at a given iteration). Thus, the energy variation is expressed as a function of the change in the coefficient with respect to a normalized reference state $|0\rangle$ defined as

$$|0\rangle = \sum_i C_i^{(0)} |i\rangle \tag{3.19}$$

with the coefficients fulfilling the same normalization condition

$$\sum_i \left(C_i^{(0)}\right)^2 = 1. \tag{3.20}$$

Thus, the variation with respect to the reference state is evaluated using a projection operator

$$\hat{P} = 1 - |0\rangle \langle 0| \tag{3.21}$$

and the parametrization of the CI wavefunction can be written as

$$|\boldsymbol{C}\rangle = \frac{|0\rangle + \hat{P}\,|\boldsymbol{c}\rangle}{\sqrt{1 + \langle \boldsymbol{c}|\,\hat{P}\,|\boldsymbol{c}\rangle}} \tag{3.22}$$

where $|\boldsymbol{c}\rangle$ is the (non-projected) CI wavefunction

$$|\boldsymbol{c}\rangle = \sum_i c_i\,|i\rangle\,. \tag{3.23}$$

The energy as function of the variational parameters c is obtained by inserting the expression of the CI wavefunction (eq. 3.22) into the expectation value of the energy

$$E(c) = \langle \boldsymbol{C}|\,\hat{H}\,|\boldsymbol{C}\rangle = \frac{\langle 0|\,\hat{H}\,|0\rangle + 2\,\langle \boldsymbol{c}|\,\hat{P}\hat{H}\,|0\rangle + \langle \boldsymbol{c}|\,\hat{P}\hat{H}\hat{P}\,|\boldsymbol{c}\rangle}{1 + \langle \boldsymbol{c}|\,\hat{P}\,|\boldsymbol{c}\rangle} \tag{3.24}$$

To obtain the CI solution, there are two possible approaches. The first one is to get the solution by directly solving the eigenvalue problems of eq. 3.18 by iterative methods or diagonalization of the matrix. The second option is to employ iterative process to converge the energy with respect to the variational parameters. In order to use the Newton-Raphson method for the optimization of the CI energy, the energy evaluation is done up to second order by differentiating the energy expression in eq. 3.24 with respect to the variational parameter c.

In the CI method, the orbitals are not optimized and thus, generally, the configurations are generated based on set of orbital occupations in the canonical MO basis which are obtained from an initial HF procedure.

In the case where an expansion is done in the full set of determinants by distributing all electrons among all the available orbitals, the method is known as Full Configuration Interaction (FCI). The cost of the computation and number of configuration grows very rapidly with the number of electrons and orbitals. A more affordable approach is where the configurations generated from excitation with respect to a set of reference configurations (eg. ground state CSF) are truncated up to a limited number of excitation. Such methods are called truncated CI and

there are various versions such as Configuration Interaction Singles and Doubles (CISD) and Configuration Interaction Singles, Doubles and Triples (CISDT) to cite a few.[93,94]

The FCI method is generally consider as exact solution for a given basis set and all correlation is included but the number of determinants grows exponentially with the number of electrons and orbitals. Thus, the method is only affordable for a very small molecular systems. The truncated CI method is able to capture part of the missing dynamic and static correlation. However, it suffers the same shortcoming as the FCI method with respect to the cost of computation, although to a lesser extent.

3.2.3 Complete Active Space Self-Consistent Field

In the HF method, the orbitals obtained by the SCF procedure are optimized for a single reference and thus, they are not optimal for the treatment of electronic states described with more than one main configuration. In the MultiConfigurational Self-Consistent Field method (MCSCF),[95–99] both the orbitals and coefficient of electronic configuration are optimized simultaneously. The wavefunction is parametrized in the following way

$$|MCSCF\rangle = e^{-\hat{K}} \sum_i C_i |i\rangle \tag{3.25}$$

with a linear combination of electronic configurations $|i\rangle$ and orbital-rotation matrix $\hat{K}$.

The MCSCF wavefunction is obtained by variationally optimizing the energy with respect to these parameters. Similar to the HF method, at convergence, the orbital-rotation matrix $\hat{K}$ becomes zero and the set of orbitals obtained are called canonical MO. The CI expansion is done in the basis of these MO.

Similar to the CI parametrization of the wavefunction, a projector operator (see eq. 3.21) is employed to monitor the variation of the MCSCF wavefunction

with respect to a reference state $|0\rangle$

$$|MCSCF\rangle = e^{-\hat{K}} \frac{|0\rangle + \hat{P}\,|\boldsymbol{c}\rangle}{\sqrt{1 + \langle \boldsymbol{c}|\,\hat{P}\,|\boldsymbol{c}\rangle}} \tag{3.26}$$

The energy expression is then obtained by evaluating the expectation value of the electronic Hamiltonian with the MCSCF parametrized wavefunction

$$E = \frac{\left(\langle \boldsymbol{c}|\,\hat{P} + \langle 0|\right) e^{\hat{K}} \hat{H} e^{-\hat{K}} \left(|0\rangle + \hat{P}\,|\boldsymbol{c}\rangle\right)}{\langle 0|0\rangle + \langle \boldsymbol{c}|\,\hat{P}\,|\boldsymbol{c}\rangle} \tag{3.27}$$

where the variables are $|c\rangle$ the CI coefficients and $\hat{K}$ the orbital-rotation parameters. For convenience, the energy function is expanded around the reference point $\boldsymbol{\lambda}^{(0)}$ with respect to a vector $\boldsymbol{\lambda}$ which contains both parameters

$$\boldsymbol{\lambda} = \begin{pmatrix} \boldsymbol{c} \\ \boldsymbol{K} \end{pmatrix} \tag{3.28}$$

and it yields the resulting equation

$$E(\boldsymbol{\lambda}) = E^{(0)} + \boldsymbol{E}^{(1)^T}\boldsymbol{\lambda} + \frac{1}{2}\boldsymbol{\lambda}^T \boldsymbol{E}^{(2)} \boldsymbol{\lambda} \tag{3.29}$$

where $E^{(0)}$ is the MCSCF energy at the current iteration (i.e. expansion point), $\boldsymbol{E}^{(1)}$ the electronic gradient and $\boldsymbol{E}^{(2)}$ the electronic Hessian. In the Taylor expansion of the MCSCF energy, the energy is differentiated with respect to both the CI and orbital-rotation parameters

$$E^{(0)} = \langle 0|\,\hat{H}\,|0\rangle \tag{3.30a}$$

$$\boldsymbol{E}^{(1)} = \begin{pmatrix} \boldsymbol{E}^{C} \\ \boldsymbol{E}^{K} \end{pmatrix} \tag{3.30b}$$

$$\boldsymbol{E}^{(2)} = \begin{pmatrix} \boldsymbol{E}^{CC} & \boldsymbol{E}^{CK} \\ \boldsymbol{E}^{KC} & \boldsymbol{E}^{KK} \end{pmatrix} \tag{3.30c}$$

and all derivatives are evaluated at the expansion point ($\boldsymbol{\lambda} = 0$).

The condition for the convergence is by setting the first derivative to be zero. Thus, the wavefunction is obtained by varying optimally both the CI coefficients and the orbitals. The optimization with respect to both parameters is done in a

sequential order. For a given set of MO, a (partial) diagonalization of the Hamiltonian matrix is done to solve the CI eigenvalue problem and a step size is evaluated for the orbital optimization using an intermediate Fock matrix which allows the computation of the first $\boldsymbol{E}^{K}$ and second $\boldsymbol{E}^{KK}$ derivatives of the energy. Each macro iteration corresponds to a step in the optimization of the MCSCF orbitals and the micro iteration corresponds to obtaining the eigenvalues (energies) and eigenvector (electronic state) of the Hamiltonian matrix in the configuration basis.

Due to the high cost of computation of any CI-based method, an accurate description of the electronic states is restricted to small molecules and using MCSCF for the full set of configurations set up in the orbital space. Moreover, the full MCSCF method is mostly a theoretical framework for getting a wavefunction that is more suitable for describing state with strong static correlation (heavily multiconfigurational). The FCI and MCSCF methods both theoretically yield the same answer. The strengths and weaknesses of both approaches becomes apparent when using truncated versions or partial expansions. In the case of MCSCF, the truncated version can provide a set of better orbitals for description of electronic state with restricted CI expansion compared to the truncated CI methods. A solution for the exponential rise of number of configurations is to constrain the number of electrons and orbitals where the permutations occur. One straightforward way of selecting the configurations is to partition the full set of orbitals into different subspaces with a restriction on the occupancy. In the Complete Active Space Self-Consistent Field (CASSCF) method,[100] the orbital space is divided into a set of occupied orbitals (doubly occupied in all configurations), virtual orbitals (empty in all configurations) and active orbitals (no restriction). The list of configurations is obtained by generating all the possible permutations of electrons in the set of active orbitals (called the active space) using a method such as the Generalized Unitary Graphical Approach (GUGA) of Shavitt.[101,102]

A special way of using the CASSCF method is to disable the convergence in the orbital-rotation optimization. This method is known Complete Active Space Configuration Interaction (CAS-CI)[56,103] where only one step in the orbital optimization is done. The solution from CAS-CI is exactly the same as CASSCF for a set of optimized MO. Mathematically, in the energy expansion of eq. 3.28, only the electronic gradient with respect to the CI coefficient is set to zero for the convergence criteria.

In the case of CASSCF and CAS-CI, the energy ($E^{(0)}$) can be written in a similar manner as the HF SCF energy (see eq. 3.14) using the Fock operator

$$E^{(0)} = \epsilon^c + \sum_{mn}^{val} F^c_{mn} A_{mn} + \frac{1}{2} \sum_{mnop}^{val} g_{mnop} B_{mnop} \tag{3.31}$$

where ϵ^c is the 'HF' energy of the core electrons (i.e. occupied orbitals)

$$\epsilon^c = 2 \sum_{i}^{core} h_{ii} + \sum_{ij}^{core} (2g_{iijj} - g_{ijji}) \tag{3.32}$$

and F^c_{mn} are the element of the Fock matrix for an effective 1 active electron operator

$$F^c_{mn} = h_{mn} + \sum_{i}^{core} (2g_{mnii} - g_{miin}) \,. \tag{3.33}$$

A_{mn} and B_{mnop} are elements of the one and two electron density matrix (sum over all the configurations)

$$A_{mn} = \sum_{KL} C_K C_L A^{KL}_{mn} \tag{3.34a}$$

$$B_{mnop} = \sum_{KL} C_K C_L B^{KL}_{mnop} \tag{3.34b}$$

where A^{KL} and B^{KL} are the symbolic matrix elements of the one and two electron density matrix between two configuration K and L. C is the CI coefficient for a given configuration.

The non-redundant parameters of the orbital-rotation are the ones involving orbitals of different subspaces and they are the occupied-active, occupied-virtual and

active-virtual rotations. A Fock operator is defined for each set of non-redundant parameters

$$ {}^{1}F_{qr} = {}^{c}F_{qr} + \sum_{mn} \left[g_{mnqr} - \frac{1}{2} g_{mqnr} \right] A_{mn} \tag{3.35a} $$

$$ {}^{2}F_{qm} = 2 \sum_{n} {}^{c}F_{qn} \boldsymbol{A}_{mn} + 4 \sum_{n,o,p} g_{opqn} B_{mnop} \tag{3.35b} $$

$$ {}^{3}F_{mr} = {}^{1}F_{mr} - {}^{2}F_{mr} \tag{3.35c} $$

where ${}^{1}F_{qr}$ is the Fock matrix element for the occupied-virtual rotation and ${}^{2}F_{qm}$ for the active-virtual rotation. The core-virtual contribution ${}^{3}F_{mr}$ can be constructed as a combination of both. These quantities are needed for the evaluation of the orbitals gradients $\boldsymbol{E}^{K}$ and Hessians $\boldsymbol{E}^{KK}$.

For the optimization of several electronic states at the same time, a State-Average (SA) formalism is employed to obtain a set of MO that provides a balanced description for all states included.[104,105] The former approach of CASSCF presented is also known as state-specific. The state-average energy is defined as followed

$$ E_{SA} = \sum_{I} W_I E_I \tag{3.36} $$

where W_I and E_I are the weight and energy of the individual state I (i.e. eigenstate of the Hamiltonian in the determinant basis). By introducing the state-average ansatz in the full MCSCF parametrized wavefunction and by expanding it into a quadratic function for the evaluation of the energy, the MO are optimized in a balanced way for an arbitrary number of states based on their respective weights. The vector $\boldsymbol{\lambda}$ will contain $I + 1$ parameters where I is the number of CI state included in the state-average.

$$ \boldsymbol{\lambda}_{SA} = \begin{pmatrix} \boldsymbol{c}_1 \\ \vdots \\ \boldsymbol{c}_I \\ \boldsymbol{K} \end{pmatrix} \tag{3.37} $$

The resulting electronic energy, gradient and Hessian in the SA formalism are

given by the following set of equations

$$E_{SA}^{(0)} = \sum_I W_I \langle 0_I | \hat{H} | 0_I \rangle \tag{3.38a}$$

$$\boldsymbol{E}_{SA}^{(1)} = \begin{pmatrix} \boldsymbol{E}_1^C \\ \vdots \\ \boldsymbol{E}_I^C \\ \sum_I W_I \boldsymbol{E}_I^K \end{pmatrix} \tag{3.38b}$$

$$\boldsymbol{E}_{SA}^{(2)} = \begin{pmatrix} \boldsymbol{E}_1^{CC} & 0 & 0 & \boldsymbol{E}_1^{CK} \\ 0 & \ddots & 0 & \vdots \\ 0 & 0 & \boldsymbol{E}_I^{CC} & \boldsymbol{E}_I^{CK} \\ W_1 \boldsymbol{E}_1^{KC} & \dots & W_I \boldsymbol{E}_I^{KC} & \sum_I W_I \boldsymbol{E}_I^{KK} \end{pmatrix} \tag{3.38c}$$

where the subscript I denotes for which electronic state the quantities have been evaluated. The simultaneous optimization of multiple states is reflected in the electronic gradient where only the weighted average of the orbital gradient is set to zero for convergence rather than the individual $\boldsymbol{E}^K$ term. As for optimization with respect to the CI parameters, the electronic states included in the state-average are optimized individually (i.e eigenvector of the electronic Hamiltonian in the CSF basis) and the energy of the state is evaluted by using the eigenvector for a given set of MO.

The CASSCF method and its extensions are suitable for the treatment of static correlation due to the inclusion of multiple configuration state functions for the description of an electronic state. If the active space is built using only the valence orbitals, barely any dynamic correlation is captured with CASSCF as most of dynamic correlation is included by double excitations into the virtual orbitals.[88] The inclusion of this correlation can be done by a variational approach by expanding the active space using CASSCF or with the Restricted Active Space Self-Consistent Field (RASSCF)[106,107] where the active space is further divided into three subspaces with different occupation restrictions. Another approach for capturing electronic correlation is by using a perturbative approach such as the Complete Active Space Perturbation Theory second order (CASPT2)[108–110] where

the missing correlation is added as a correction. The consequence of the perturbative approach is that the variational condition is no longer fulfilled and thus, the lower-bound set for the energy is not usable to assess the convergence of perburbative methods.

The advantage of using CASSCF and RASSCF is the availability of analytical gradients and Hessians which allows affordable computations for on-the-fly *ab initio* dynamics.

3.3 Nuclear dynamics

3.3.1 Direct Dynamics variational Multi-Congurational Gaussian method

The methods described here is the variational Multi-Configurational Gaussian (vMCG)[111] and the variant where the PES is calculated on-the-fly using electronic structure methods known as DD-vMCG.[44,112,113] The QuEh method presented in the next section is a variant of DD-vMCG where the basis function evolved on a time-dependent PES (i.e. Ehrenfest PES).[38,56,57]

In this section, the Equations-Of-Motion (EOM) of DD-vMCG are derived starting from the time-dependent Schrödinger equation (TDSE) for the nuclear wavefunction and associated nuclear Hamiltonian $\hat{H}_N$ (see eq. A.14 in appendix).

$$i\frac{\partial}{\partial t}\chi(\boldsymbol{R},t) = \hat{H}_N\chi(\boldsymbol{R},t) \tag{3.39}$$

One approach in the single-set formalism presented previously in chapter 2 is to expand the nuclear wavefunction

$$\chi(\boldsymbol{R},t) = \sum_j \sum_s A_{j,s}(t) g_j(\boldsymbol{R},t)\,|s\rangle \tag{3.40}$$

using a basis set of gaussian functions g_j (referred as GWP) with their respective expansion coefficients $A_{j,s}$. In the single-set formalism, only one set of basis

functions is defined for a manifold of electronic states $|s\rangle$. The multidimensional gaussian functions in matrix notation have the following form:

$$g_j(\boldsymbol{R}, t) = \exp\left(\boldsymbol{R}^T \cdot \boldsymbol{\zeta}_j \cdot \boldsymbol{R} + \boldsymbol{\xi}_j \cdot \boldsymbol{R} + \eta_j\right) \tag{3.41}$$

The complex parameters of the gaussian functions, generally time-dependent,

$$\boldsymbol{\Lambda}_j = \{\boldsymbol{\zeta}_j, \boldsymbol{\xi}_j, \eta\} \tag{3.42}$$

are represented by a square matrix $\boldsymbol{\zeta}_j$ containing the widths of the gaussians, a vector $\boldsymbol{\xi}_j$ which is the linear parameters containing the momentum and coordinate of the centre of the function and a scalar η_j which corresponds to the phase. The TDSE is solved using the ansatz provided in eq. 3.40 and the Dirac-Frenkel variational principle[114,115]

$$\left\langle \delta\chi \middle| H - i\frac{\partial}{\partial t} \middle| \chi \right\rangle = 0 \tag{3.43}$$

to guarantee a variationally optimal time evolution of the approximate nuclear wavefunction. This yields the EOM for the expansion coefficients in the following form:

$$i\dot{\boldsymbol{A}}_s = (\boldsymbol{S})^{-1}\left[\left(\boldsymbol{H}^{(ss)} - i\boldsymbol{\tau}\right)\boldsymbol{A}_s + \sum_{s'\neq s} \boldsymbol{H}^{(ss')}\boldsymbol{A}_{s'}\right] \tag{3.44}$$

where $\boldsymbol{S}$ is the overlap matrix with the elements

$$S_{jl} = \langle g_j | g_l \rangle\,, \tag{3.45}$$

$\boldsymbol{H}$ is the nuclear Hamiltonian matrix with the elements

$$H_{jl}^{(ss')} = \left\langle g_j, s \middle| \hat{H}_N \middle| g_l, s' \right\rangle \tag{3.46}$$

with $\hat{H}_N$ being the nuclear Hamiltonian operator (see eq. A.14 in appendix) and $\boldsymbol{\tau}$ is the overlap time-derivative matrix where the diagonal elements are zero to keep the gaussian normalised during the propagation and the off-diagonal element are obtained using the chain rule,

$$\tau_{jl} = \langle g_j | \dot{g}_l \rangle = \sum_\alpha \left\langle g_j \middle| \frac{\partial g_l}{\partial \lambda_{l\alpha}} \dot{\lambda}_{l\alpha} \right\rangle. \tag{3.47}$$

The gaussian parameters evolve in time according to the following EOM (in compact matrix form):

$$i\dot{\boldsymbol{\Lambda}} = [\boldsymbol{C}]^{-1}\boldsymbol{Y}. \tag{3.48}$$

The matrix $\boldsymbol{C}$ and the vector $\boldsymbol{Y}$ are expanded:

$$C_{j\alpha,l\beta} = \sum_{s} \left(\rho_{jl}^{(ss)}\right) \left(S_{jl}^{(\alpha\beta)} - \left[\boldsymbol{S}^{\alpha 0)} \left(\boldsymbol{S}\right)^{-1} \boldsymbol{S}^{(0\beta)}\right]_{jl}\right) \tag{3.49a}$$

$$Y_{j\alpha} = \sum_{s,s'} \sum_{l} \rho_{jl}^{(ss')} \left(H_{jl}^{(ss',\alpha 0)} - \left[\boldsymbol{S}^{(\alpha 0)} \left(\boldsymbol{S}\right)^{-1} \boldsymbol{H}^{(ss')}\right]_{jl}\right), \tag{3.49b}$$

where ρ is the density matrix with the elements,

$$\rho_{jl}^{(ss')} = \left(A_{j,s}\right)^{*} A_{l,s'}, \tag{3.50}$$

and various derivatives of the overlap and Hamiltonian matrix,

$$S_{jl}^{(\alpha\beta)} = \left\langle \frac{\partial g_j}{\partial \lambda_{j\alpha}} \middle| \frac{\partial g_l}{\partial \lambda_{l\beta}} \right\rangle \tag{3.51a}$$

$$S_{jl}^{(\alpha 0)} = \left\langle \frac{\partial g_j}{\partial \lambda_{j\alpha}} \middle| g_l \right\rangle \tag{3.51b}$$

$$H_{jl}^{(ss',\alpha 0)} = \left\langle \frac{\partial g_j}{\partial \lambda_{j\alpha}} \middle| H^{ss'} \middle| g_l \right\rangle. \tag{3.51c}$$

The nuclear Hamiltonian in the GWP basis in DD-vMCG is expanded using a Local Harmonic Approximation (LHA) around the centre q_j of each GWP g_j

$$V_j^{(s)}(\boldsymbol{R}) = V_{j0}^{(s)} + \sum_{\kappa} V_{j,\kappa}^{(s)'}(R_\kappa - q_{j\kappa}) + \frac{1}{2}\sum_{\kappa\mu} V_{j,\kappa\mu}^{(s)''}(R_\kappa - q_{j\kappa})(R_\mu - q_{j\mu}) \tag{3.52}$$

where the derivatives are evaluated at the GWP centres. In the DD-vMCG algorithm, the electronic structure method has to provide the energy V_{0j}, the gradient $V_{j,\kappa}^{'}$ in each nuclear degree of freedom κ and the Hessian $V_{j,\kappa\mu}^{''}$ in each nuclear degree of freedom κ and μ. The LHA expansion is done for every electronic state s. Alternatively, the information on the PES can be retrieved from a database containing previous electronic structure evaluations. The DD-vMCG method performs dynamics on diabatic surfaces, built from the adiabatic PES using a diabatisation scheme due to the mathematical simplicity and smoothness of the diabatic PES.

In this method, the main computational effort is on the evaluation of the PES in the LHA expansion at each centre of GWP and the integration of the EOM. For a small number of basis functions, most of the computational time is on the electronic structure calculations which can be replaced by a data reading from a database. However, a simulation with a large database has additional memory requirement in order to save all the larges arrays such as gradients and Hessians.

3.3.2 Quantum-Ehrenfest method

Starting from the single-set DD-vMCG ansatz (see eq. 3.40), the set of electronic states $|s\rangle$ is contracted on a single weighted-average PES, the Ehrenfest PES.[38,56,57] The individual weights of each electronic state are time-dependent and thus, the single PES becomes time-dependent.

The evaluation of the relevant quantities for the propagation of the nuclear wavefunction simplifies due to having only a single time-dependent electronic state. The electronic wavefunction is propagated within the electronic structure method to make use of the ability of evaluating the energy and derivatives of an Ehrenfest state in the CASSCF algorithm of GAUSSIAN.

Within the time dependent section of CASSCF algorithm implemented in a development version of GAUSSIAN, the electronic wavefunction ψ is expanded in a basis set of orthonormal time-independent electronic functions ψ_s for a given nuclear geometry $\boldsymbol{R}$.

$$\psi(\boldsymbol{r}, t; \boldsymbol{R}) = \sum_s c_s(t)\psi_s(\boldsymbol{r}; \boldsymbol{R}) \tag{3.53}$$

The EOM for the nuclear wavefunction (in the diabatic representation) is similar to DD-vMCG without the coupling between different electronic states s and s'. Then, the matrix elements of the nuclear Hamiltonian are written as follows

$$H_{ij}^N = \langle g_i|\hat{T}_N|g_j\rangle + \langle g_i|\hat{V}|g_j\rangle \tag{3.54}$$

where $\hat{V}$ is the potential energy operator. The Ehrenfest PES V_{ii} is evaluated at

the center of each GWP and then expanded using a LHA for couplings between different GWP

$$V_{ii} = \sum_{st} c_s^* H_{el}^{ss'} c_{s'}. \tag{3.55}$$

The EOM for the electronic state coefficient is

$$i\dot{c}_s(t) = \sum_{s'} H_{el}^{ss'} c_{s'}(t). \tag{3.56}$$

In QuEh, the electronic EOM are solved with a CAS-CI approach in a development version of GAUSSIAN. From the nuclear dynamics driver, only one time-dependent electronic state is considered for each GWP. Thus, the computational cost for the propagation of the nuclear wavefunction is reduced but at the cost of a more complicated evaluation of the PES from the electronic structure method.

3.3.3 Initial Conditions and Protocols

In QuEh, the initial conditions are defined in two separate ways for both the electronic and nuclear wavefunction. The electronic wavepacket is defined in the input of the electronic structure program and can be defined in three ways. The first one is a combination of two diabatic states represented by vector in a 3-D space (i.e. Bloch sphere) where the in-plane angle θ determines the weight of the two states and the rotation of the plane defined by the angle ϕ corresponds to the phase between the states (see Fig. 3.1).[116] The second way is by defining a linear combination of diabatic states using normalized coefficients for each state. The final option is by entering an arbitrary CSF vector that can be projected as a linear of combination of adiabatic states spawned by the number of CSF defined by the active space size.

The initial nuclear wavepacket centered at the initial geometry is represented as a linear combination of N GWP distributed in phase space with a momentum distribution, i.e. they have the same initial geometry but different velocity for

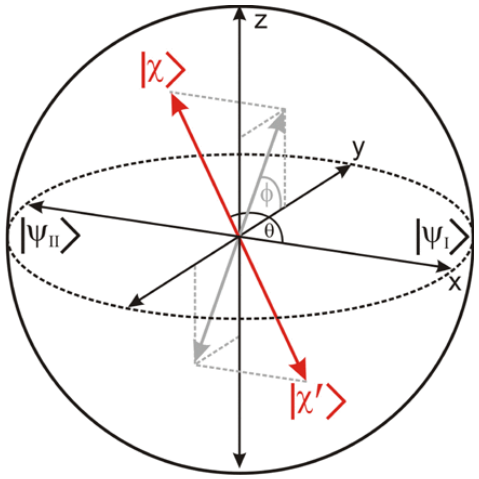

Fig. 3.1: Representation of the superposition of two orthogonal electronic diabatic states $|\Psi_I\rangle$ and $|\Psi_{II}\rangle$ as vector on the Bloch sphere. The mixing angle is represented by θ and the phase between state is defined ϕ. Reproduced with permission under Creative Commons CC-BY from ref. 116.

the centre of the GWP. We also use a narrower width than the actual ground vibrational eigenstate of a harmonic oscillator for the GWP to avoid numerical problems for the integration in region of turning points in electron dynamics.

For the purpose of nonadiabatic dynamics with a method such as QuEh where the electronic wavefunction is defined as a linear combination of configurations, a rotation in the orbital space (even within active-active) is undesirable and thus, using a CAS-CI algorithm will prevent that situation from occuring. The lack of information on individual adiabatic/diabatic states from the electronic structure program prevents the use of the database in the DD-vMCG algorithm for the QuEh method. For both of these reasons, a very small time step has to be adopted for the dynamics to ensure optimal relaxation of the orbitals between each steps and consistency in the electron dynamics. The orbital guesses are projected and renormalized at each step to adjust for the small change in geometry. Furthermore, the small step size and non-full optimization of the MO ensure that the (quasi-)diabatic electronic basis remains fairly unchanged throughout the dynamics.

3.4 Data Analysis

In dynamics simulations with a trajectory approach, the averaged quantities are computed by summing over the contribution of the individual trajectories (i.e. weight). In DD-vMCG, the GWP basis possess a localized nature around their centres and follow quantum trajectories. Due to the non-orthogonality of the set of basis functions, the actual weight of the GWP cannot be defined just by the gaussian populations GP

$$GP_i^{(s)}(t) = \left| A_i^{(s)}(t) \right|^2 \tag{3.57}$$

as the GWP overlap matrix $\boldsymbol{S}$ (see eq. 3.45) contains non-zero off-diagonal elements and thus, by using the vMCG ansatz for the wavefunction (see eq. 3.40), the normalization condition for the nuclear can be written as

$$\sum_{ij} \sum_{s} S_{ij}(t)^{(s)} A_j^{(s)*}(t) A_i^{(s)}(t) = 1. \tag{3.58}$$

An approach to evaluate the effective weights of the individual GWP is by using a method similar to the Mulliken formalism for the analysis of orbital populations.[117] By applying this to the DD-vMCG method, the weight is then defined by the Gross Gaussian Populations (GGP)[45,118,119] given by the following equation

$$\mathrm{GGP}_i^{(s)}(t) = \mathrm{Re}\left\{ \sum_j S_{ij}^{(s)}(t) A_j^{(s)*}(t) A_i^{(s)}(t) \right\}. \tag{3.59}$$

where the population value accounts properly for the non-zero overlap between basis functions. A direct consequence of the normalization condition is that the sum over the imaginary terms yields zero and thus, the GGP can be calculated directly by taking the real part of the product.

The expectation values for quantities such as the nuclear geometries, electronic populations are approximated in the first instance as a weighted summation over the individual quantum trajectories using the GGP values.

$$\langle o(t) \rangle \approx \sum_i \sum_s \mathrm{GGP}_i^{(s)}(t) o_i^{(s)}(t) \tag{3.60}$$

In QUANTICS, the nuclear degrees of freedom are defined using a set of vibrational coordinates, called Normal Mode displacement (NM), as an orthogonal basis. The coordinates Q employed for the dynamics correspond to a mass-frequency scaled NM displacement coordinate with respect to an initial reference geometry.[120,121] The conversion between cartesian coordinate displacement (with respect to the reference geometry) $\boldsymbol{r}_\alpha$ and the NM displacement Q_i is given by eq. 3.61 below. A matrix $\boldsymbol{K}$ containing the NM i, expressed in mass-weighted coordinates α, is required as input to transform the cartesian coordinates into NM coordinates which have been obtained from a frequency calculation. The coordinate Q_i is then obtained by scaling it with the mass M_α of the atom of coordinate α and the frequency ω_i of NM i. From the mathematical expression and by taking standard quantum chemistry atomic unit, we can see that the NM unit is a mass and frequency scaled atomic unit.

$$Q_i = \sqrt{\frac{\omega_i}{\hbar}} \sum_\alpha K_{\alpha i} \sqrt{M_\alpha} \boldsymbol{r}_\alpha \tag{3.61}$$

For the data analysis, it is convenient to employ the set of NM as basis for representing the overall change in geometry of the system. Furthermore, the individual degrees of freedom can be assigned an irreducible representation when the molecule has a symmetry point group higher than C_1. For systems with high symmetry, the resulting dynamics can then be explained using group theory to rationalize the observed behaviour.

The electronic wavefunction can be represented using various approaches. In DD-vMCG, the electronic degree of freedom is defined by a single particle function which contains the diabatic state vector. In QuEh, the QUANTICS program does not possess any information related to the electronic state as it only sees an effective time-dependent PES. The electronic wavepacket composition is defined in GAUSSIAN and is stored as a vector of configuration's (complex) coefficients

which can be projected onto a set of adiabatic/diabatic states. A set of reference diabatic states or pseudo diabatic states can be defined using a specific combination of CSF to monitor the electron dynamics. An alternative method is to compute the spin density for systems with unpaired electrons. In the development version of GAUSSIAN, a procedure implemented by Polyak et al.[122] allows us to retrieve the spin density in the context of a CI type calculation using CSF that are S^2 eigenfunctions. The spin density for a given total spin value is

$$\rho^S(r) = \frac{M}{S(S+1)} \sum_{i,j}^{N} \phi_i^*(r)\phi_j(r) \left(\left(2 + n - \frac{N}{2} \right) \langle \Psi | \hat{E}_{ij} | \Psi \rangle - \sum_k \langle \Psi | \hat{E}_{ik}\hat{E}_{kj} | \Psi \rangle \right) \tag{3.62}$$

where S is the spin, M the spin projection, n the number of spin-orbitals, N the number of electrons, $\hat{E}_{ij}$ the one electron excitation operator, ϕ the spin-orbital and Ψ an arbitrary molecular wavefunction. The two last terms correspond to the one- and two-electron density matrix. Thus, the spin operator is defined as

$$Q = \frac{M}{S(S+1)} \left(\left(2 - \frac{N}{2} \right) R_1 - 2Sp_2 R'_{12} \right) \tag{3.63}$$

where R_1 is the one-electron density matrix, R_{12} the two-electron density matrix (the prime denote the transposition in the second pair of coordinate) and Sp_2 defines the reduction with respect to the second electron coordinate. The density matrices are quantities that are computed in most of the electronic structure methods and using a Mulliken formalism[117] to account for the non-orthogonality of the spin-orbital basis, the spin density can be partitioned (by atom for example) to follow electron dynamics.

3.5 Summary

This chapter highlights the main methods and relevant equations to understand the nature of the electron and nuclear dynamics simulated. The electronic structure is treated using a multiconfiguration approach with CASSCF/CAS-CI to obtain a

balanced treatment of excited states with diverse nature. The orbital optimization in CAS-CI allows us to keep a set of pratically unchanged orbitals to define a reference quasi-diabatic state in a unambiguous way.

The nuclear dynamics is treated within the framework of DD-vMCG where the nuclear wavefunction feel the effect of a single time-dependent Ehrenfest PES. Some approximations are made as a result for the overall definition of the molecular wavefunction starting from the exact factorization. The Ehrenfest PES are only defined properly locally within the centre of the GWP and a LHA expansion is done with frozen parameters. The QuEh method expands the nuclear wavefunction as a linear combination of frozen width GWP with a local definition of the electronic wavefunction. To ensure stability in the dynamics and account for the nature of the fast electron dynamics, a small time step is required and a quantum chemistry evaluation at fixed time step ensure a balanced treatment for the electronic wavefunction of each GWP.

The basis function dynamics in DD-vMCG and QuEh can be seen as individual GWP following quantum trajectories and each trajectory is assigned time-dependent coefficients which can be used to extract the GGP. The GGP corresponds to the weight of the individual basis function and it accounts for the non-orthogonal nature of the GWP. So the expectation values such as the geometry, adiabatic/diabatic electronic population, spin density can be approximated as a weighted sum over the GWP.

Chapter 4

Development

4.1 Introduction

The Direct Dynamics variational Multi-Configurational Gaussian (DD-vMCG) and Quantum-Ehrenfest (QuEh) methods introduced in chapter 3 are implemented in the QUANTICS program.[123] However, due to the expensive cost of the computations, only small organic systems can be studied within a reasonable time frame. Both methods require information on the Potential Energy Surfaces (PES) computed by an external quantum chemistry program which is the main limiting step in the computational effort for a single iteration in the propagation of the nuclear wavepacket. From a practical approach, QuEh and DD-vMCG are implemented within the same portion of the code in QUANTICS and the former method is just a particular case of the latter where the electronic structure provides information about one single effective time-dependent PES rather than the full set of adiabatic states employed in DD-vMCG.

Multiple developments has been implemented to improve the speed of these methods such as parallelizing the interface to external programs and storing calculated points of the PES in a database to circumvent the call to an expensive computation. QUANTICS v1.3 currently has an Open Multi-Processing interface (OpenMP) for the DD-vMCG and QuEh method and the database has been implemented via the use of flat binary file containing the information required to

build the PES. There are multiple restrictions on the current code such as database readings and writings on a single computer node using shared memory protocols.

In this chapter, works toward further optimizing the code are presented. An extra layer of parallelization using the Message Passing Interface (MPI) is added to the existing OpenMP section of the DD-vMCG code. To reduce the impact of single processor access to data in the section involving the database, an interface employing Server Query Language (SQL) is written for a more optimal handling of the database. These projects were conducted from 2020 to 2021 in collaboration with Dr. Simon J. Clifford and Dr. Christopher Cave-Ayland from the Research Software Engineer team at Imperial College London.

In the DD-vMCG method, the effect of an external pulse can be included by defining a specific operator in the Hamiltonian section of the input file in QUANTICS. Such an approach cannot be employed for the QuEh method due to the nature of the time-dependent PES and the lack of information of individual adiabatic/diabatic states. To solve this problem, an implementation of the pulse incorporated directly within the electronic structure method is presented in the last section of this chapter. The last part of this work is done in the development version of GAUSSIAN within the Complete Active Space Self-Consistent Field (CASSCF) code. The work in this last section has been published by Tran et al.[124] in the Journal of Chemical Physics 2020 (Vol. 153).

4.2 Parallelization with Message Passing Interface

4.2.1 Overview of the DD-vMCG algorithm

In DD-vMCG, due to the coupled motion of the nuclear basis functions and the evaluation of the PES, a single iteration in the dynamics loop can be rather expensive. Running a program on parallel architecture allows one to reduce the

total time of computation at the cost of using more ressources (i.e. processors). To build a parallel code, either an interface with shared memory system such as OpenMP or a distributed memory system with MPI is employed to make use of the multi-threading capability of the hardware.[125–128]

The advantage of using a shared memory architecture parallelization is that the individual threads execute the instructions without any interaction between processes thanks to the shared access to the memory. Thus, it yields a parallel environment with little overhead which is only limited by the memory bandwidth.[127]

Parallelization for nonadiabatic methods with independent trajectories such as surface hopping[49] is straightforward and efficient as they display a linear scaling for the cost of computation with respect to the number of basis functions (i.e. trajectories) as well as independent computation for each individual trajectory. Whereas DD-vMCG with the coupled nature of the GWP, the cost of computation for the propagation of the nuclear wavepacket shows a non-linear scaling with respect to the number of GWP and thus, there is part of the algorithm that cannot be parallelized in a simple way with respect to the number of GWP. An efficient parallelization can be achieved for DD-vMCG in case where the main limiting step is the evaluation of the PES.

The structure of the QUANTICS program is given in Fig. B.1 in Appendix B. In the DD-vMCG algorithm, the main two limiting steps are the evaluation of the matrix elements in the basis of the Gaussian Wavepackets (GWP) using a Local Harmonic Approximation (LHA) expansion around the centre of each GWP and the integration of the Equations-Of-Motion (EOM). Due to the coupled nature of the motion of the basis functions, only a few sections of the code are currently written in a parallelizeable way using a OpenMP/MPI layer.

There is already an existing layer of parallelization using OpenMP or MPI in the QUANTICS program for Multi Configuration Time Dependent Hartree

(MCTDH) calculations and for the relevant section of DD-vMCG, there is an OpenMP parallelization for the evaluation of the PES and handling of the database. The advantage of using an OpenMP approach is the straightforwardness of the implementation around a parallelizeable loop (i.e. independent calculation for each index of the loop). The work presented in this section involves adding an extra layer of MPI on top of the existing OpenMP to allow a parallel execution of the program on multiple nodes.

In the OpenMP section of DD-vMCG code, the parallelization is done over the call to the external program for the evaluation of the PES up to second order (adiabatic energy, first and second derivatives) and their values in the diabatic representation in the getddpes subroutine. The full algorithm of the routine can be found in Algorithm 1 in Appendix A. At the end of the direct dynamics section, these values are written in the database and that section is handle by a single processor.

The main consideration is properly defining the global and local variables. The communication between OpenMP 'processes' relies on a shared memory and thus, it is straightforward to handle the evaluation of array elements such as the matrix element of the Hamiltonian in the basis of the GWP. However, the biggest drawback of OpenMP is that it restricts the program's execution to a single hardware with shared memory (i.e. single computing rack/node in a cluster). Parallelization across multiple hardwares requires a different protocol due to the lack of shared memory.

4.2.2 Basic principle/structure of MPI

A parallelization with MPI relies on message/communication to circumvent the lack of a shared memory system and thus, this interface is suitable for parallelization of the code on distributed memory system such as internode multi-threadings where only processors on the same node has a physical shared memory. The dis-

advantage of the use of MPI is the increase in overhead compared to the OpenMP parallelization since now, there is a need to synchronize and allow communications between processes.

A program compiled with the MPI library can be run using the mpirun/mpiexec executable to run multiple time the same program on different logical processor unit in hardware with parallel computing architecture. The interface allows the parallel execution of the program to interact with each other through message passing (i.e. communication) without the need of a shared memory.

To ensure compability of the QUANTICS program for serial or OpenMP run only (i.e. compilation without the MPI library), Fortran preprocessor directives are employed to isolate the MPI sections of the code. These directives start with a # character and by writing the code within a "#ifdef MPI" and "#endif" statement will allow the compiler to ignore these section in case the parallel interface is not used.

The protocol employed by MPI for the interaction between parallel processes is through messages in a communicator (MPI_COMM_WORLD) where the individual processes are assigned an unique mpirank, starting from 0 for the first one.

All parallel processes will run the program exactly the same way initially. One way of separating the processes into a main one and multiple sub-unit is by using an if condition with the value of the mpirank. In QUANTICS this is done during the initialization part of the execution of the DD-vMCG algorithm and the processes with a rank above 0 are sent into the mpipropmod subroutine and wait for a communication from the main unit (see Fig. 4.2).

For the current development project, the main goal is to speed-up the DD-vMCG code for the call to the external quantum chemistry program. The communication in the parallel region is achieved through the use of four MPI routines

which are MPI_Barrier(), MPI_Bcast(), MPI_Scatter() and MPI_Gatherv(). A visual representation of their task is shown in Fig. 4.1. A more detailed description of the routines is given in Appendix B.2

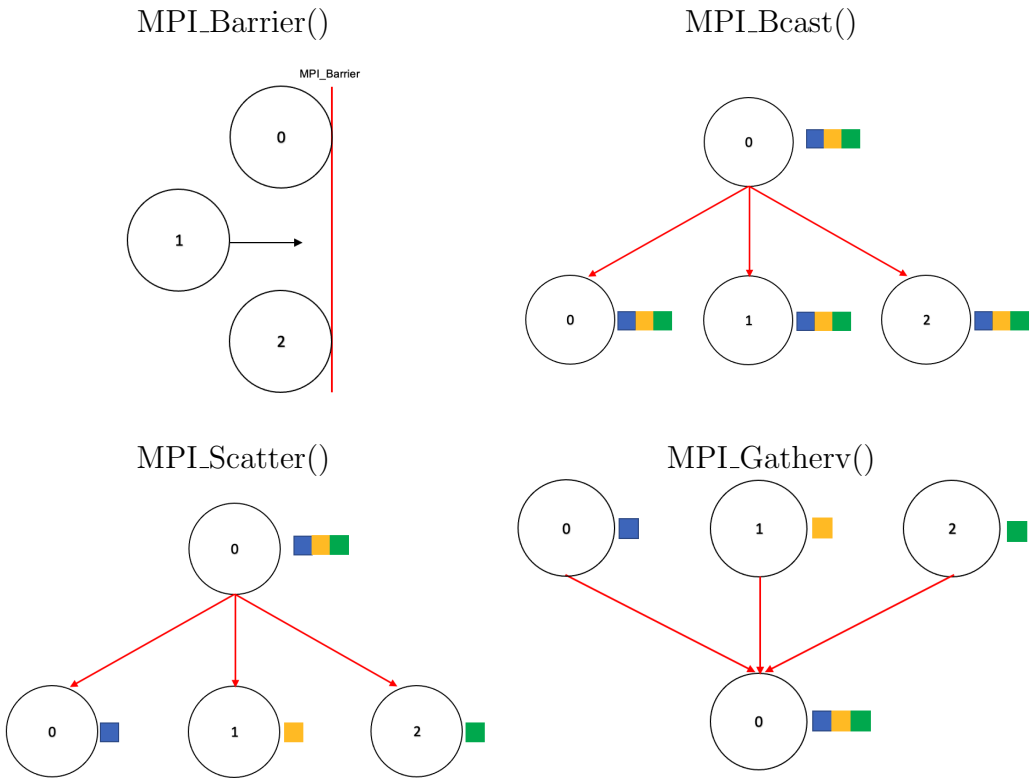

Fig. 4.1: A visual representation of the effect of the main MPI routine employed in the parallelization of DD-vMCG. The number corresponds to the mpirank of the process in the communicator and the squares represent data in an array.

4.2.3 MPI algorithm

To design the algorithm for the DD-vMCG method that can be run in parallel, first there is a need to isolate a part of the code that can be run independently for each computing unit. Furthermore, another restriction is to minimize the need of reshuffling the code or making parallel adapted version of some subroutine.

For the main subroutine tasked with evaluation of the PES, a parallel adapted version of it is written by isolating the OpenMP section of the subroutine getddpes presented in the Algorithm 1 which are copied and transferred into a new

Table 4.1: Input variable needed by the DD-vMCG code within the OpenMP section.

name	type	description
totdim1	Int	Number of basis functions
ndofddpes	Int	Number of degrees of freedom
nddstate	Int	Number of electronic states
nsymop	Int	Number of replica (use in symmetry)
ddlaenge	Int	Length of the ddname string
dbdlength	Int	Length of the DB path string
nroot	Int	Number of root in CAS calculation
maxdim	Int	Maximum number of degrees of freedom
qcsubform	Int	Number of arguments to be taken by external program
nbasis	Int	Number of basis function for the MO
maxhpar	Int	Maximum number of parameters used in the Hamiltonian
maxhop	Int	Maximum number of primitive operators
lhaorder	Int	Order for the expansion around the center of GWP
dddiab	Int	Diabatization scheme
time	DP	Time
dde0	DP	Reference energy (the zero value)
lpestest	Bool	Flag for testing the directdyn section
lupdhes	Bool	Flag for Hessian update
ldbsave	Bool	Flag for saving values in database
lddrddb	Bool	Flag for reading the values in database
lqcsaveall	Bool	Flag for concatenating quantum chemistry output file
ddextcmd	Char(64)	Command for executing the external program
fchkcmd	Char(64)	Command for formatting the chk file of Gaussian
ddname	Char(240)	Path to the direct dynamics directory

Int = Integer
DP = Float Double Precision
Bool = Boolean
Char = Character (with number of characters in parenthesis)

subroutine named mpigetddpes. The argument required for that MPI adapted subroutine is reduced to a minimum by using some variable defined in the initialization section (i.e. global variable with fixed value). Inside the mpigetddpes section, the OpenMP layer is still present and thus, a hybrid parallelization using both interfaces are possible.

The parallel algorithm for the DD-vMCG is shown schematically in Fig 4.2, 4.3, and 4.4. The optimization of the parallel computing is done by minimising the amount of communication between the processes and the amount of data

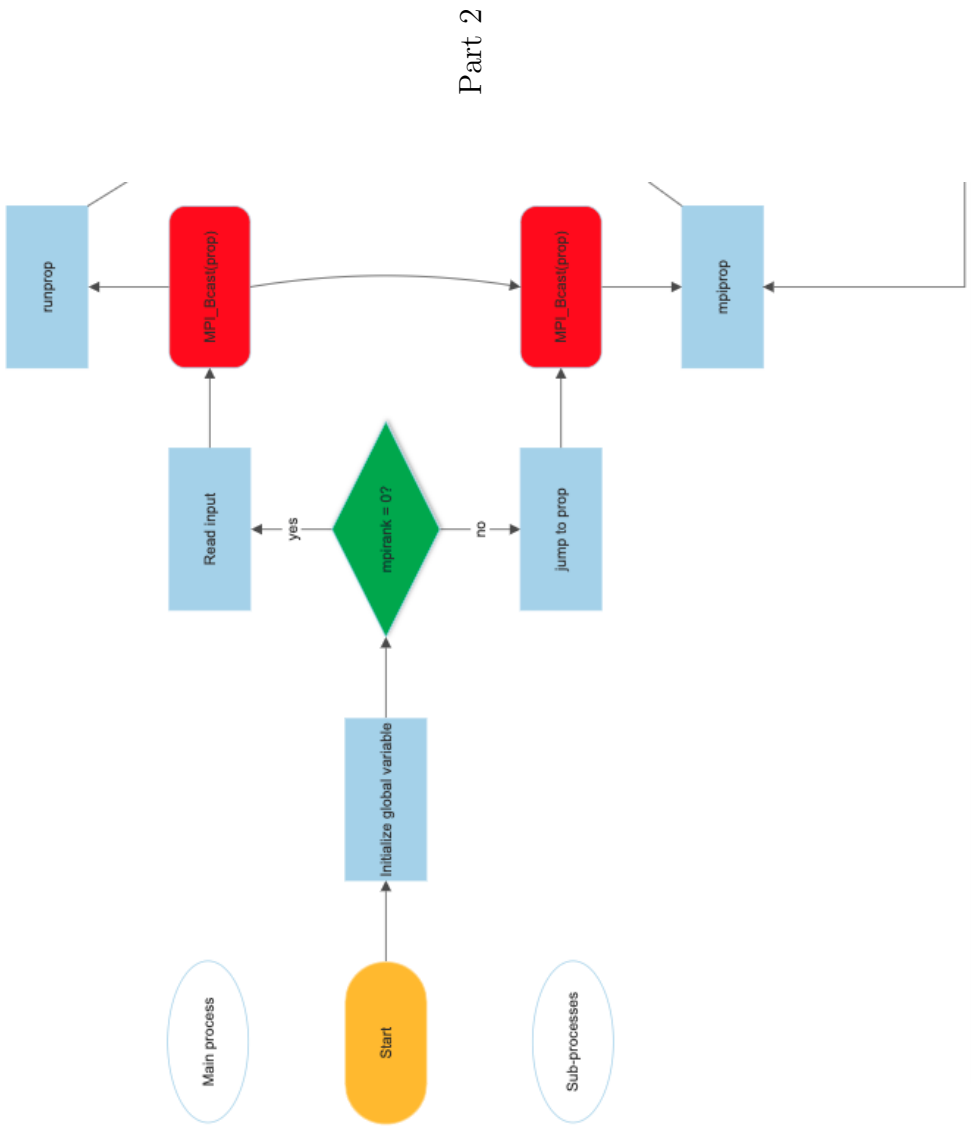

Fig. 4.2: Algorithm for the MPI implementation in DD-vMCG (part 1: Initialization)

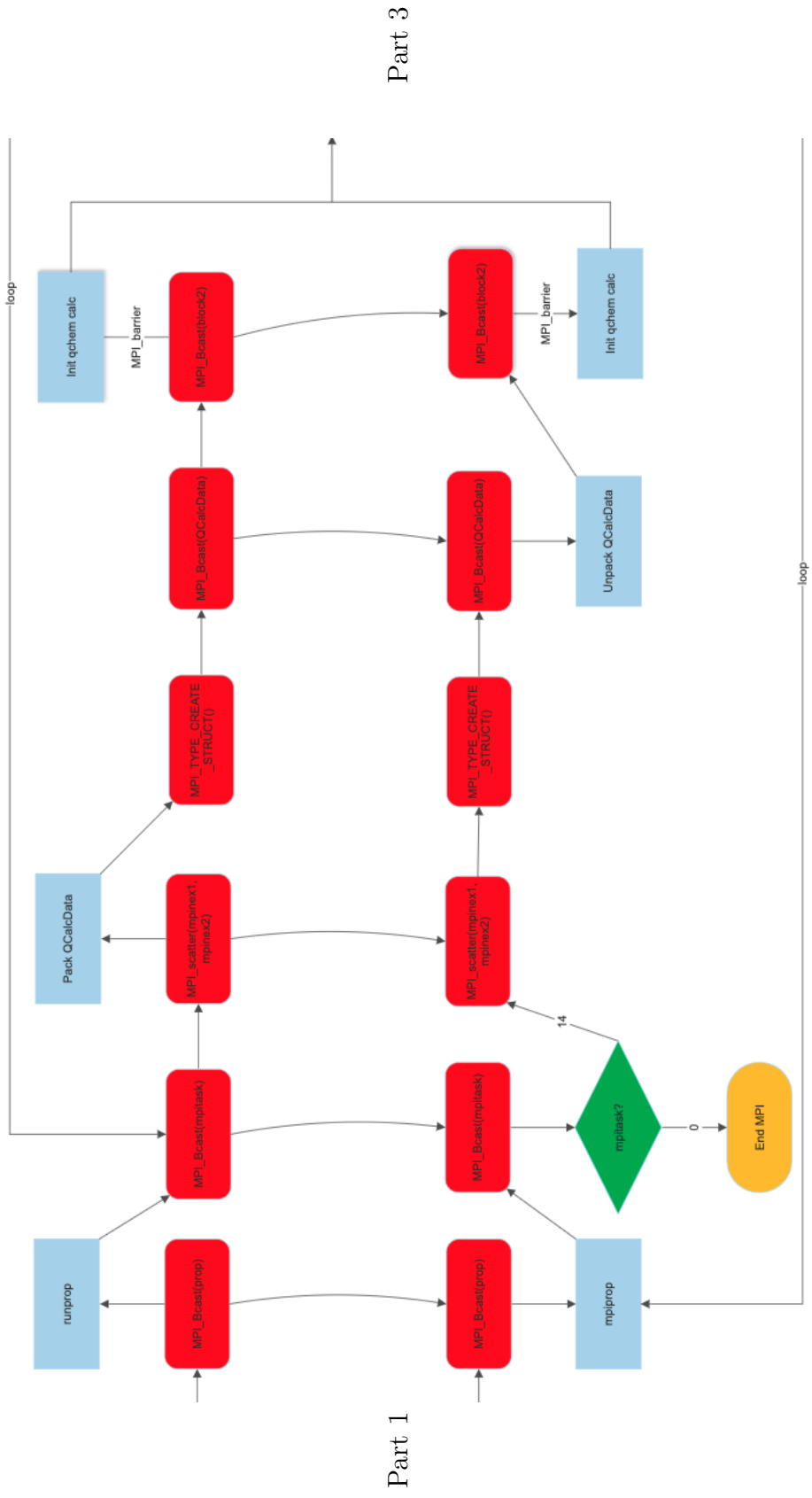

Fig. 4.3: Algorithm for the MPI implementation in DD-vMCG (part 2: Propagation and MPI setup)

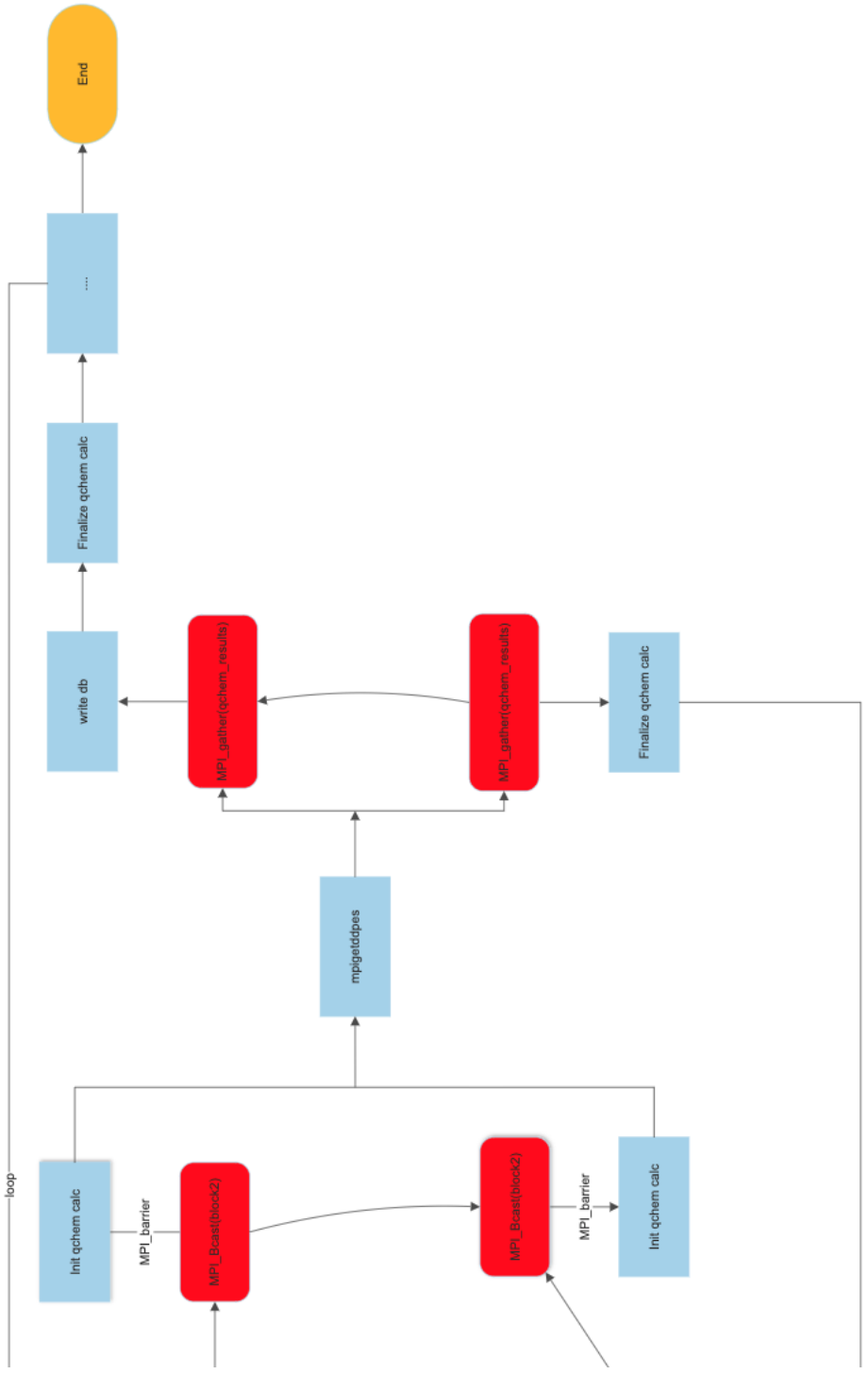

Fig. 4.4: Algorithm for the MPI implementation in DD-vMCG (part 3: Loop and end)

Table 4.2: Input arrays of variable needed by the DD-vMCG code within the OpenMP section for a single GWP.

name	size	description
eex2[a]	ngp	Mapping of required calculation and GWP
idbloc[a]	nsymop,ngp	List of data to be read in database
hopipar[a]	maxhpar,maxhop	Options for evaluating the Hamiltonian
r1[b]	dbnrec,totdim1	Coordinates of points in database
xgp[b]	ndd,nsymop,totdim1	Coordinates of the basis functions
atnam[c]	natm,c1	List of atom label

[a] = Integer
[b] = Float Double Precision
[c] = Character
c1 = string with 16 characters length (global QUANTICS variable)
dbnrec = number of record in the database
natm = number of atoms
ndd = nddofdddpes = number of degrees of freedom
ngp = number of basis function (equal to totdim1 in most cases)

communicated. Thus, the parallel execution of the program will only communicate at two blocks. The first set of communications will consist of the main process sending all the required information to be able to write the input to the external electronic structure program and run it. The second block of communication happens once all the electronic structure calculation for the current iteration has been run (either successfully or failed which will require an interpolation through the database).

The task of the mpigetddpes routine is to evaluate the PES around the center of each GWP through a call to the lhaqchem subroutine which contains the interface to various electronic structure program. The MPI adapted routine will then diabatize the adiabatic energies, first and second derivatives returned from the lhaqchem subroutine. The use of the global diabatization requires special attention due to the use of the database in this method (see section on SQL). In the case of a run using the Hessian update algorithm for the evaluation of the second derivatives, the procedure is done at the end of mpigetddpes.

Before all the processes can run the central subroutine, there are three impor-

Table 4.3: Output variables produced by the DD-vMCG code within the OpenMP section. The size is given for each dimensions separated by a comma. The last dimension which corresponds to the number of electronic calculation is not specified explicitly.

name	size	description
adv[a]	ndd, ndd, nsym	Adiabatic energies
adder1[a]	ndd, ndd, ndof, nsym	Adiabatic first derivative
adder2[a]	ndd, ndd, ndof, ndof	Adiabatic second derivative
addip[a]	ndd, ndd, 3	Adiabatic dipole
ddv[a]	ndd, ndd, nsym	Diabatic energies
ddder1[a]	ndd, ndd, ndof, nsym	Diabatic first derivative
ddder2[a]	ndd, ndd, ndof, ndof, nsym	Diabatic second derivative
dddip	ndd, ndd, 3	Diabatic dipole
nac[a]	ndd*(ndd-1)/2, ndof, nsym	nonadiabatic coupling
soc[a]	ndd*(ndd-1)/2	Spin-orbit couplings
moco[b]	nbasis, nbasis	Molecular Orbitals

[a] = Float Double Precision
[b] = Float Single Precision
ndd = nddstate = number of electronic states
ndof = ndofddpes = number of degrees of freedom
nsym = nsymop = number of replica

tant sets of information that need to be known on all parallel computing units. The first one is the number of quantum chemistry calculation required for the current iteration. The second set of data needed is all the relevant input to be able run the mpigetddpes routine and the last part is the output array to store all the results which will be subsequently written in a database by the main process.

For the first requirement, the main process stores the number of calculations required in the variable nex2 and its mapping with the correct basis function in eex2. To make full use of the parallel capability, the number of electronic calculations should be spread as much as possible among all the processes using the arrays mpinex1 and mpinex2 that contain the starting and the final point, respectively. The MPI_Scatter routine is employed to distribute the number of quantum chemistry evaluations and to make the arrays straightforward to send with that routine (with size of mpinex1 and mpinex2 being the number of parallel processes). A smaller communicator is initiated in order to exclude process that

doesn't have any electronic calculation to perform. This reduces the number of communications required at each MPI routine employed.

For the second part, the input for that section of the code are given in Table 4.1 and 4.2 and thus, a communication between the main and sub-processes is required before the call to mpigetddpes to obtain all the relevant quantities. Due to the large number of variables required as "input" to run the parallel section, multiple broadcasts are needed to be able to transfer all the values of the relevant variables to the sub-processes. To optimize that section and make the code clearer, a data structure (QCalcData) is employed for the variables in Table 4.1. The data structures are also known under the name of structured types or derived types. The advantage of that approach is that only one communication is needed to send the whole data structure to other processes. Furthermore, data structures can be used through MPI which possess their own set of routine for dealing with it. The array of variables required in the direct dynamics section need to be transfered over a subsequent communication due to the need of knowing the size of the array to allocate it beforehand. However, the value of these variable such as totdim1, ngp, etc. are not known in the sub-processes. Thus, the structure needs to be sent first and the global variables needed for direct dynamics are assigned the correct value by unpacking the data structure.

To simplify the definition of the data structure QCalcData as well as avoid the need of sending the information needed to create it, the data structure is declared generally (as a global 'variable', see Fig. 4.5) with a fixed size and number of variables so that the information is consistent between each processes using the data structure. The variable in the structure are accessed using the % symbol (eg. struct%variable1 = value1).

Upon creation of the data structure, it will occupy a block in the memory (i.e. without getting split) and thus, the variable can be accessed directly in

```
integer(long), parameter :: DATA_N_TYPES=4,&
  DATA_N_INTS=19,DATA_N_REALS=2,DATA_N_LOGICALS=4,&
  DATA_N_CHARS_C3=2,DATA_N_CHARS_C5=1
type :: QCalcData
  integer(long) :: totdim1,s1,hl,ngp,mxmpi,ndofddpes,&
    nddstate,nsymop,dbnrec,ddlaenge,dbdlength,nroot,&
    maxdim,qcsubform,nbasis,maxhpar,maxhop,lhaorder,&
    dddiab
  real(dop) :: time,dde0
  logical(kind=4) :: lpestest,lupdhes,ldbsave,lddrddb,&
    lqcsaveall
  character(len=c3) :: ddextcmd, fchkcmd
  character(len=c5) :: ddname
end type QCalcData
```

Fig. 4.5: Definition of the QCalcData structure and its size given as Integer parameters in the mpistructure.F90 source file in the include directory

a sequential way by knowing the memory address. In the current development version of QUANTICS, the data structure (see top part of Fig. 4.5) consists of 4 types of data, 19 integers, 2 double precision float numbers, 4 booleans and 3 string of characters (2 with size c3 and 1 with size c5). The variable c3 and c5 are among the global variables with fixed value and thus known by all processes as long as the module with the global variables is loaded.

Before the QCalcData can be broadcast between processes, there is a need to create a MPI type of the data structure. This is achieved through the use of two routines which are MPI_TYPE_CREATE_STRUCT and MPI_TYPE_COMMIT. The first routine deals with the layout of the data structure by taking in arguments such as the number of datatypes, arrays containing the length of each datatype, memory address displacements between each block and the variable's type in each block. The output parameter is the MPI_datatype which is used as an argument for MPI_TYPE_COMMIT to commits the datatype and thus, it will make the data structure usable in MPI communications.

In the initialization process before the execution of the mpigetddpes routine,

the main process assigns all the values to the variables in the data structure (i.e. packing of QCalcData) and then both the main and sub-processes create the MPI data structure to allow transfer over MPI communication routine. Once the broadcast of QCalcData by the main unit is finished, the sub-processes unpack the structure and then proceed to allocate all the relevant input arrays necessary for the central routine evaluating the PES. Once the array are initialized and properly allocated, the main process can broadcast all the array listed in Table 4.2 (with the name block2 in Fig. 4.3).

The third part is the allocation of the arrays for the output of the quantum chemistry calculations. The output of the subroutine mpigetddpes are the adiabatic/diabatic energies, first and second derivatives as well as the dipole, Molecular Orbitals (MO), nonadiabatic couplings and spin-orbit couplings (see Table 4.3). To ensure consistency between the parallel process on the output array size and number of arrays, a subroutine init_qchem_calc is written which main task is to allocate all the arrays employed for storing the results from quantum chemistry calculation and their diabatic representation. The other advantage of having that separate small routine is the possibility to easily add new quantities if needed in future development of the code.

Once all the MPI processes have finished the run through the mpigetddpes subroutine, the data are all communicated to the main unit through the MPI_Gatherv. Multiple wrapper functions around the MPI routine are written to handle arrays of arbitrary number of dimensions to be able to send any result arrays in a straightforward way in the second block of communication of the parallel section. The sub-processes are then sent back to the beginning of the mpipromod subroutine to await further instruction from the main process which will execute the rest of the DD-vMCG code for a propagation of the nuclear wavepacket.

Due to the restriction of the serial part of QUANTICS, the main MPI paral-

lelization algorithm evaluates all the relevant quantities through a main process and uses collective communication to let the sub-processes evaluate the matrix elements in the parallel part of the code. Furthermore, any I/O with the database, due to its heavy memory requirement, can only be done on the main process in MPI due to the lack of shared memory.

4.2.4 Speed-up test

To evaluate the efficiency of the MPI parallelization of DD-vMCG, a test case was used to monitor the total computation time (i.e. walltime) based on the number of processors requested for the simulations. The model system used for the test is the ethylene cation and the full computational details as well as the extensive discussion on the results are given in chapter 5.

The simulation on the nonadiabatic dynamics of ethylene has been performed using the QuEh method with a basis of 16 GWP to represent the nuclear wavefunction for the purpose of the test. A momentum distribution has been employed for a set of Normal Mode (NM) defined by a frequency calculation at the neutral ground state structure of ethylene with a B3LYP/6-31G* level of theory. The integrator for the nuclear dynamics is Runge-Kutta 5th order and a time step of 0.01 *fs* is used for a total propagation time of 5 *fs*.

A benchmark of the speed-up with the number of processors employed is reported in Fig. 4.6. The speed-up is defined as ratio of the walltime of the simulation with N processors over the total walltime for the single MPI process run which is 32 hours and 36 minutes. All simulations were done on the same computer node with a dual Xeon Gold 5218R CPU which has 20 cores each with hyperthreading and a base frequency of 2.10 *GHz*

The green line on Fig. 4.6 shows the ideal speed-up of N times where N is the number of processors. With the current test set used on QuEh, a perfect speed-up is almost achieved. There are three reasons for that optimal parallelization. The

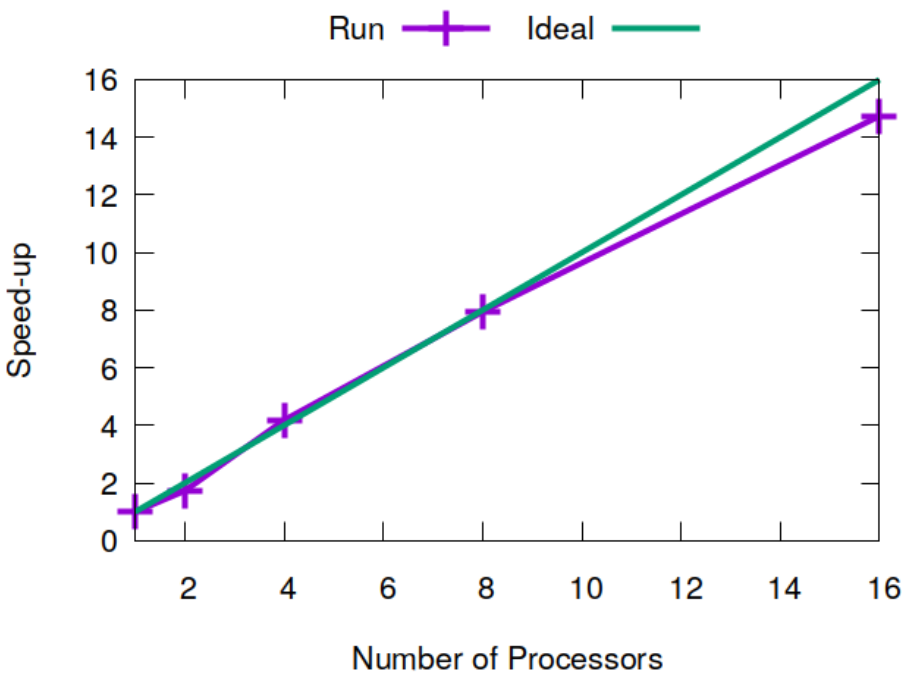

Fig. 4.6: Test of the MPI version of DD-vMCG with different number of parallel processes and the reported speed-up in total walltime as a function of the number of processors. The dynamics was run for a total simulation of 5 *fs* with a time step of 0.01 *fs* (walltime of 32 hours and 36 minutes for the single MPI process run)

first one is that the number of MPI processes requested is a divider of the number of quantum chemistry calculation at each step (i.e. GWP), so no idle process during the evaluation of the PES. The second reason is that the QuEh method updates the PES at each nuclear time step and cannot employ the database to circumvent the need of an electronic structure calculation (due to the time-dependent nature of the PES). Thus, at each time step, there is exactly N tasks to share among the MPI processes where N is the number of GWP. The last justification is that the main limiting step in the wavefunction propagation in that specific example is the call to the external quantum chemistry software.

For these specific reasons, an almost ideal parallelization of the QuEh method is possible. However, for simulations with very fast evaluation of the PES by the external program, the limiting step can become the integration steps and thus, a decrease in the speed-up with the number of processors is expected. Another way

of increasing the cost of computation in the integration steps is by increasing the number of GWP. The current simulations on ethylene are a representative test for the speed-up of the QuEh method due to the fast evaluation of the PES (on average 30 seconds) and despite the fast electronic structure calculations, the limiting steps still reside in the execution of the external program. So it is expected that as molecular systems get bigger the time spent on the quantum chemistry software will remain the main cost of computation and more GWP will be needed to properly describe the system due to the increase in number of degrees of freedom which implies more electronic structure calculations at each step. Thus, the MPI parallelization for QuEh will still provide a substantial speed-up for larger molecules. The exact number of GWP needed for a system of a given size cannot be easily determined as the convergence of the dynamics is heavily system dependent (i.e. based on the shape of the PES for example).

In a propagation where the database is not used, it is easy to predict the number of electronic structure calculations to do at every time step in method like QuEh and the user can easily choose the number of MPI processes to achieve optimal parallelization. In the test case presented here, the number of processors requested are a divider of 16 which corresponds to the number of GWP. Thus, each MPI process evaluates the same number of electronic structure calculations without one or more process being idle. In case, there are idle processes, the MPI algorithm has been written in a way to isolate them to reduce the overhead of the communication.

In the case of a DD-vMCG simulation with global diabatization (i.e. imply use of database) and Hessian updating, the number of electronic structure calculations cannot be easily predicted at each step (both nuclear step and integration step) and thus, an optimal parallelization for DD-vMCG won't be possible unless with small number of parallel processes. The general suggestion for running DD-vMCG

is with multiple propagations to complete the database due to the nature of the global diabatization where the database is rediabatized with all the available points at the beginning of a simulation. In this kind of case, the parallelization can be used in the initial runs to converge the database by spreading the GWP in the configuration space and the final run is done with a database only (no call to external quantum chemistry software).

4.3 Database with SQL

4.3.1 Usage of database for DD-vMCG

The use of a database allows the program to circumvent the expensive external electronic structure calculations by interpolating the quantities of points close in the configuration space (i.e. coordinates in NM). In the current development version of QUANTICS (v1.3), the interaction with the database is through direct data access in the memory and its content is also written on flat binary files.

There is one file per quantity provided in the DD-vMCG code. A list of all the current outputs of the main subroutine can be found in Table 4.3 which consists of the energies, first and second derivatives plus any couplings between states of same spin multiplicity (nonadiabatic couplings) or different total spin (spin-orbit couplings). In the DD-vMCG algorithm, a modified Shepard interpolation algorithm[129] is employed to approximate new data points that are close in NM space. In case of a simulation employing the database, the main control a user has over its usage is through the *dbmin* keyword which defines the maximum distance (i.e. Euclidian norm of the vector difference for all NM between two points) to employ the interpolation scheme. If the distance between a new point and any previous points in the database is larger than *dbmin*, the quantum chemistry program is invoked to evaluate the PES.

Any new data originating from an on-the-fly evaluation of PES are appended

Table 4.4: List of file used for storing the database. The flat binary files has the ".db" extension and the ASCII formatted files has the ".dba" extension.

name	description
geo	Geometry in cartesian
adpes	Adiabatic energies
pes	Diabatic energies
adgra	Adiabatic gradients
gra	Diabatic gradients
adhes	Adiabatic Hessian
hes	Diabatic Hessian
addip	Adiabatic dipole
dip	Diabatic dipole
nact	Nonadiabatic couplings
adsoc	Adiabatic spin-orbit couplings
soc	Diabatic spin-orbit couplings
moco	Molecular Orbitals
trans	Adiabatic transformation Matrix
nmode	Geometry in normal mode (with respect to a ref geo)
coord	Coordinates for GAP potentials
civec	Vector of configuration interactions coefficient

to the relevant file and thus, the data are not ordered in a specific way other than in order of appearance. All data are related to each other by an unique record number. At the initialization of any DD-vMCG run, the algorithm checks for the existence of the database and loads its entire content in the memory. Any browsing through the list of data is done in a sequential manner on the main process and there is possibility of using OpenMP parallel code thanks to the existence of shared memory protocol for that interface.

The database is also used for data analysis such as plotting the adiabatic/diabatic PES along specific NM coordinate. There is also the possibility to convert the files from a binary to ASCII format and vice-versa using some QUANTICS utilities.

The current limitations on the usage of the database is the low speed sequential access to the data and the large memory requirement with the increasing number of points. For a simulation on a shared memory system, the database reading has

been parallelized using OpenMP. However, the data writing to the flat file can only be done sequentially by the main thread.

4.3.2 Principle of SQL

The SQL is a standard query language used for the interaction with relational databases. The information in the database is related to each other by means of an unique number (ID) and a relational table which links data from different tables together (see Fig. 4.7). Thus, a more intuitive handling of it would be storing the results as a table with an ID assigned to each new data entry. In the case of QUANTICS, a single relational table using the dbentry ID is enough to link all the data between each tables together. The number of tables will depend on the option specified by the user for a particular simulation.

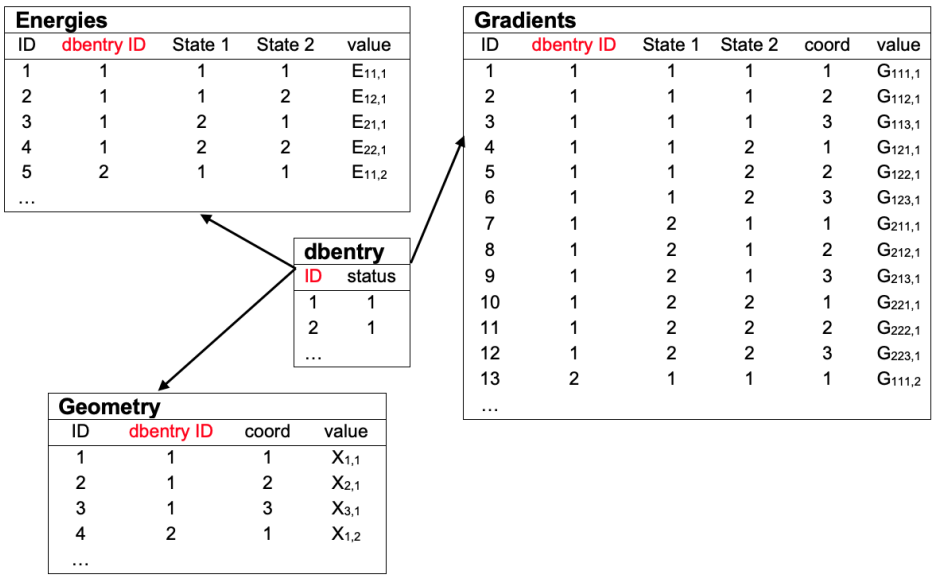

Fig. 4.7: Example structure of the table used in QUANTICS for the storage of geometries, energies and gradients for an arbitrary system with 2 electronic states and 3 nuclear degrees of freedom (in cartesian). The relational table is the dbentry table with the dbentry ID (in red) as the primary key and link to others table. The number of rows for each entry is based on the dimensionality of the arrays, the number of electronic state (State 1 and State 2) and number of atoms (coord, with 1,2 and 3 corresponding to the x,y and z coordinates of each atoms).

By using SQL, all data quering to the database is done through the engine

(i.e. using SQL commands) rather than a direct search by memory address in pre-allocated arrays. There are different database manage software solution available for the handling of the database and there is a need to compile QUANTICS with the correct library. For the current development project, the SQLite database engine has been chosen for multiple reasons over the more common OracleSQL:

- database handling without requiring a server to run
- self-contained (database engine runs as part of the program)
- low memory overheads
- Easy portability with all data stored in a single file

The main disadvantage is the poor scalability of SQLite compared to OracleSQL and the restriction to a single writing thread due to the lack of specific thread management functionality. The first limitation is not a major drawback considering the small volume of data needed for DD-vMCG (up to a few thousands points). The second restrcition can be mitigated by rewriting part of the MPI code to dedicate a thread for the interaction with the database engine to append new data. However, considering the cost of the electronic structure calculations, the overhead generated by the data writing should be very small in comparison.

The advantage of using SQL interface for the management of the database rather than previous flat file based solution allows a more robust I/O with a protocol in place to prevent corruption of the data upon appending new results. Furthermore, the reading of a database using SQL is possible on multiple processes without the need of a shared memory. Thus, it should make the handling of the database compatible with an MPI parallelization of QUANTICS in addition to reducing the requirement in memory for runs with a large database.

4.3.3 SQL implementations

SQLite provides a C-language library and to use the database in QUANTICS, a wrapper for Fortran is required. Thus, the fsqlite module created by Markus[130] which has been developed to interact with SQLite3 is used and statically linked.

The quantum chemistry results are stored in their respective tables listed in Table 4.4. The number of columns in each table is based on the dimensionality of the array used to store the results in the getddpes routine for a single GWP. This approach is to ensure flexibility of the implementation for arbitrary number of states and degrees of freedom and thus all tables are created with a set number of N columns based on their dimension (i.e. rank of arrays). The number of states and nuclear degrees of freedom will determine the number of lines required for each entry (i.e. geometry) in each table (see Fig. 4.7). For example, a gradient will need $s^2 \cdot M$ lines to store the first derivative for a system with s electronic states and M nuclear degrees of freedom. Two extra columns (one at the second column and one at the end) is added to each table which contains the dbentry ID and the value of the quantities (i.e. energies, gradients, etc.) at specific index respectively. The dbentry ID allows the program to relate the data to a specific geometry and the information stored in column 3 to N-1 correspond to the index of the location of the value in the full array. In the case of the gradient for example, these indexes related to the electronic states and nuclear dimensions.

The relational table is the dbentry table which is use to monitor the status of each entry in the database. The other function of the dbentry table is to keep track of the size of the database by using a SQL command for counting the number of elements in the table.

To ensure compatibility between different versions of QUANTICS, two programs have been written to allow conversion of the database from SQL to flat binary files and vice-versa. These two programs are named convdbfromsql and

convdbtosql, respectively and they are part of the analysis program contained in QUANTICS (see Fig. B.1. Thus, databases created by the new version of QUANTICS with SQL can be used by older versions that only have database handling with flat binary files and vice-versa.

At the start of the DD-vMCG algorithm, the program checks for the existence of a database file. The program then either creates the SQL database (database.sql) or converts existing flat binary files into it. The general reading of a database is done by first quering for the existence of a specific table in the database and then initiating the read transaction followed by a retrieval of the data corresponding to a dbentry ID in the appropriate array. All the data are linked to a specific geometry which is tied to its entry number ID in the database. Once the results of the saved PES, the processes finalize the reading transaction with database for each table queried with the appropriate SQL command.

The writing of the database is done using the same order of instruction as the reading procedure. In the dddb_wr1 subroutine, a transaction is initiated with the database and then all the data evaluated in the getddpes subroutine is written to the database using the appropriate SQL command. Finally, once all data is written for a single entry (i.e. one geometry), the transaction with the database is committed.

As mentioned previously, the lack of multiple processes management in the SQLite engine eliminates the possibility of having multiple threads writing to the database at the same time. The advantage of using a SQL library for database is that it provides a more efficient data searches/queries and minimizes risk of data corruption. Moreover, the diabatization procedure or Hessian updating requiring previous points could be done in parallel through the MPI and/or OpenMP section.

However, the database for a particular work is tied down to the molecule and level of theory employed. Thus, the data is not flexible or restricted in its utility

across different simulations. However, the quantities in the database could be used for PES fitting for more accurate simulations with MCTDH and thus, the easy portability could have further use for future development.

4.4 Implementing a pulse in the QuEh method

4.4.1 Pulse in DD-vMCG

In the QUANTICS package, it is possible to include the presence of an external oscillating pulse in the dynamics for the Multi Configuration Time Dependent Hartree (MCTDH) or DD-vMCG method by defining a new operator in the Hamiltonian section in the input file. The operator can be declared as a product of an oscillatory function (sine, cosine) and an envelope function (eg. a gaussian). In the general case of a DD-vMCG simulation, the dynamics occurs on PES of multiple electronic states and the operator can be defined for interstate excitations in the case of a resonant pulse (for photoexcitation) or for intrastate effects. In the latter case, an extra time-dependent term is thus added to the diabatic state energy.

However, for the QuEh method, the nuclear dynamics driver on QUANTICS only has information on a single effective PES and thus, no interstate couplings can be added to include effect of a resonant excitation during the dynamics.

To include the time-dependent term in QuEh, a different approach from DD-vMCG is employed where the operator for electric field is added directly at the electronic level rather than in the nuclear Hamiltonian explicitly. Due to the nature of the time-dependent PES for the QuEh nuclear Hamiltonian (see eq. 3.54), a straighforward inclusion of the pulse involves putting all the time-dependent terms together (i.e. put the electric field operator in the Ehrenfest PES $V(\boldsymbol{R}, t)$).

4.4.2 Implementation in CASSCF/CAS-CI

We now discuss including the effect of an external pulse in the QuEh dynamics algorithm. This is accomplished by including the time-dependent term in the electronic Hamiltonian.[131–133]

The interaction between the electronic wavefunction and the oscillating electric field $\vec{E}(t)$ is included by adding the dipole-electric field term $\langle i|h_0|j\rangle \cdot \vec{E}(t)$ to the one-electron operator of the electronic Hamiltonian h_{el} as shown in eq. 4.1. $\langle i|\vec{r}|j\rangle$ are the dipole integrals in an orbital basis $|j\rangle$. In the current work, the interaction between the field and the electronic wavefunction is only accounted for up to the first order (i.e. dipole term only). The term $\langle i|h_0|j\rangle >$ is simply the nuclear-electron attraction term plus the electronic kinetic energy. This implementation is straightforward in the QuEh method due to the use of a single time-dependent PES and thus, all the time-dependent terms are added at the electronic level.

$$h_{el}(t) = \langle i|h_0|j\rangle + \langle i|\vec{r}|j\rangle \cdot \vec{E}(t) \tag{4.1}$$

The implementation is done in a development version of GAUSSIAN in the MultiConfiguration Self-Consistent Field (MCSCF) code (link 510). The additional interaction term is added to the one-electron term of the Fock matrix (see eq. 3.35a, 3.35b and 3.35c). The MCSCF wavefunction is optimized for a set of "dressed" electronic states which correspond to a set of eigenstates of the time-dependent electronic Hamiltonian with an external electric field. One particular aspect of the CASSCF method is that all integral evaluations are in the MO basis. In GAUSSIAN, the dipole-electric field integrals are computed by link 303 and stored in the atomic orbital (AO) basis. Thus, an unitary transformation is required to transform the dipole-electric field integral from the atomic basis $\mathbf{D}^{AO}$ to the molecular basis $\mathbf{D}^{MO}$. This is accomplished through the matrix multiplcation

$$\mathbf{D}^{MO} = \mathbf{C}\mathbf{D}^{AO}\mathbf{C}^{T} \tag{4.2}$$

where **C** is the unitary matrix transformation from the atomic to MO basis.

To properly interface the electronic structure evaluation with the external field in QuEh, special attention is given in the template file reading (the file used by QUANTICS to write input for the quantum chemistry calculation) in order to properly assign the time value for the computation of the electric field at a time t by using a tag for substitution ($time$ in QUANTICS).

4.4.3 Computational Details

To test the effect of the pulse in QuEh, we investigate the dynamics of the allene cation. For allene, the Ehrenfest electronic structure method is used with Complete Active Space Configuration Interaction (CAS-CI)[56,103] formalism with an active space of 3 electrons in 2 localized π orbitals shown in Fig. 4.8. The nuclear dynamics is described within QuEh using a set of 16 GWP to represent the nuclear wavefunction which evolves on the time-dependent Ehrenfest potential.[50,134,135] The basis functions sample the initial nuclear wavefunction using a momentum distribution and the width of the GWP is narrower than usual (0.1 instead of the 0.7071 which corresponds to a ground state vibrational wavefunction in a harmonic potential) to avoid numerical problems for the integration in regions of turning points in electron dynamics.

The initial geometry is the neutral ground state structure with the dihedral angle between the carbon and hydrogen atom set at 45°. The NM are defined using a frequency calculation performed at that specific geometry with B3LYP/6-31G* level of theory.

The pulse, employed for the current theoretical simulation, models an experimental setup with a Ti:sapphire chirped-pulse amplification laser system with short IR pulses. The pulse $E(t)$ is represented (see eq. 4.3) by a gaussian with parameters given in Table 4.5). The field is polarized in the direction of the molecular axis (along the C=C bond). In the GAUSSIAN program, the length of the pulse

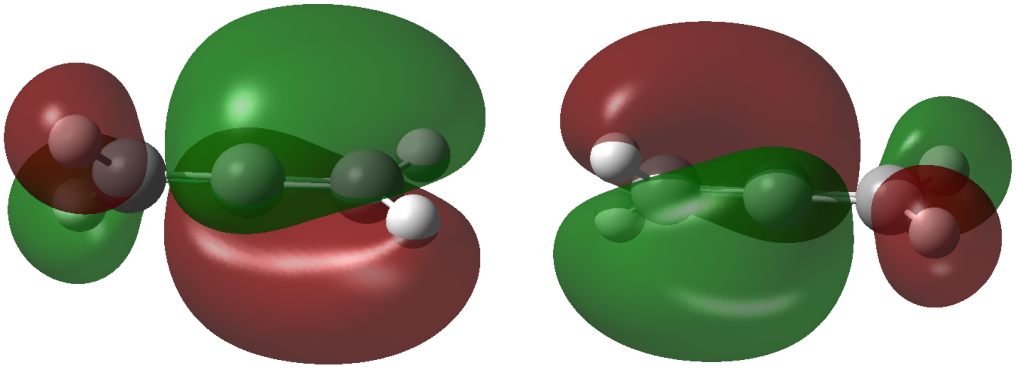

(a) (b)

Fig. 4.8: Localized π orbitals included in the active space

Table 4.5: Parameters of the pulse included in allene cation dynamics.

Quantity	SI unit	Atomic unit
E_0	5 x 10^9 V/m	0.0098 a.u.
ω	3.7 x 10^{14} Hz	0.05625 a.u.
t_0	15 fs	620.1206 a.u.
γ	0	0
W	15 fs	620.1206 a.u.
σ	0.0785 fs^{-1}	0.001899 a.u.

is defined by the width σ parameters rather than the full width at half maximum W and the mathematical relationship is given in eq. 4.4

$$E(t) = E_0 \cdot cos(\omega(t - t_0) + \gamma) \cdot \exp\big(-(\sigma(t - t_0))^2\big) \tag{4.3}$$

$$\sigma = \sqrt{\frac{2\ln(2)}{W^2}} \tag{4.4}$$

The ionization process with the pump pulse is treated with the sudden approximation where the dynamics is initiated on a superposition of the 2 lowest cationic states. For the simulation, we assume an initial electronic state that corresponds to the situation with a lone electron localized on one of the π orbitals (Fig. 4.8). This situation corresponds to a superposition of the 2 adiabatic states wherein each have an equal weight.

4.4.4 Results

In previous theoretical work, the QuEh method was used to follow the electron dynamics associated with a pulse that creates a superposition of adiabatic states. In this work, we discuss incorporating a subsequent IR control pulse in the QuEh simulations.

The interaction of an external electric field with the molecular wavefunction is included only at the electronic level, directly in the one-electron Hamiltonian. However, further terms could be added such as the molecular dipole moment interaction for the equation of motion of the GWP or including the derivative dipole moment in the calculation of the gradient. The pulse used in the dynamics as well as the orientation of the field with respect to the molecule has been chosen for investigating non-resonant interaction[136] of the field with electron dynamics with the purpose of steering the dynamics near a Conical Intersection (CoIn).

The time-evolution of the system can be followed either by monitoring the evolution of centre of the nuclear wavefunction or by monitoring individual GWP. We shall discuss the overall behaviour of the complete nuclear wavepacket first, using the spin density, and then via NM displacement analysis. We focus our analysis on the torsional motion and the asymmetric C=C bond stretching that spans the branching space of the degenerate lowest 2 cationic states of allene.[137] We also look at the symmetric C=C stretching to monitor the overall change for the C=C bond length due to the formation of localized hole (i.e. CM). Subsequently we will also look at the behaviour, in detail, of GWP 6 that initially has an excitation in momentum along the NM for torsion. The basis of 16 GWP was employed to fill the half-shell in the momentum distribution (i.e. only the positive momentum of each NM is described with a function). In the current work, we do not focus on the convergence of the dynamics with the number of basis functions. However, it is known in the literature that full quantum dynamics methods can converge with

a small number of basis functions,[46,138] and the basis chosen resulted in functions that retains a low weight throughout the propagation, which is an indication that it is large enough for reasonable results.

We have chosen to follow the spin density of the unpaired electron to understand the electron dynamics. The spin density provides us with information about the location of the lone electron and has the advantage that it is not dependent on the details of the electronic structure method.[122] The analysis of the propagation of the nuclear wavefunction is done in the NM diplacement basis. We use this representation for the GWP because of the orthogonality of this representation and the ability to easily identify the relevant degrees of freedom compared to the cartesian representation where the degrees of freedom are strongly coupled together.[139]

We first discuss the electron dynamics, which we visualize with the spin density on the two terminal carbon atoms (C_2 and C_3) (averaged using the Gross Gaussian Populations (GGP) of the GWP). The labelling of the atom can be found in Fig. 4.9. In Fig. 4.10, we show the average spin density (in white) as well as the spread in this distribution (corresponding to contributions of the individual 16 GWP which are displayed using a blue colour gradient). In Fig. 4.11, we show the corresponding averaged adiabatic populations.

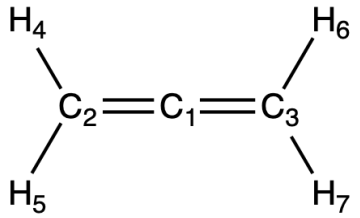

Fig. 4.9: Scheme of allene with the labelled atoms.

In general, the period of the electron dynamics depends on the energy gap between the two states that corresponds to the location of an unpaired electron on either C_2 or C_3. Thus, the larger the energy difference is, the shorter the period

of the oscillations will be. Thus, at a CoIn where the energy is zero, the period is infinite and the electron dynamics collapses. Thus, the change in the period of the electron dynamics reflects a change in the energy gap as the geometry is changed.

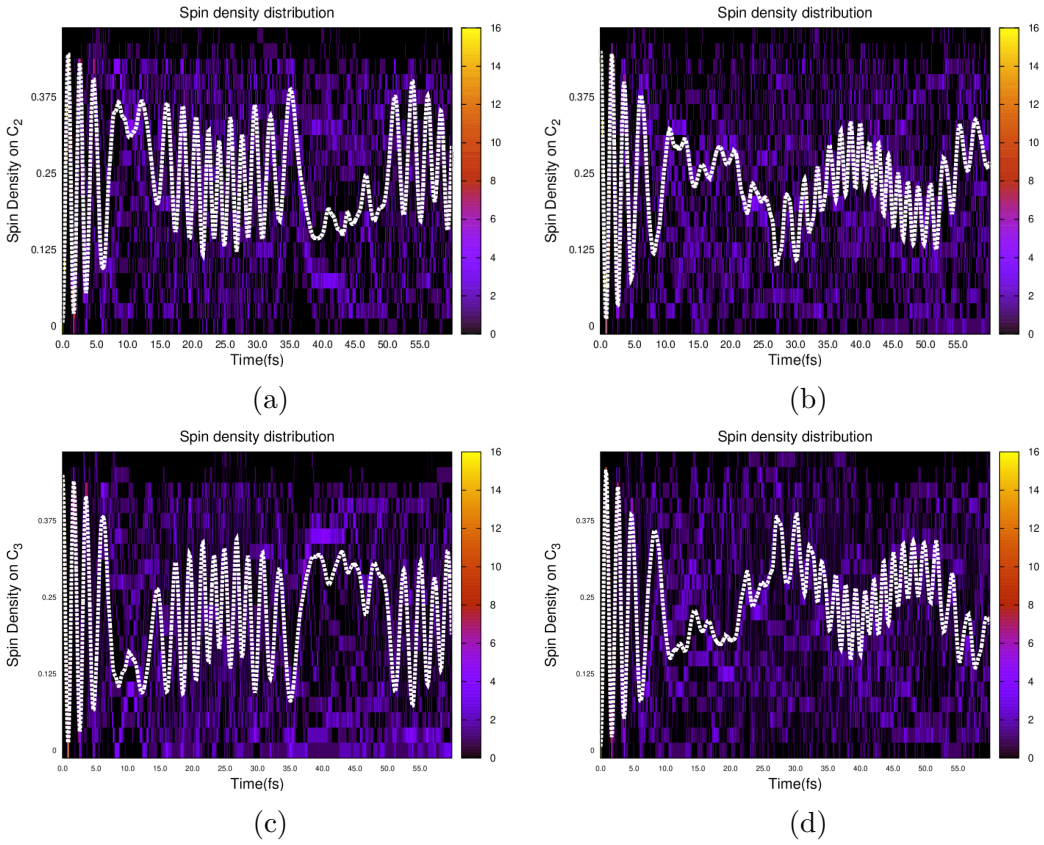

Fig. 4.10: Average spin density (in white) and its spread on the terminal carbon C_2 (top) and C_3 (bottom) for the 16 GWP dynamics without pulse (left) and with pulse (right).

We now discuss the case where we have no pulse where the dynamics begins with an equal superposition of the 2 adiabatic states. Looking at Fig. 4.10a and 4.10c, we can see there are 4 distinct segments of the electron dynamics: segment 1: 0-8 *fs*, where we have oscillatory electron dynamics and the unpaired electron moves between the 2 carbon atoms, segment 2: 8-15 *fs* where the system passes near the CoIn, segment 3: 15-35 *fs* where the electron dynamics revives again and segment 4: 35-55 *fs* where we again pass the CoIn. In contrast, for the case where the pulse switched on, Fig. 4.10b and 4.10d, we see that segments 1 up to 8 *fs*

have not changed significantly. However, beginning in segment 2-3: 8-25 *fs*, we see that the electron dynamics only partially collapses and continues with a longer period (larger gap) until 25 *fs*. At 25 *fs* the electron dynamics partly recovers and is composed of a slow and fast oscillation. Thus the electron dynamics of the average of the 16 GWP for the dynamics is strongly affected by the pulse particularly in the CoIn region near 15 *fs*. However, a large spread can also be observed for the spin density on the individual GWP as displayed by the purple lines in Fig. 4.10. Thus, one must look at the individual GWP for a detailed understanding and we return to this subsequently.

The response to the pulse also manifests itself in the adiabatic state populations shown in Fig. 4.11. On comparing segment 1 (0-8 *fs*) in Fig. 4.11a and 4.11b we can see that pulse partly destroys the equal superposition of the 2 adiabatic states from the outset (0 *fs*) and one has a partial collapse then revival of the adiabatic populations in the CoIn region (segment 2). There remains an attempt to try to understand this behaviour of the adiabatic state populations and the spin density in terms of the nuclear motion.

Accordingly, we now turn to the motion of the nuclei in response to the electron

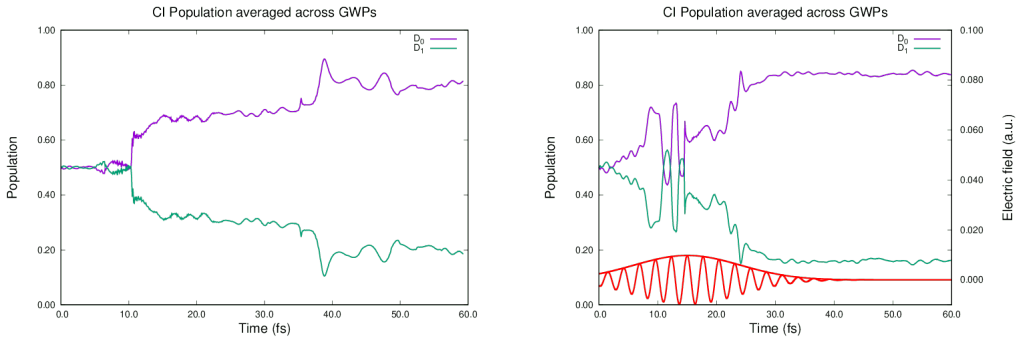

(a) (b)

Fig. 4.11: Adiabatic state populations averaged over GWP for (a) no pulse and (b) with pulse dynamics (electric field of the pulse shown in red with a width of 15 *fs* and full pulse parameters given in Table 4.5).

dynamics. The motions of the nuclei are monitored either by following a given NM displacement coordinate for the centre of the nuclear wavepacket or using the nuclear displacement of a specific GWP. The changes in the period of the electron dynamics arise from changes in the nuclear motion. Since the electron dynamics involves the carbons of the two terminal methylenes, we expect that the important nuclear motion involves the torsion and the C-C-C stretches. These NM are displayed in Fig. 4.12 with arrows showing the direction of motion of the individual atoms.

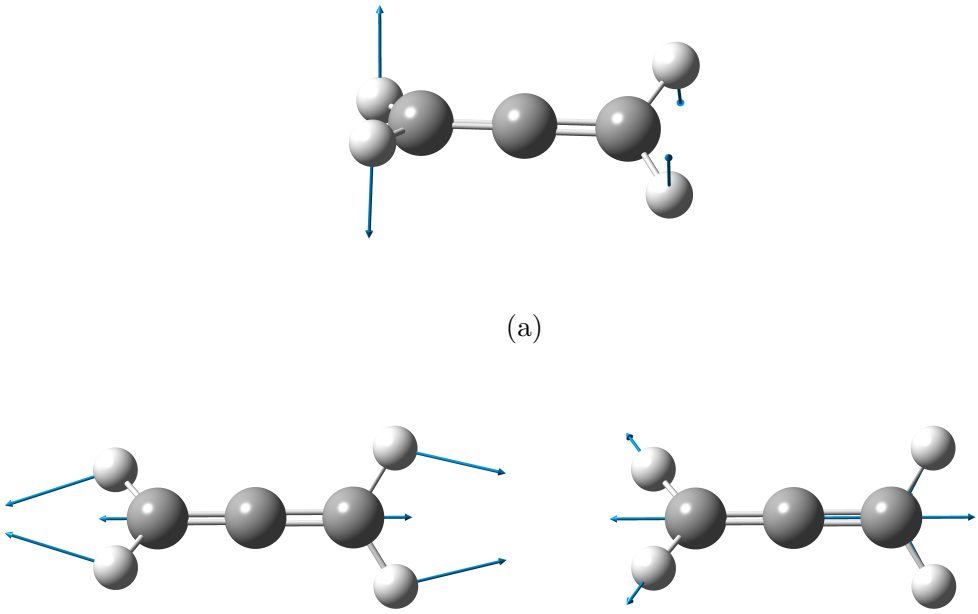

(a)

(b) (c)

Fig. 4.12: Vector representation for (a) NM 5 (torsional motion), (b) NM 8 (symmetric C-C-C stretch coupled to HCH bend) and (c) NM 11 (C-C-C asymmetric stretch).

Table 4.6: Turning point (TP)/torsional angle of NM 5 in Fig. 4.13

Time (fs)	No pulse	Pulse
23	113 (TP)	95 (TP)
48	73	67 (TP)
60	58	81

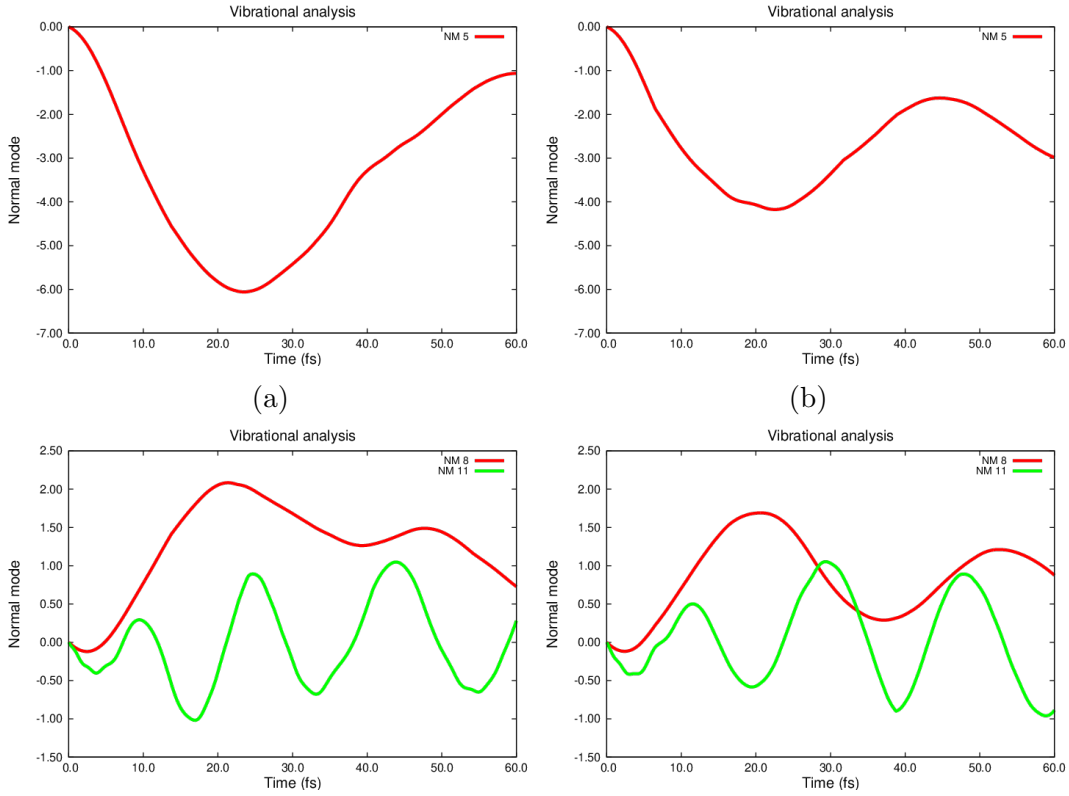

Fig. 4.13: NM displacement for the centre of nuclear wavefunction for (top) the torsional motion with NM 5 and (bottom) C-C stretching and H-C-H bending with NM 8 and 11 for dynamics without pulse (left) and with pulse (right).

In Fig. 4.13a and 4.13b and Table 4.6 we collect the data for the torsional motion (NM 5). In Table 4.6, we report the data for one specific dihedral angle (H_4-C_2-C_3-H_6) to provide an alternative interpretation of Fig. 4.13a and 4.13b which effectively show the combined motion of all four HCCH dihedral angle in the dimensionless units used for NM motion. The plot of the dihedral angles for the four HCCH can be found in Fig. 4.14. Without the pulse, the centre of the

Table 4.7: Bond length in angstrom for C_1-C_2 and C_1-C_3 for the sum of NM 8 and NM 11 in Fig. 4.13

Time (fs)	No pulse		Pulse	
	C_1-C_2	C_1-C_3	C_1-C_2	C_1-C_3
17	1.41	1.32	1.37	1.34
40	1.33	1.37	1.36	1.29
60	1.34	1.32	1.38	1.30

nuclear wavefunction follows the path from 45° to 113° (turning point at 23 *fs*) and thus goes through the CoIn (90° for dihedral angle and about -4 for NM 5) twice as shown by Fig. 4.13a (the NM shows a motion down to –6 units and back). With the presence of the pulse (see Fig. 4.13b), the turning point still occurs at 23 *fs* with a smaller angle (95°) (with a value of -4 units). With the pulse, there is a turning point at 67° at 48 *fs*. While for the case without the pulse, the torsional motion continues. Thus, without the pulse, there is a larger torsional motion observed compared to the simulations with the pulse.

Now, we focus on the C-C-C stretching motion represented by the symmetric stretch with NM 8 and the asymmetric stretch with NM 11 (see Fig. 4.13c and 4.13d and Table 4.7). Without the pulse, NM 8 shows a motion up to a value of 2 units with NM 11 reaching a minimum of -1 units which corresponds roughly to a bond length of C_1-C_2 of 1.41 Å and 1.32 Å for C_1-C_3 bond length. Both C-C bond lengths show little variation over time oscillating between 1.3 and 1.4 Å . With the presence of pulse, a smaller bond stretching is observed for the bond length which is shown by a smaller amplitude for NM 8.

It now remains to understand the relationship of the nuclear motion (Fig. 4.13 and Table 4.6-4.7) and the electron dynamics (shown in Fig. 4.10) focusing on

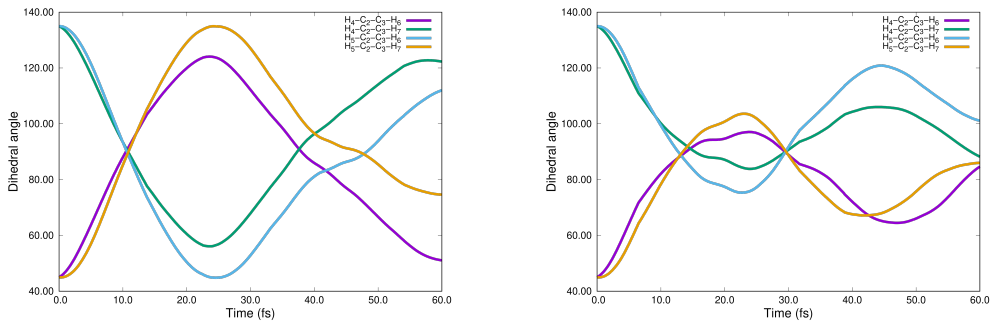

(a) (b)

Fig. 4.14: Plot of the 4 dihedral angles of HCCH in allene (based on atom labelling given in Fig. 4.9 average over the 16 GWP for dynamics (a) without pulse and (b) with pulse.

the energy gap between the two electronic states. Let us look at the energy gap for the GWP corresponding to NM 5 (GWP 6) shown in Fig. 4.15. The energy gap plot for dynamics initiated in the direction of NM 8 and NM 11 with GWP 9 and NM 12 can be found in the supporting information of the full paper in Ref. 124. NM 5 is the torsional motion which is one of the degrees of freedom responsible for the nonadiabatic events between the two lowest cationic states.[137] In contrast, NM 8 and NM 11 correspond to the symmetric and asymmetric C-C-C stretches respectively and are useful for monitoring the asymmetry in the bond lengths as a direct consequence of the asymmetry of the charge location (induced by CM). In contrast in Fig. 4.15a and 4.15b we can see that the behaviour of the energy gap before and after the pulse is very different. Thus, it would appear that the electron dynamics and the torsional motion are strongly coupled, but the stretching is hardly affected by the pulse. For example, at 15 *fs* without a pulse (Fig. 4.15a) the energy gap is almost zero in correspondence with the collapse of the electron dynamics between 5-15 *fs* in Fig. 4.10a and 4.10c. In contrast, in Fig. 4.15b we see a substantial gap at 15 *fs*. Thus between 5-15 *fs*, in the case of the pulse, we see electron dynamics with a longer period (i.e. small but non-zero gap).

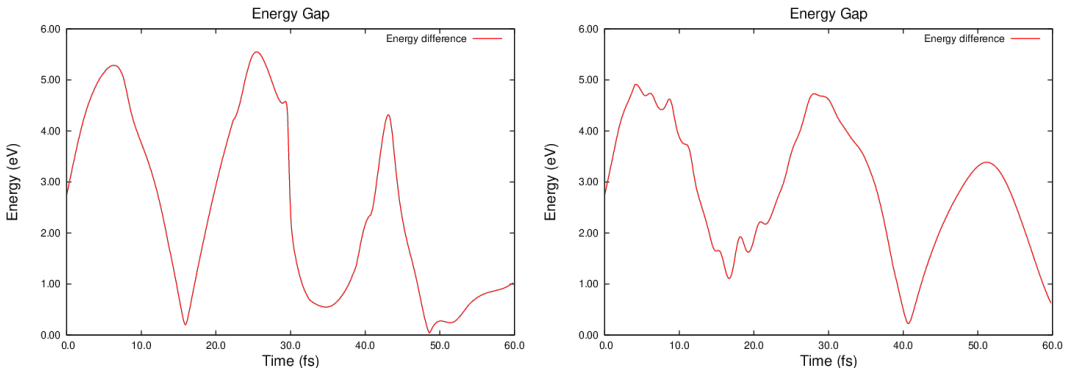

(a) (b)

Fig. 4.15: Energy gap between the 2 adiabatic states as a function of time for GWP 6 for dynamics (a) without pulse and (b) with pulse

The preceding discussion has been focused mainly on the NM motion averaged

over the whole nuclear wavefunction. Furthermore, the adiabatic population shown in Fig. 4.11 are for the complete nuclear wavefunction. In contrast, if we look at individual GWP (isolated points from the complete nuclear wavefunction) as in Fig. 4.15 we can obtain additional physical insight. The individual GWP represent points that were initiated with velocity on a particular NM in the momentum distribution. Thus, GWP 6 corresponds to the GWP that was started with NM 5 excited. For comparison with Fig. 4.15, Fig. 4.16 shows the adiabatic populations and the associated spin density along GWP 6. Notice that GWP 6 decays to the ground state at 15 *fs*. In contrast, the pulse maintains the mixed state that leads to electron dynamics which manifests itself in the change in spin density. Thus, without the pulse as shown in Fig. 4.16a and 4.16c the electron dynamics collapses at 15 *fs*. In contrast, with the pulse the electron dynamics persists. The effect of the pulse is shown more emphatically by examining the spin density of the individual atoms (see Fig. 4.16c and 4.16d). Without the pulse, there is oscillation of the spin density between the two terminal carbons for 30 *fs* before the lone electron becomes localized onto one specific carbon (C_2); whereas in the presence of pulse, the CM persists beyond 30 *fs* with a spin density oscillation between the two terminal carbons (C_2 and C_3).

In this work our objective has been to describe the effect, on nuclear-electron dynamics, of including the field of a short probe IR pulse in the electronic structure method. The pulse was applied near the CoIn geometry. We have used a two-level electronic state model for the allene cation so that the results can be easily understood. The electron dynamics was observed by monitoring the spin density on the carbon atoms of the two methylene groups. The pulse strongly perturbs the electron dynamics at the CoIn. As a consequence, the nuclear motion is changed, and we observe a smaller displacement amplitude for both the torsional motion and the C-C stretching with the presence of the pulse. The individual GWP have

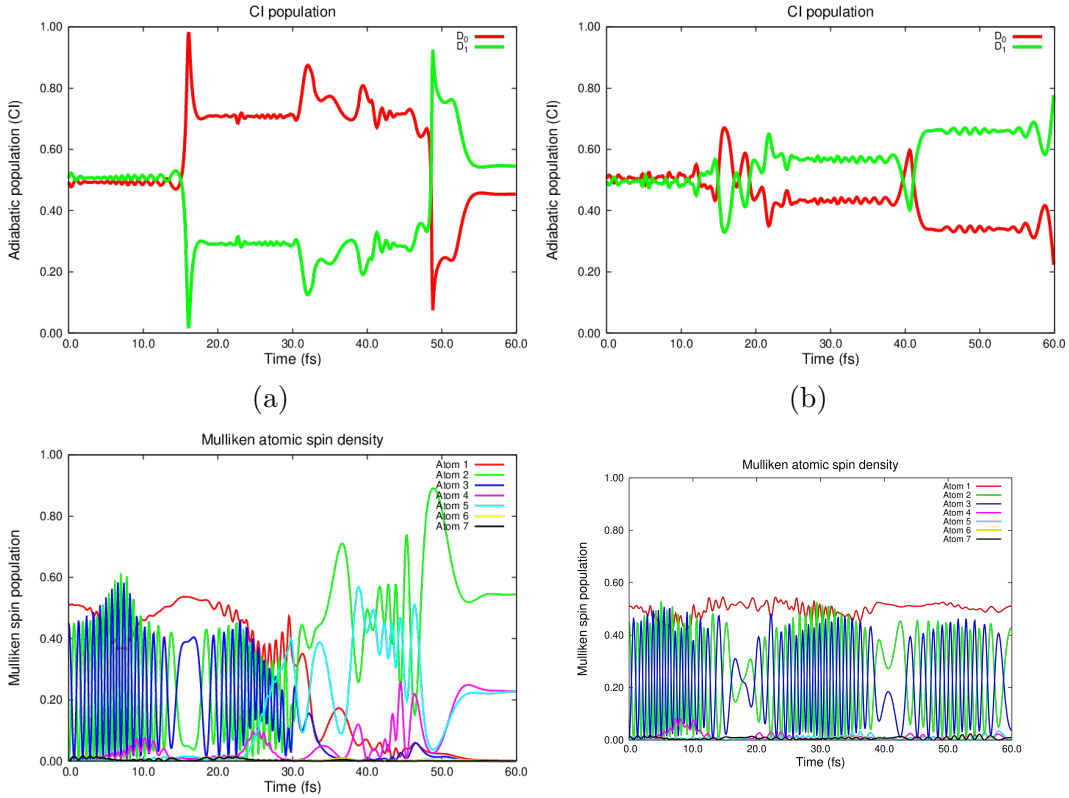

Fig. 4.16: Adiabatic populations along GWP 6 (a) no pulse adiabatic state populations (b) adiabatic state populations with pulse and (c) and (d) their corresponding spin densities.

a wide range of behaviours for the electron and nuclear motion. The expectation values of the nuclear (NM) and electron (spin density) dynamics allows us to get a global picture on the effect of the pulse in the dynamics of the complete nuclear wavefunction. The possibility of a direct study on how a short pulse affects the molecular wavefunction opens the door for investigating how fast electron dynamics interacting with an electric field can influence the nuclear dynamics.

4.5 Summary

The purpose of this chapter is to show the development work on the QUANTICS program for the QuEh method. To improve performance, a MPI layer has been added on top of the existing OpenMP one for the subroutine responsible for eval-

uating the PES at the center of GWP. A more optimized approach is employed with the use of structure data to reduce the overhead of the communication. An almost perfect speed-up is observed when running the dynamics in a set of specific options. Due to QuEh algorithm being part of the DD-vMCG one, the MPI implementation have to be usable with the latter too. The main restriction in the MPI parallelization is the lack of shared memory between the processes and thus, the usage of a database using memory and flat files isn't possible unless the whole database is through communication which would multiply the requirement in memory.

To solve this problem, a SQL implementation is written for the handling of the database and various executables are written to allow retro-compatibility of the QUANTICS program. The fastest method for database reading is through the memory. However, the size of the arrays to hold in memory grows with the number of degrees of freedom and states quadratically and linearly with the number of points. Simulation with large databases becomes impracticable unless one has access to a system with large memory.

Finally, to extend the scope of the application of QuEh, a dipole-electric field integral is added to the Fock matrix in the CASSCF code of Gaussian. This implementation will allow us to simulate the effect of external pulse on the nonadiabatic dynamics of the system and rationalize the mechanism behind to achieve photo-control of the molecules.

Chapter 5

Results

5.1 Introduction

To rationalize the effect of electron dynamics and its effect on the nuclear motion, the nonadiabatic dynamics of three model systems are investigated using the Quantum-Ehrenfest (QuEh) method presented in chapter 3 and the results presented here are ordered following a gradual increase in the complexity of the dynamics. The works shown in this chapter on octa-3,5,6-trieniminium cation and benzene cation are published in the *Journal of Physical Chemistry Letters* 2021 (vol. 12)[140] and *Communication Chemistry* 2021 (vol. 4),[141] respectively. The ethylene (ethene in IUPAC nomenclature) cation results are part of a manuscript in preparation.

The first example is on the all-trans octa-3,5,6-trieniminium cation where the control of the nuclear dynamics (photoisomerization of a double bond) is achieved by carefully selecting the initial weight of the two lowest singlet excited states. The application to benzene, with a D_{6h} symmetry, allows the rationalization of the effect of the coherent superposition of 8 electronic cationic states on the nuclear dynamics using symmetry arguments where only few selected nuclear modes of correct symmetry can be activated due to the symmetry of the electronic state. Finally, a pulse is employed to control the nuclear and electron dynamics (5 lowest states) of the ethylene cation, with a D_{2h} symmetry, where the effect will be ratio-

nalized in term of symmetry and coherent superposition of states. The structure of the chapter is as follows, each work is presented individually in a section with a background on the chemical relevance of the molecule as well as previous theoretical and spectroscopic studies followed by the results obtained with the QuEh method.

5.2 Controlling passage through a Conical Intersection with initial electronic state superposition

5.2.1 Isomerization in rhodopsin

The photoinduced isomerization of a double-bond is an important mechanism in many biological systems (i.e. proteins). In some classes of proteins such as rhodopsin, phytochromes and xanthopsins, the isomerization is the main intramolecular process required for their biological activity whereas types of protein such as Green Fluorescent Protein (GFP), the rotation around the double-bond is a secondary process that can quench the fluorescence of the system.[142] In the former group, the conformational change around one of the double-bonds is known to happen on the picosecond to subpicosecond timescale. Thus, understanding the "unlocking" of the double C=C bond is of key importance to rationalize the efficiency of such systems as well as controlling the formation of the photoproducts.

In vertebrates, rhodopsin is one of the photoactive proteins allowing dim-light vision.[142,143] The photoactive unit in rhodopsin is the retinal Protonated Schiff Base (rPSB). For example, in bovine rhodopsin, upon absorption of a photon, the 11-cis rPSB (see Fig. 5.1a) undergoes a fast isomerization around the C11=C12 double bond inside the rhodopsin cavity which will interact with the rest of the protein and initiate the function known as vision.[142,144] The chromophore changes into an all-trans isomer which is the key step of the protein's photocycle and it

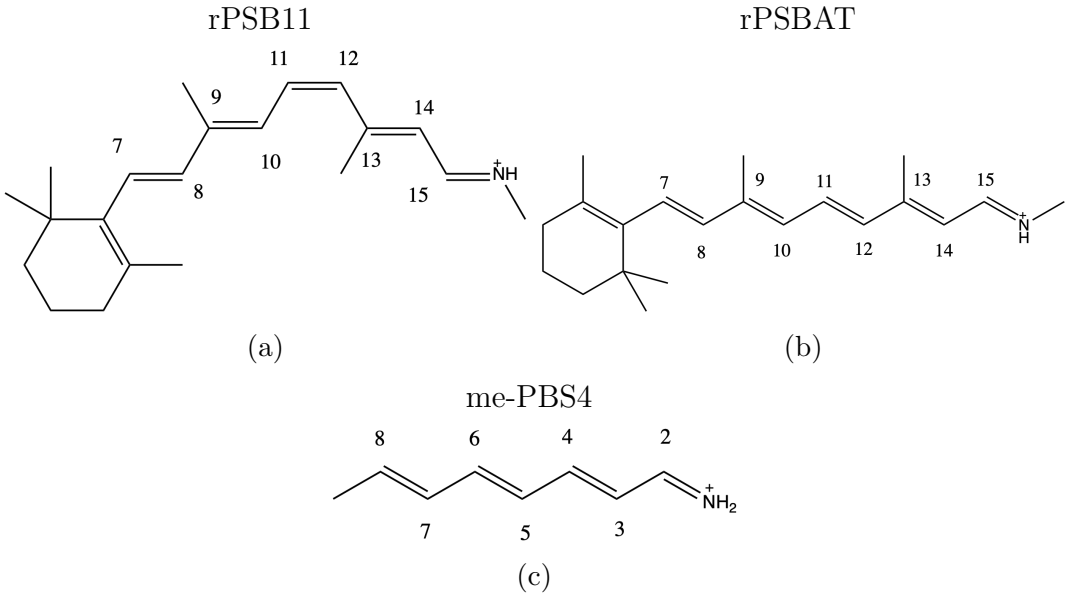

Fig. 5.1: Molecular structure of (a) rPSB11, (b) rPSBAT found in bovine and bacteria rhodopsin, respectively. (c) Model system investigated with the atom labelling employed in this work

happens on a sub 200 *fs* timescale upon photoexcitation in gas phase.[142,143,145] Further details of the full cycle mechanism can be found in the literature.[146]

In bacterial rhodopsin, the chromophore is the all-trans isomer of rPSB (rPSBAT, see Fig. 5.1b) and it fulfills the function of light-dependent ion pumping protein.[144,147] In this molecule, the photoisomerization happens around the C13=C14 double bonds yielding the rPSB13 product and is known to happen as a slower timescale compared to the rPSB11 of bovine rhodopsin. Decay through a Conical Intersection (CoIn) occurs within 1 ps and the isomerization events take place in 4 ps compared to rPSB11 in which the events happen in 50 *fs* and 200 *fs*, respectively.[142,143,145,148]

The actual mechanism of rPSB has been extensively investigated from both theoretical and experimental approaches. It has been found that the electron and nuclear dynamics is heavily coupled (i.e. vibrationally coherent) in that chromophore and the actual photophysics of the system involved multiple CoIn between the 3 lowest singlet states.[142,145,148–151] In the literature, these three states

are commonly labeled as $1A_g$, $1B_u$ and $2A_g$, respectively. The symmetry allows one to relate the electronic character to the one in polyene hydrocarbon, described using a C_{2h} point group. The $2A_g$-like state corresponds to a covalent or diradical state and the $1B_u$-like state to a Charge Transfer (CT) state.[152]

The critical nuclear motions responsible for excited state dynamics and passage through the CoIn is the Bond Length Alternation (BLA) stretching, out-of-plane hydrogen motion and the isomerization around the C=C bonds.[150] The unlocking event of the double-bonds happens through an alternation of single and double bond (i.e. BLA) through the polyene chain driven by electron dynamics.[142,151]

In rPSB11, the main photophysics takes place on the S_1 state where, upon excitation from the Franck-Condon (FC) point, a decay to the ground state via an energetically accessible CoIn is observed which leads to a fast isomerization. There is also a CoIn between the S_1 and S_2 state relatively close to the FC point which has been hypothesized as responsible for the slow mechanism observed in some of the rhodopsin chromophores. Therefore, the unlocking of the double bond can be affected by nonadiabatic events between the 2 lowest singlet excited states. From previous theoretical works, it has been shown that a 3-state model is required to properly describe the nonadiabatic dynamics of bacterial rhodopsin.[142,144,153–157]

In computational studies, it is commonly found in the literature that smaller model system of the full rPSB are used for dynamics due to practical reasons such as cost of computation.[142,158] Furthermore, multiple theoretical works have included the effect of solvation[157,159] and shown that the main solvent action is to slow down the processes observed in the gas phase. Thus, the main photochemistry remains qualitatively the same for the different systems and environments. In the case of the bacterial rhodopsin, the presence of a polar solvent has shown the ability to further mix the 2 lowest excited states (S_1/S_2 CoIn more energetically accessible from the FC point).[154,160] For that reason, the current work is done on

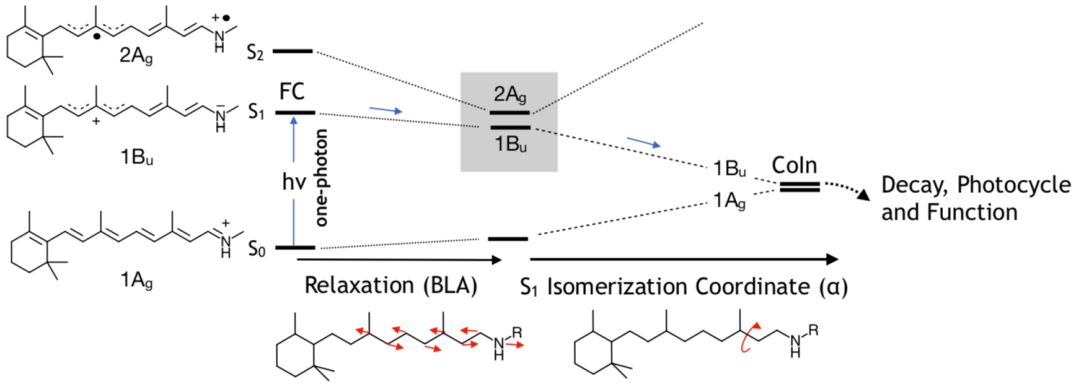

Fig. 5.2: Schematic representation of the reaction coordinate for the rPSB photoisomerization. The Lewis formulas represent the electronic character of the ground state and first two singlet excited states. The CoIn corresponds to a $1B_u/1A_g$ crossing delivering the chromophore to S_0. Notice during the initial BLA nuclear relaxation the $2A_g$ and $1B_u$ states transit in the vicinity of a $2A_g/1B_u$ CoIn, become nearly degenerate, and mix

a small rPSB4 system where the environment presence is not considered.

By mixing the electronic states, it is possible to alter the main conformational change and how fast the isomerization happens. Carefully selecting the initial electronic wavepacket with a coherent superposition should allow us to rationalize how electronic coherence affects the dynamics. Previous computational work by Manathunga et al.[154] highlighted the possibility of controlling the efficiency of the molecular twisting responsible for the actual isomerization event by mixing the S_1 and S_2 states. It is possible to create such conditions experimentally by means of an ultrafast laser (i.e. broad in energy) which will lead to a simultaneous population transfer to multiple electronic states in a coherent way. While the coherent control via mixing is still an open question, modulation of the rPSB electronic wavepacket via a spectroscopically induced S_1/S_2 mixing could provide a novel experimental tool to control an important photobiological event.

5.2.2 Computational Details

The QuEh simulation on rPSB4 is done using 47 Gaussian Wavepackets (GWP) to represent the nuclear wavefunction and a Complete Active Space Configuration Interaction (CAS-CI(6,6)/6-31G*) level of theory for the electronic structure method (see Fig. 5.3 for active space). The nonadiabatic dynamics is initiated with different electronic initial conditions by varying the mixing ratio between the S_1 and S_2 states. The simulation is run using a time step of 0.1 *fs* with the Runge-Kutta 5th order integrator for a full propagation time of 20 *fs*. All dynamics are initiated from the FC point, on the S_0 ground state. The ground state optimization and frequency calculation has been performed at the B3LYP/6-31G* level of theory.

One important feature of the QuEh method is that the electronic wavepacket is described using a linear combination of (quasi)-diabatic states and thus, the gradient driving a specific electronic mixture is computed as the expectation value of the derivative of the electronic Hamiltonian (off-diagonal gradient, i.e. derivative couplings, are included in the full gradient). As shown in Fig. 5.5, one can predict the initial nuclear relaxation by combining the gradient of the individual pure state and the derivative coupling obtained as a consequence of the electronic mixing. Another important consideration is that we assume that the dynamics start using a sudden approximation. Thus, the change in electronic population due to the pulse in a laser experiment is not included.

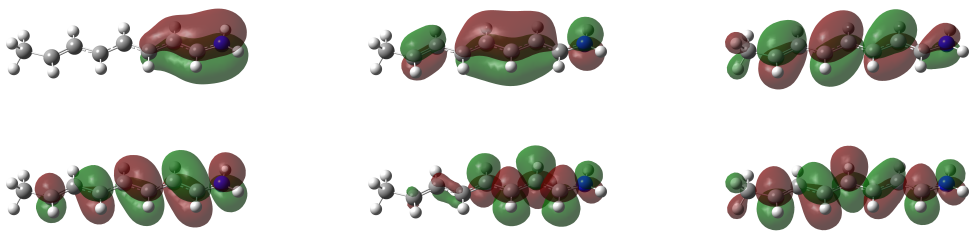

Fig. 5.3: Active space employed for the rPSB4 simulation.

5.2.3 Results

For this work, we focus on the dynamics initiated on a pure S_1 state and a mix of S_1/S_2 with a ratio of 50:50 at the FC point. Furthermore, the objective is to show where the initial vibrational energy is deposited for the first few *fs* of the dynamics and thus, a short simulation time of 20 *fs* is adequate in that context.

By monitoring the critical Normal Mode (NM) motion and the C-C bond length as a function of time, we can rationalize the effect of electron dynamics and initial superposition of states on the resulting nuclear dynamics. Moreover, the C-C bond length gives a visual cue on the BLA motion and allows us to determine how the double-bond evolved for a specific electronic state mixing.

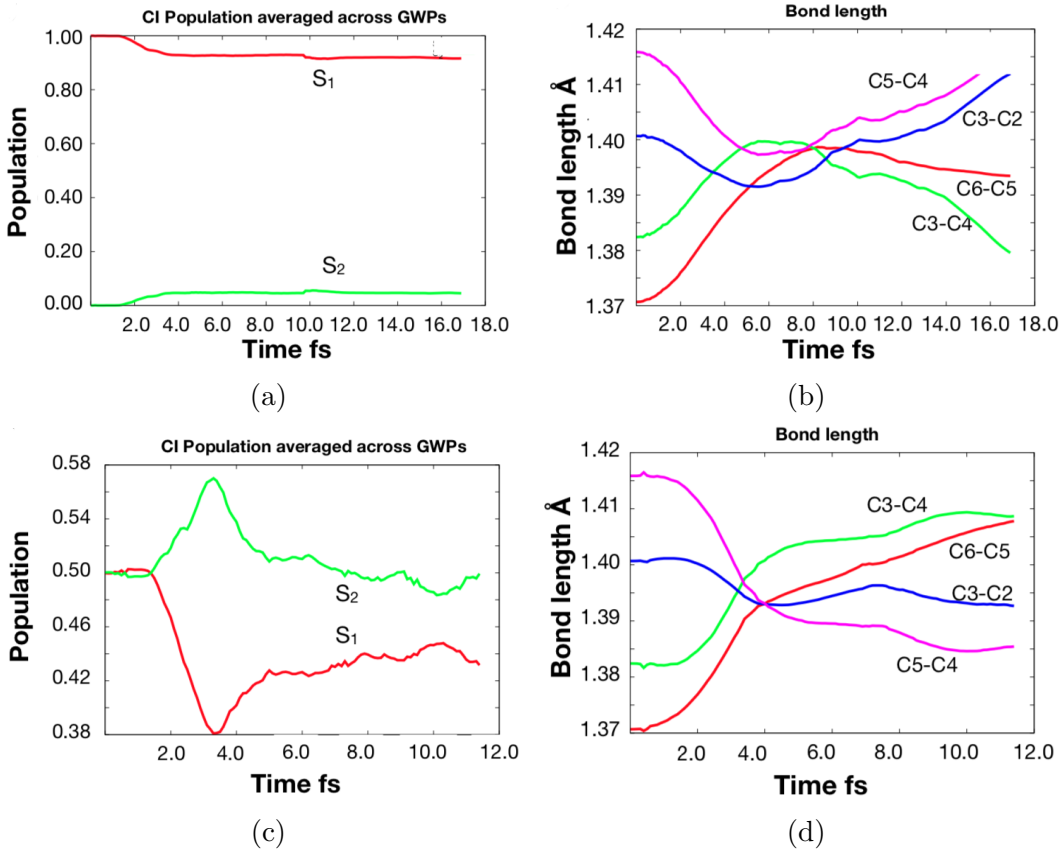

Fig. 5.4: Adiabatic electronic state population for rPSB4 with dynamics initiated on (a) the S_1 state and (c) a mix of 50/50 for the S_1 and S_2 states. The resulting nuclear dynamics in term of C-C bond length are displayed on the right for (b) pure S_1 and (d) mixture of states.

Table 5.1: Bond length in Ångstrom of rPSB4 optimized at the CASSCF(6,6)/6-31G* level of theory and atoms labelling in Fig. 5.1c

	N1-C2	C2-C3	C3-C4	C4-C5	C5-C6
S_0	1.33	1.43	1.35	1.40	1.29
S_1	1.45	1.36	1.49	1.37	1.34
S_2	1.45	1.42	1.43	1.40	1.32
S_1/S_2 CoIn	1.51	1.46	1.45	1.41	1.28

By focusing first on the pure adiabatic state for the initial condition and the location of minima and CoIn on the three states of interest, one can determine the initial relaxation step from the FC point. The bond length of the S_0 and S_1 optimized structures (see table 5.1) shows that initial excitation on the first excited state will primarily lead to an inversion of single and double bond length (i.e BLA). Thus, a fast unlocking of the double bond is observed which is then followed by an isomerization.

Upon excitation to the S_1 state (see Fig. 5.4a), we can observe some electronic population transfer to the S_2 state due to the CoIn being located close to the FC point and the initial nuclear relaxation leading it close to the region of degeneracy. Even by initially populating only the first excited state, the diradical state does participate actively in the nonadiabatic dynamics and thus, the results are consistent with the 3 state model suggested previously in the literature for bacterial rhodopsin.[142,161] Furthermore, the single and double bond inversion happens in a relatively short timescale, with a full oscillation cycle in 15 *fs*. This result is consistent with the BLA reported in the literature from previous quantum-classical trajectory calculations using a Quantum Mechanic/Molecular Mechanic (QM/MM) model where the solvent effects are included.[154]

By initiating the dynamics with a coherent superposition of 50:50 for the 2 lowest singlet excited states, one can observe a fast nonadiabatic event at around 4 *fs* with a rapid rise and decrease of the S_2 state population which then persists at an almost constant value for the remaining part of the dynamics (up to 12

fs). The nuclear dynamics shows similar BLA trends to the pure S_1 dynamics. The main difference appears after the inversion point (at around 4 *fs*) where the elongated bonds stays at a similar value for a few *fs* and thus, the double bond remains geometrically unlocked for a longer time. Whereas in the case of the single state nonadiabatic dynamics, we could observe an oscillatory BLA motion. Using a mixing of the two excited states, the dynamics enter a different regime where the restraining force (i.e. gradient, shape of the Potential Energy Surface (PES)) of the S_1 state is mixed with the derivative couplings on top of the gradient coming from the S_2 state as shown by equation 5.1.

Generally, for a superposition of two electronic states $|\psi_I\rangle$ and $|\psi_{II}\rangle$, the nuclear gradient , approximated by the Hellmann-Feynman term (i.e. only the derivative of the electronic Hamiltonian $\hat{H}_{el}$ with respect to the nuclear coordinate is included), is a sum of the two state gradients and the derivative couplings.[116] The weight of each term is dependent on the mixing angle θ and relative phase ϕ (see Fig. 3.1).

$$\begin{aligned}\nabla_R \langle\psi_{el}|\hat{H}_{el}|\psi_{el}\rangle &\approx \langle\psi_{el}|\nabla_R\hat{H}_{el}|\psi_{el}\rangle \\ &\approx \cos^2\left(\frac{\theta}{2}\right)\ \langle\psi_I|\nabla_R\hat{H}_{el}|\psi_I\rangle \\ &\quad + \sin^2\left(\frac{\theta}{2}\right)\ \langle\psi_{II}|\nabla_R\hat{H}_{el}|\psi_{II}\rangle \\ &\quad + \sin(\theta)\cos(\phi)\ \langle\psi_I|\nabla_R\hat{H}_{el}|\psi_{II}\rangle\end{aligned} \tag{5.1}$$

The nuclear dynamics is thus directly controlled by the initial relaxation and the electronic dynamics created as a consequence of the coherent superposition. By visualizing the initial gradient of the mixed states (see Fig. 5.5), we can see that the vectors are dominated by a type of bond-order inversion coordinate. However, the gradient of the mixed initial conditions at the FC point also shows a clear nuclear relaxation that is in a different direction to the BLA motion. Both dynamics display fast BLA motion within the first 4 *fs* of the dynamics and the deviation from the S_1 dynamics is mainly due to the persistence of the superposition of electronic states after the main nonadiabatic events. Thus, the nuclear dynamics

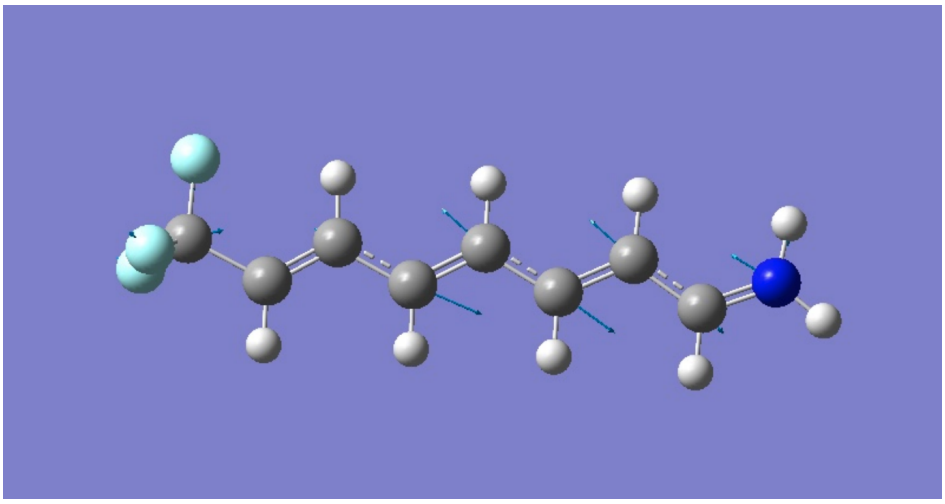

Fig. 5.5: Initial gradient of the superposition of S_1/S_2 states.

of the superposition of states displayed some similarities to the dynamics through a S_1/S_2 CoIn despite the two states being nondegenerate at the FC point and at 'longer' timescale dynamics.

In conclusion, one may achieve control of the nuclear dynamics if the initial superposition of electronic state can be tuned with a specific ultrashort laser pulse. In the current work, we show that electronic coherence leads to a vibrational coherence that can control the reactivity of the system. Another possibility of achieving photocontrol is by the mean of a control/probe pulse.

5.3 Using symmetry to predict the outcome of dynamics initiated on a superposition of states

5.3.1 Background on benzene cation

In the previous section, it was shown that one can control the photoisomerization process of rPSB by controlling the initial superposition of the important spectroscopic states responsible for the nonadiabatic dynamics of the bacterial rhodopsin. In the current section, the nuclear dynamics resulting from a specific superposition of electronic states are analyzed using a symmetry model on the benzene system

with a D_{6h} symmetry point group.

We will demonstrate that a coherent superposition of adiabatic states can lead to nonadiabatic effects that occur even far away from regions of degeneracy or for nonadjacent adiabatic states. The current work is focused on the 8 lowest cationic states of benzene which has been the subject of recent spectroscopic and theoretical works.[162] In the work of Galbraith et al., they photoionized benzene with an extreme ultraviolet (XUV) pulse generated from a High-Harmonic Generation (HHG) source which populated multiple cationic states at the same time. Subsequently, they probed the system with a visible/near-infrared (VIS/NIR) pulse and the experimental observable is a time-resolved $C_4H_3^+$ fragment yield. The benzene in the neutral ground state has an ionization threshold of 17.5 eV for the production of $C_4H_3^+$ and $C_4H_2^+$ fragments. Without a probe pulse, the main fragments collected on the mass spectrum are the $C_3H_3^+$ and $C_4H_4^+$ fragments. Upon probing with a VIS/NIR pulse, the mass spectrum displayed some intensity for a $C_4H_3^+$ and $C_4H_2^+$ that is dependent on the time delay between the two pulses. The experimental data for the $C_4H_3^+$ fragment yield was fitted with a bi-exponential decay with time constants of 11 *fs* and 110 *fs*. They performed nonadiabatic dynamics with the Multi Configuration Time Dependent Hartree (MCTDH) method to unravel the mechanism following the photoionization event. In this work, they employed a model Hamiltonian defined with a linear vibronic coupling model for the 8 lowest cationic states (up to the E state) and 9 nuclear degrees of freedom. The dynamics was initiated on the E state from the FC geometry of the neutral ground state. The central conclusion of their work is that their XUV pulse is able to simultaneously populate the 8 lowest cationic states of benzene and the two measured lifetimes corresponds to a successive decay through CoIn between the E/D states and D/B states (see Fig. 5.6).

In previous theoretical work in the field of attosecond science, much of the effort

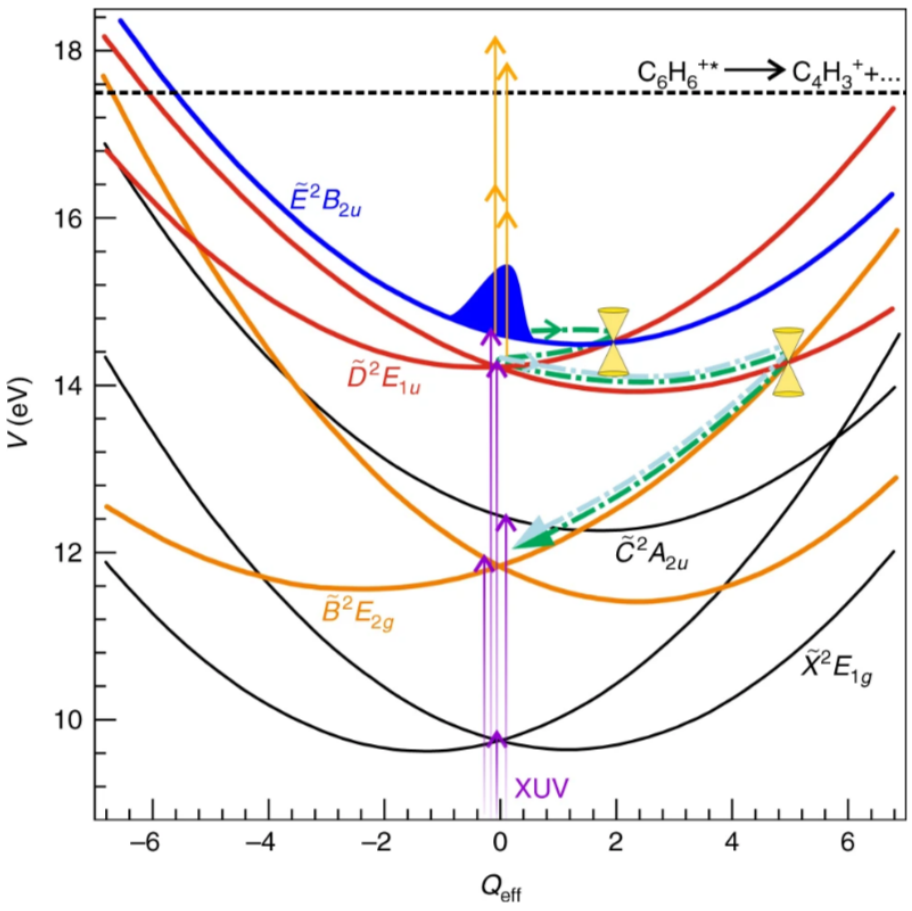

Fig. 5.6: Schematic of the dynamics of the benzene cation initiated on the E state followed by successive decays through CoIn. The PES of the 8 cationic states are expanded along a dimensionless effective nuclear coordinate Q_{eff}. The photoionization and two-photon process (photoexcitation) are shown by the purple and orange arrows, respectively. Reproduced with permission under Creative Commons CC-BY from ref. 162

has been focused on electron dynamics, simulated within the framework of frozen nuclei.[163–165] However, some recent studies has shown the importance of the nuclear motion on the electron dynamics as well as the lifetime of the coherence.[57,166,167] Thus, the effect of moving nuclei cannot be neglected in order to rationalize the mechanism upon photoionization to multiple states. In this work, we focus our attention on the 8 lowest cationic states of benzene where we create initial coherent superpositions to rationalize how the nuclear dynamics evolved based on a specific state combination (by groups of two or three states) with equal weighting for each

state. We also consider a full superposition of the 8 states where the weights are obtained from photoelectron cross sections. However, we cannot determine to what extent the states are coherently excited in the experimental part of the work of Galbraith et al.[162] We also assume a full coherent photoionization with a sudden approximation approach where the effect of the width of the ionization pulse is ignored. Thus, while we cannot provide a full comparison with the experiment, the current work should unravel some general interpretation of the XUV induced dynamics.

Using a model with successive CoIn, the system evolves from the E state and descends to the D through the region of degeneracy where the derivative couplings driving the nuclear dynamics can break the symmetry of the system. In this work, we show that electron dynamics and the resulting gradient coming from a specific coherent superposition of adiabatic states, where phase matters, is responsible for the observed nuclear dynamics. By creating a superposition of two or more states, the initial electronic wavepacket is no longer an eigenstate of the electronic Hamiltonian and thus, the electronic wavefunction will show an oscillatory behaviour involving the initial composition of states. In a case of a two state system, it is known that the weight of the 2 states oscillate in time with a frequency which is inversely proportional to the energy gap between the states. Furthermore, the individual term of the full gradient (see eq. 5.1) can be evaluated using symmetry product and thus, we can determine which nuclear degrees of freedom Q_i (i.e. NM) can contribute to the overall gradient for a composition of electronic states I and II. The term is non-zero when the product of irreducible representations α yields the totally symmetric term E. Thus, the intrastate gradient is along the totally symmetric direction and the non-totally symmetric contributions come from the derivative couplings. In the case of benzene, the totally symmetric character is A_{1g} in the D_{6h} point group and A_g for the subgroup D_{2h}.

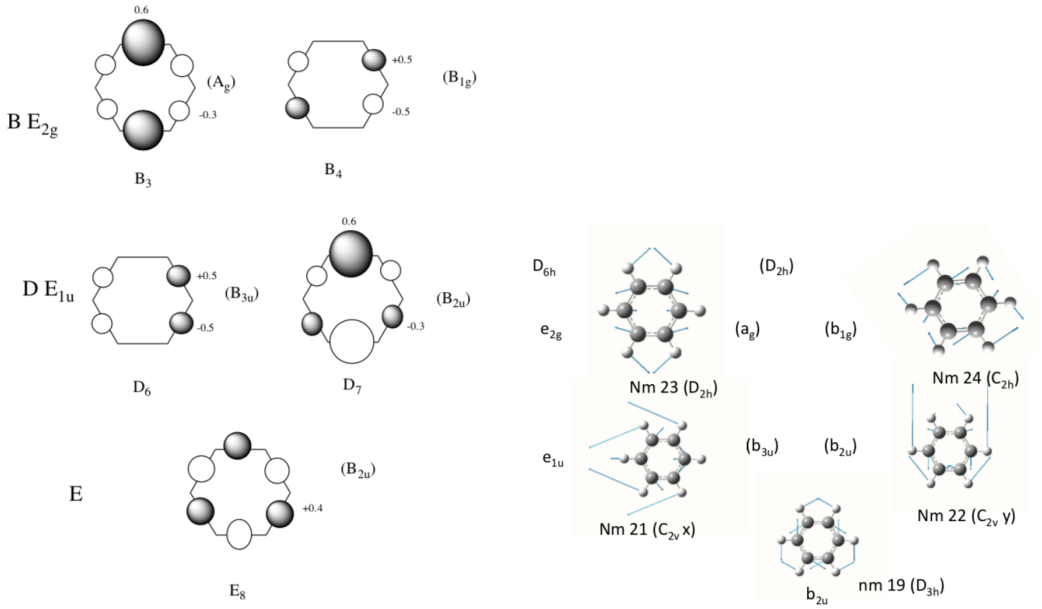

(a) (b)

Fig. 5.7: (a) Diabatic states (at time 0) in the permutation representation. E D B are spectroscopic notation (the π states are shown with orbital plots in Fig. 5.8), E_{1u}, E_{2g}, etc. refer to D_{6h} symmetry while the additional labels in brackets (B_{2u}) refer to irreducible representations in the D_{2h} symmetry point group. Each shaded lobe represents a positive contribution while an unshaded lobe is negative. (b) Computed NM spanned by the same permutation representation. They are ordered from lowest energy to highest. The nature of the symmetry lowering for each NM is indicated in parenthesis. The couplings of the electronic states and NM are indicated on Table 5.2

$$\alpha^{I} \otimes \alpha^{Q_i} \otimes \alpha^{II} = E \tag{5.2}$$

The main results shown in this section are presented as the average NM displacement and diabatic state populations (based on the initial quasi-diabatic states at the reference geometry). The reference states are defined using the Configuration State Functions (CSF) vector for the adiabatic states computed at the optimized geometry. The expectation values of these quantities are computed using a Gross Gaussian Populations (GGP) weighted average among all the 25 GWP. The reference diabatic states are given in Fig. 5.7a with their corresponding symmetry label.

As introduced before, there are two main driving factors for the nuclear and electron dynamics. The first one is the initial gradient (at time zero) that has components along non-totally symmetric modes due to the initial electronic state being a linear combination of two or more eigenstates. Because of the non-stationnary nature of the electronic wavefunction, the individual eigenstates population will oscillate in time and this phenomenon is referred to as Charge Migration (CM). Thanks to the rich symmetry of the benzene molecule, much of the electronic structure and nuclear dynamics is governed by symmetry rules.[162,168,169] Using the symmetry tools to determine the NM responsible for spawning the CoIn between pair of states, we can relate the specific compositions of electronic states to a specific set of nuclear motions (i.e. C-C stretches) and these NM would be part of the initial gradient. The other components of the nuclear dynamics we can predict are the NM that arises from CM due to the asymmetry of the electronic wavefunction (i.e. localized hole). The cationic eigenstates that are part of the superposition will display an oscillation in the diabatic state populations and by varying the weight of these cationic states, we can qualitatively determine the localized holes where the CM will occur. These oscillation patterns can be related to specific NM by visual correspondence using permutations representations by applying the symmetry operations on the localized hole using a localized orbital basis such as the 2p orbital on the carbon atoms in benzene. Thus, we can qualitatively determine where the CM occurs using the permutation obtained by applying the symmetry operation of the D_{6h} point group. Alternatively, the patterns of the CM can be determined by performing a simulation using frozen nuclei where there is no decoherence or dampening of the electron dynamics.[41,170]

5.3.2 Computational Details

In this work, we employed an active space of 15 electrons in 8 orbitals (see Fig. 5.8)with the initial orbitals optimized at the Complete Active Space Self-

Table 5.2: Nuclear degrees of freedom (NM) that displayed non-zero (i.e. asymmetric) gradient at the FC point due to derivative couplings and electron dynamics from a superposition of pair of states.

S Btates	NM from electronic coupling	NM from electron dynamics
E8 B3	19 22	19 23
E8 B4	21	19 24
E8 D7/D6	23/24	19 21/19 22
B4 B3	24	23 24
D7 D6	24	21 22

Consistent Field (CASSCF) level at the benzene D_{6h} neutral equilibrium geometry. The NM definition and geometry optimization of the neutral ground state of the molecule has been done using B3LYP/6-31G* level of theory. The dynamics have been performed in a reduced dimensionality where only 12 nuclear degrees of freedom are considered out of all 30 available for benzene. The degrees of freedom included in the dynamics are the in-plane C-C stretches and C-C-C angle bends. The nuclear wavefunction is described using a linear combination of 25 GWP, with a width of 0.1 NM unit (frequency and mass scaled atomic units) in position, using a momentum distribution around the FC point of the neutral optimized geometry and is propagated for 50 *fs* using a time step of 0.1 *fs* with the Runge-Kutta 5th order integrator. The initial electronic wavepacket is built using positive weights for all 8 states considered.

5.3.3 Results

The main objective is to rationalize how various initial combinations of adiabatic states can activate a specific nuclear motion and which component involved in the electronic mixing is responsible for the observed fragmentation patterns. The highest state considered is the 8th cationic state (labelled as E) and is the main state of interest in the work of Galbraith et al.[162] where they suggested a successive decay from the E states to lower states to explain the different lifetimes reported experimentally. The first result corresponds to a QuEh dynamics initiated on the

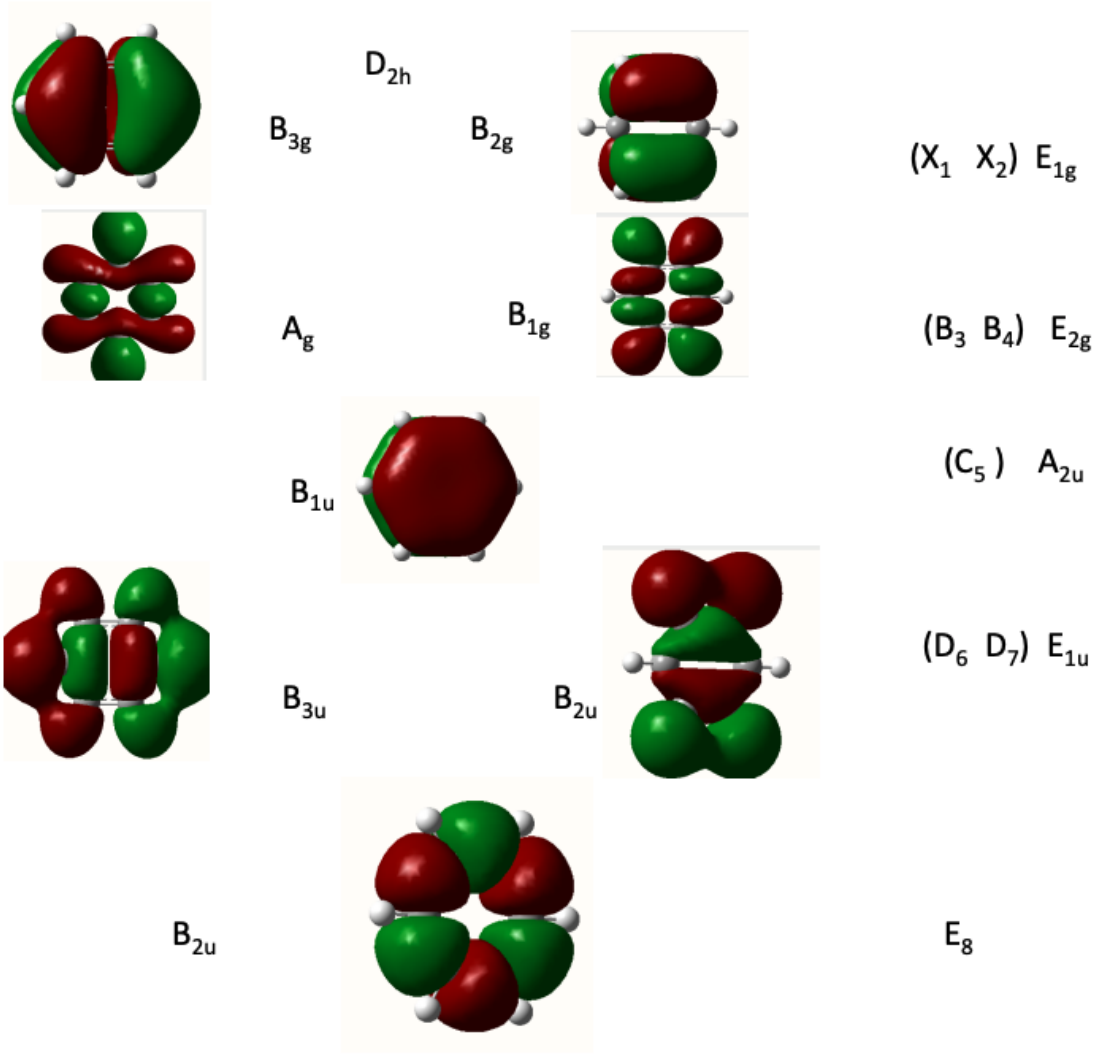

Fig. 5.8: CASSCF active space employed for the simulation. The symmetry labels for the MO are given in D_{6h} (right) and D_{2h} (left) symmetry point groups.

E state. Then, we rationalize how different 'pairs' of superpositions can steer the dynamics in a specific direction using symmetry arguments. Based on the work of Galbraith et al.,[162] we focus the mixing on the E, D and B states based on their importance in the nonadiabatic dynamics of the cationic benzene. Due to the nature of the B and D states being doubly degenerate, any superposition involving these states will include both degenerate states at the FC point. In the rest of the section, the results are presented in increasing order of number of adiabatic states involved in the initial superposition. The final goal is to explain the origin of the

different fragmentation patterns ($C_3H_3^+$ and $C_4H_4^+$) observed upon photoionization to the 8 cationic states without including the effect or the presence of the probing pulse.

Dynamics initiated on the E state

We begin with the nonadiabatic dynamics starting on the E states within the sudden approximation approach. The main goal of the dynamics initiated on a pure E state is the comparison of the QuEh results to the MCTDH simulation of Galbraith et al.[162] We can see that a simulation initiated on a single state only starts showing substantial electron dynamics once the nuclear wavepacket gets close to a region of degeneracy. Thus, pure state dynamics can be rationalized directly using a CoIn model with the underlying symmetry rules. After 7 *fs*, there is an electronic population decay from the E8 state to the D7 state and a large portion of it is transferred within 20 *fs*. Population transfer to the D6 only becomes significant at a longer time and this is a consequence of the separation of degenerate components when the symmetry of the system is lowered. Another important aspect is that while the D state is doubly degenerate at the FC point, in practice the D7 state is slightly higher in energy (by 0.0001 Hartree). Thus, D7 gets a faster population transfer from the E state compared to the D6 state. Furthermore, NM 23 is stimulated upon decay to the D state due to the symmetry nature of the mixing of E8 and D7.

E/D and E/B superpositions

From the dynamics initiated on the E state, we observe substantial nonadiabatic events leading to population transfer to the D state. By starting the dynamics on a superposition of E8 and D7/D6 states, a similar E/D population transfer can be seen at around 10 *fs* followed by a E/D7 and E/D6 electron dynamics (see Fig. 5.10). From the symmetry rule, a CoIn between E8/D7 or E8/D6 is spawned by

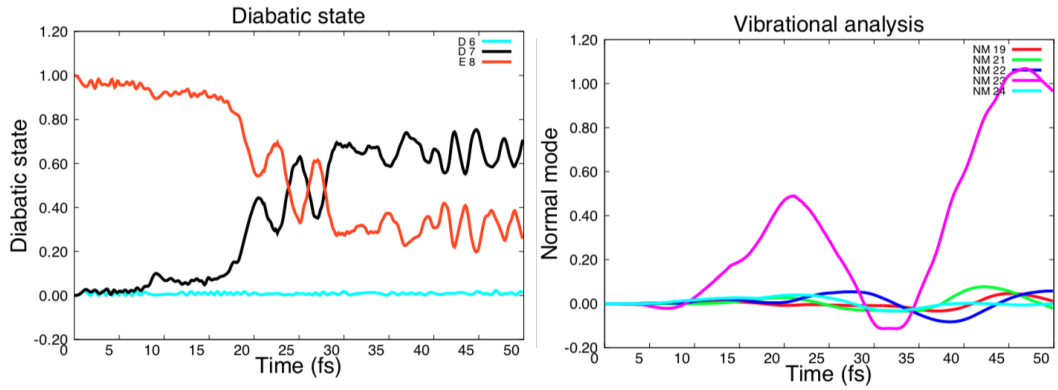

(a) (b)

Fig. 5.9: Decay of state E at an E/D CoIn and its resulting (a) electron dynamics (diabatic population) and (b) NM. All averages are computed using the GGP.

NM 23 and 24. In the case of dynamics on a pure E state, a decay to the D states slightly enhanced motion along NM 23 whereas starting from an initial coherent superposition, the dynamics are steered strongly along NM 23 and 24 from the beginning. One important note is that a small asymmetric motion along NM 19, 21 and 22 can be observed resulting from the E/D electron dynamics.

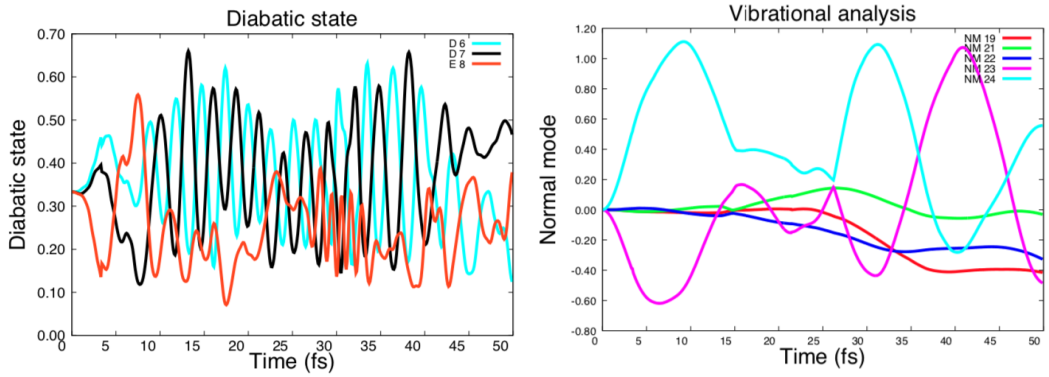

(a) (b)

Fig. 5.10: Dynamics with an initial superposition of E/D (E8, D7 and D6) and the resulting (a) diabatic state population and (b) NM. All averages are computed using the GGP.

In the case of a E/B mixing , as well as the D/B combination, the initial electronic wavepacket involves a superposition of non-adjacent electronic states (energy-wise at the FC point). By initiating the dynamics on a E/B mixing,

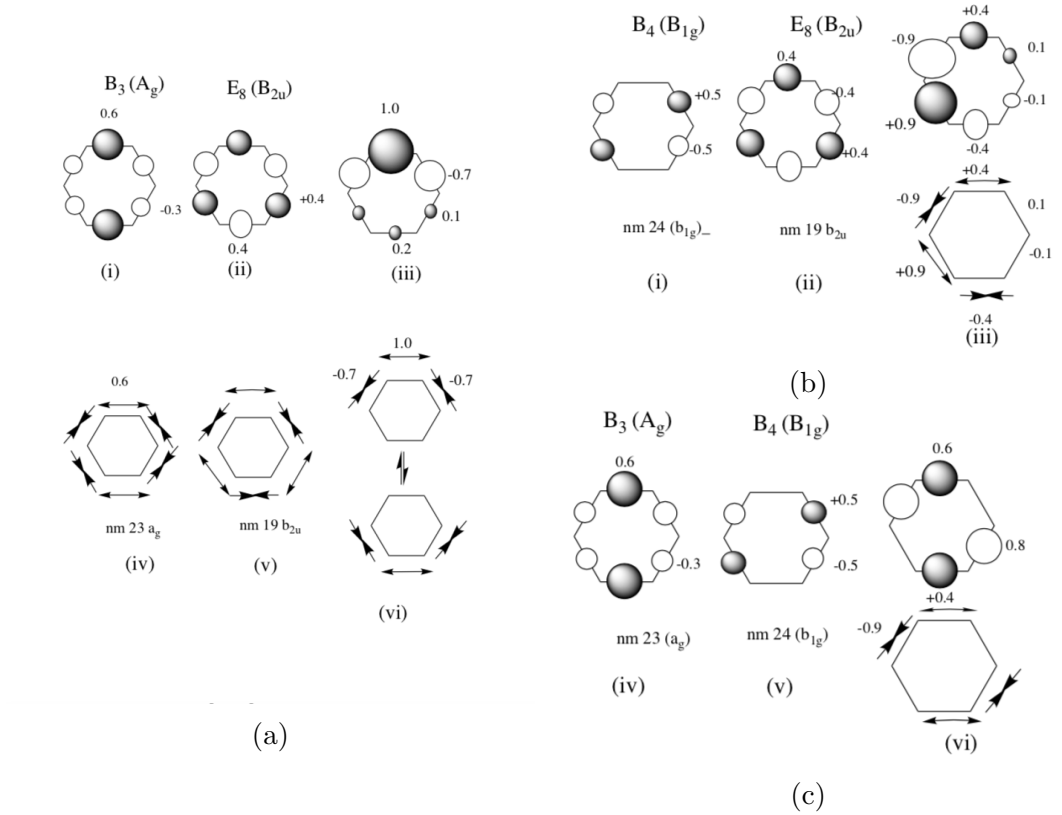

Fig. 5.11: (a) The superposition of a component of the B state (B3, part i) which is a component of the B state (with symmetry E_{2g} in D_{6h} and Ag in D_{2h}), mixed with E8 (part ii) (with symmetry B_{2u}) and a similar relation forNM 23 (part iv), and NM 19 (part v). A similar symmetry analysis is done for the mixing (b) B4 E8 (parts i and ii) and (c) B3 B4 (parts iv and v)

there is asymmetric motion for the nuclear wavepacket along multiple NM. Using symmetry, one can rationalize which pair of states is responsible for the observed nuclear motion components. A mixing of B states (B3 and B4) yields derivative couplings along NM 23/24 whereas the E/B3 and E/B4 superposition produces off-diagonal gradients along NM 19/23 and 19/24, respectively. A scheme of the symmetry analysis for the mixing of E/B states can be found in Fig. 5.11 The nonadiabatic dynamics of the combination E/B3 and E/B4 displays the typical type of motion normally seen at a Jahn-Teller CoIn.[171] Furthermore, the coherent superposition of E and B states shows population transfer to the D state after a few *fs* of dynamics.

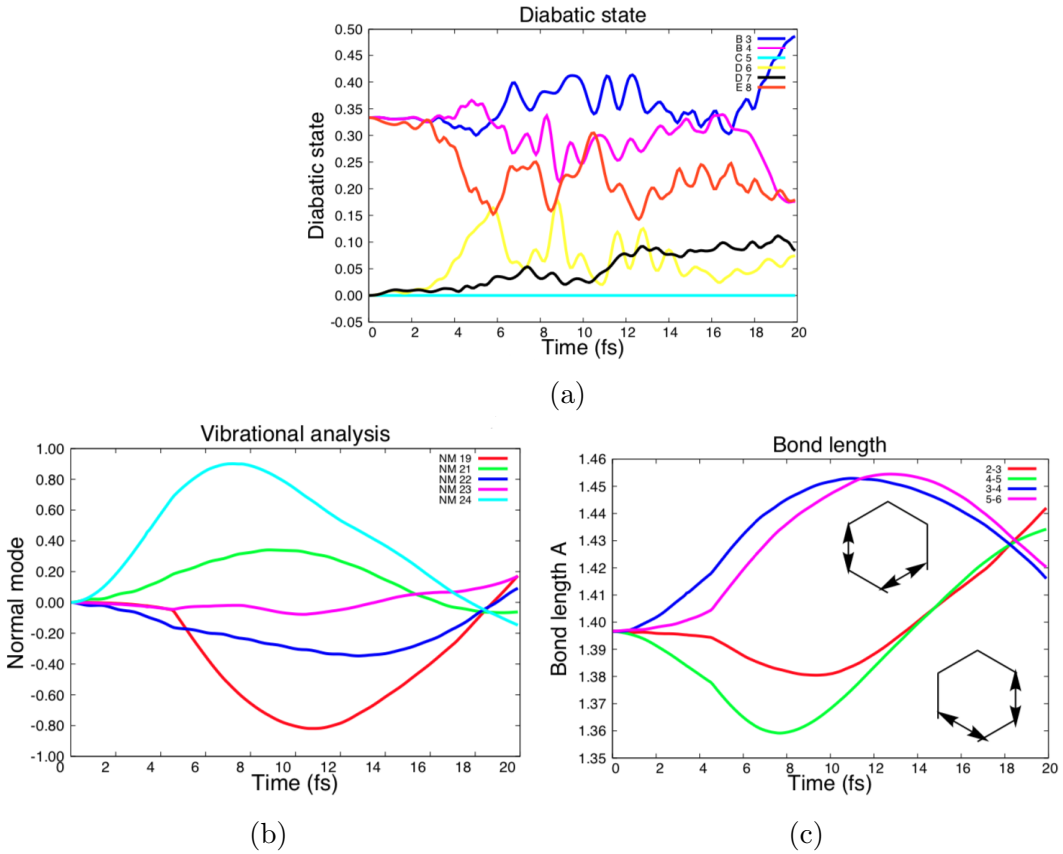

Fig. 5.12: Results of E/B, 3-state initial superposition with QuEh dynamics. The label E8, D (D6,D7), etc. refer to the singly ionized states in Fig. 5.7a. The atom labels 1-6 in the carbon atoms start at the top of the hexagon and follow the order clockwise. The results shown are the (a) diabatic state populations, (b) NM and (c) bond vibrations for dominant stretches.

The pair of states involved in the initial superposition yield different initial nuclear motion which in turn leads to a potentially different fragmentation pattern. With the E8/B3 mix, the combination of NM 19 and 23 gives rise to C_2H_2 and C_4H_4 fragment. A similar pattern is observed for the E8/B4 mix but the potential C-C bond-breaking occurs on a different part of the benzene molecule. In the case of equivalent carbon and hydrogen atoms, no difference would be found between these two pairs but from a point of view of symmetry, it displays a different energy transfer along some specific C-C stretching. In Fig. 5.12c, one can observe a coherent stretch of a pair of C-C bonds which is either a combination of C3-C4/C5-C6 or C2-C3/C4-C5. Both of these motions are individual precursors to

the C_2H_2 and C_4H_4 fragmentation patterns. Fig. 5.12b shows the nuclear motion in terms of NM which allows us to highlight the symmetry rules resulting from the superposition of electronic states. The comparison between Fig. 5.12c and 5.12b give us the links between the resulting C-C bond stretch to a combination of NM motion at a specific time. In the case of B3/B4 mixing, the initial bond stretching leads to a formation of two C_3H_3 unit. The initial motion of the E/B mixing (either B3 or B4) produces vibrations that lower the symmetry of the molecule to a C_{2v} point group while the resulting nuclear motions from a B3/B4 superposition correspond to a lowering of the symmetry to C_{2h}.

The relative phase between the states involved in the initial superposition also plays a role depending on which specific C-C bond is stretched. Taking different mixing phases, without changing the weight, yields multiple equivalent sets of results with different fragmentation pattern for the C_2H_2 and C_4H_4 part and they can be related to each other using symmetry operations. The results show the energy deposition into specific nuclear motion based on a set of specific initial conditions. However, due to the numerical challenge of the dynamics some discontinuity can be observed on Fig. 5.12b and 5.12c. These can arise from the fast electron dynamics and it can become difficult to smoothly integrate the electronic EOM. Thus, the current simulations only aim to provide a qualitative picture.

B/D superposition

A superposition of B/D states also results in electron dynamics between non-adjacent states similar to the case of the B/E mixing. The results are shown in Fig. 5.13 The D6/D7 and B3/B4 couplings yield a gradient along NM 24 which corresponds to a Jahn-Teller dynamics. We can also observe an asymmetric motion along NM 21 and 23 resulting from the electron dynamics. A similar dynamics with motion along NM 23 and 24 can be seen on the B3/B4 superposition (as a consequence of the electron dynamics too). An important aspect of the results

is the electron dynamics and population transfer between adiabatic states when starting on a superposition of non-adjacent states (as shown in the B/E and B/D mixing) and that the nonadiabatic events take place without an explicit motion through a CoIn leading to a state population decay. Furthermore, the B/E and B/D mixing can control the initial coherent bond stretching leading to either a C_2H_2 and C_4H_4 fragment or two C_3H_3 moieties.

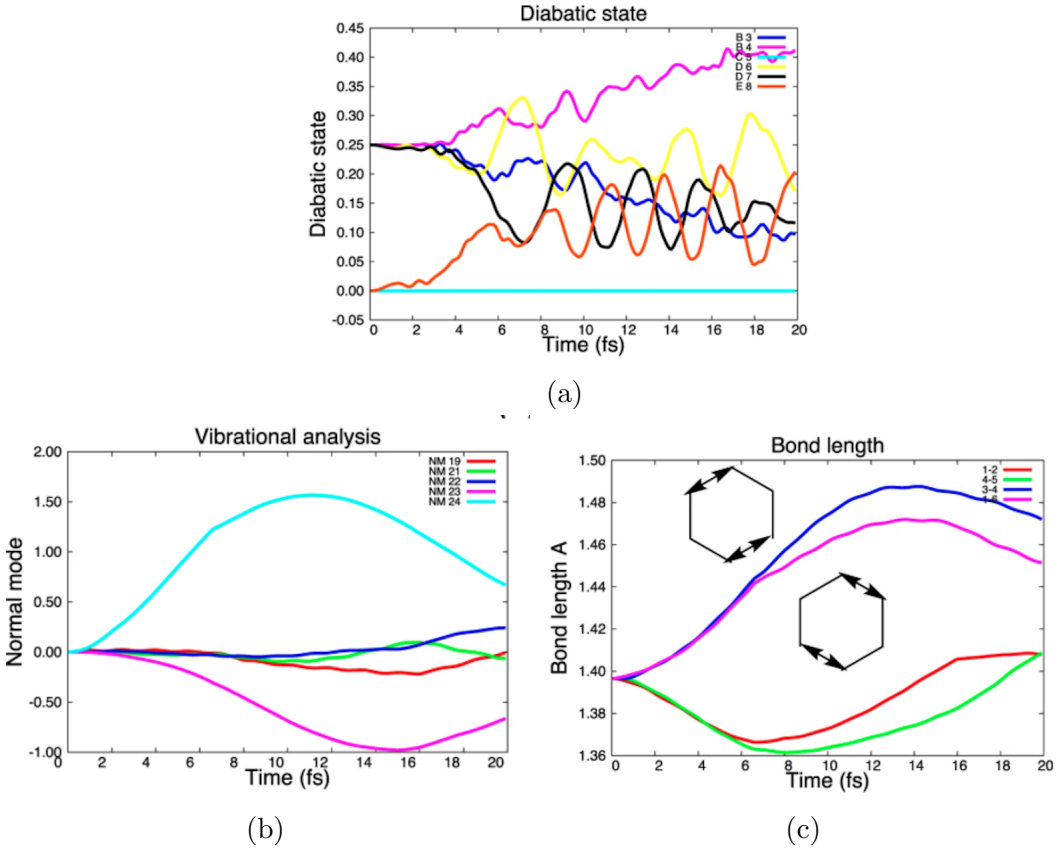

Fig. 5.13: Results of D/B, initiated on a 4-state superposition with QuEh dynamics, for the (a) diabatic state populations, (b) NM and (c) bond vibrations for dominant stretches.

8-states dynamics

We now focus on the dynamics initiated on a coherent superposition of the 8 cationic states. Using the photoelectron cross section from the work of Galbraith et al., the initial electronic wavepacket was built using the weight X1 0.051, X2 0.051, B3 0.179, B4 0.179, C5 0.449, D6 0.028, D7 0.028, and E8 0.0311. From

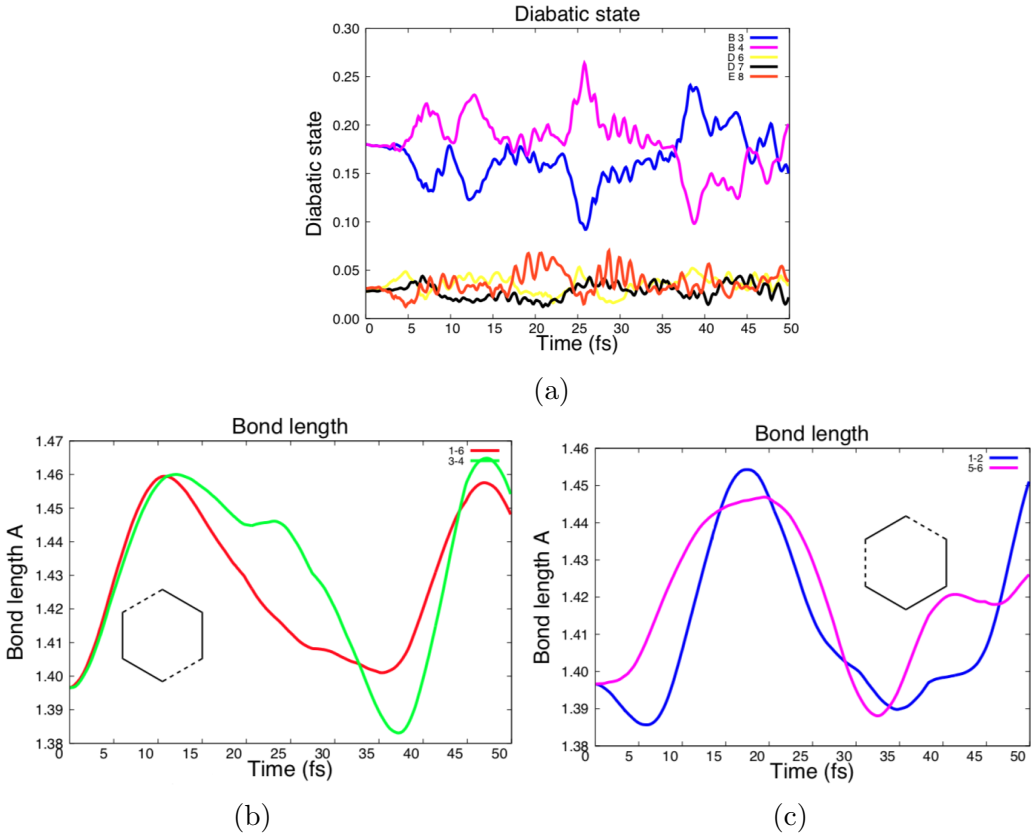

Fig. 5.14: Results of the 8-state QuEh dynamics using the coherent superposition obtained from the photoelectron cross sections. The labels E8, D7, and D6 refer to the singly ionized diabatic states according to Fig. 2a in Ref. 162. The atom labels 1-6 on the carbon atoms start at the top of the hexagon and increment clockwise. (a) Populations of the diabatic states. (b), (c) Bond vibrations for dominant stretches. The data in all panels is obtained by weighting the GWP by their GGP

the experimental cross section, we cannot determine to which extent the states are populated coherently from the photoionization pulse and furthermore, we do not have any information on the relative phase between each state. The two main assumptions we are making for the dynamics is (i) fully coherent population of the cationic states and (ii) a coefficient with positive and real values for all states involved. Upon absorption of the XUV pulse, it has been shown experimentally that the molecules will either fragment into two C_3H_3 parts or a C_2H_2 and a C_4H_4 part.

From the dynamics initiated on the 8 states, we can identify different types of coherent C-C bond oscillations. Using the positive electronic state's coefficient,

the coherent bond oscillation involves the pair C1-C6/C3-C4 and C1-C2/C5-C6 as shown in Fig. 5.14 which is consistent with the potential fragmentation pattern observed experimentally later on. Different fragmentation patterns yielding the same final fragment can be obtained by changing the relative sign of the electronic state's coefficients. However, the actual fragmentation phenomenon occurs at a longer timescale and relies on multiple factors such as the vibrational energy deposition, energy barrier to bond-breaking and orientation effects. From the current nonadiabatic dynamics, we can provide insights into where the vibrational energy is deposited and which nuclear motion are enhanced based on specific initial electronic conditions.

5.4 Controlling nuclear-electronic dynamics with a pulse

5.4.1 Background on ethylene cation

Using the rich symmetry of benzene, we were able to predict the initial outcome of the dynamics in terms of initial gradients and electron dynamics using group theory. In this section, we include the effect of a femtosecond IR laser in the simulations and we will rationalize its mechanism by comparison with simulations without pulse.

For that purpose, Ethylene is used as the simple model for investigating the dynamics of a π radical system which has been extensively studied both in an experimental and theoretical approaches. Furthermore, it is a system that possess a fairly rich symmetry with a D_{2h} symmetry point group.

From the work of Ludwig et al.,[172] it is shown that after photoionization of ethylene with an XUV pulse from HHG source, the fragment yields can be altered with an IR probe pulse. The XUV photon energy allows the ionization of ethylene up to 6 states and the excitation spectrum shows that all states can be populated

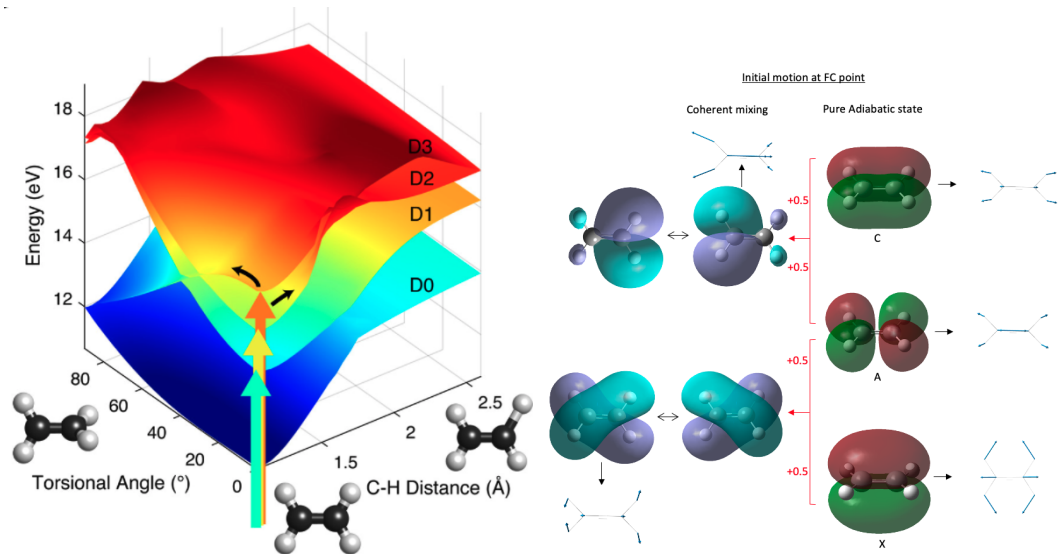

(a) (b)

Fig. 5.15: (a) PES of the 4 lowest electronic states of ethylene cation along the CH stretch coordinate and torsional motion. Reproduced with permission from Ref. 172. Copyright 2016 American Chemical Society. (b) Model for coupled electron-nuclear dynamics starting from (left) a coherent superposition of states with the resulting initial gradients or a pure adiabatic dynamics on the right. The two symmetrical structure represent the pairs of 'localized' holes for a given mixing of adiabatic states.

with a single pulse with most of the population on the 4 lowest states. The dynamics was then probed by a IR pulse to determine the timescale of the internal relaxation (isomerization) and it was reported to be 30±3 *fs*. Combined with previous theoretical works,[172,173] the mechanism of the excited state decay in the cationic manifold of ethylene is explained in term of successive decay through CoIn driven by a torsional motion and an in-plane C-H motion as show by the model in Fig. 5.15a. The overall dynamic observed experimentally upon photoionization to multiple cationic states was explained using an incoherent superposition of states which is simply a weighted contribution from individual simulation initiated on a different cationic state.

In a more recent experimental work, Lucchini et al. initially pump the ethylene on a superposition of 5 states with three different harmonics from a HHG laser source.[174] They observed different fragment yields based on the harmonics used

and they shows the dependence of these fragment yields on the time delay between the XUV pump and IR probe pulses.

While previous theoretical works used an incoherent superposition of state to rationalize the experimental results, we attempt to rationalize the dynamics as a coherent superposition of cationic states by using the QuEh method. The Ehrenfest approach of this method allow us to define coherent superposition of states and simulate the subsequent nuclear dynamics.

As introduced before, with a coherent superposition of states, there are two driving forces for the short-term dynamics: The initial gradient (see eq. 5.1) and the CM that arises because of the non-stationary nature of the electronic wavefunction (see Fig. 5.15b). The initial gradient can be determined qualitatively from symmetry product (see eq. 5.2) where the nuclear degrees of freedom that coupled the states (i.e. derivative coupling) are part of the initial gradient on top of the intrastate (i.e. adiabatic) gradient of the individual electronic state. The second component is the electron dynamics (i.e. electronic population transfer) which is a well known aspect of the coupled electron-nuclear dynamics at a CoIn and we expect to observe it at a lesser amplitude outside of regions of degeneracy as a result of coherent state mixing.

In this work we will study different coherent superpositions of 3 of 5 cationic states: those associated mainly with the CH bonds. The weights of the 3 adiabatic states have been chosen in a systematic pair wise way to rationalize the dynamics. In addition, the nuclear dynamics was steered via means of a control IR pulse.

5.4.2 Computational Details

The CAS-CI active space is generated using the cationic state-average CASSCF (over 5 states) canonical Molecular Orbitals (MO) at the neutral ground state geometry and consists of 11 electrons in 7 orbitals (see Fig. 5.16). The initial electronic wavefuncion is defined as a linear combination of two adiabatic state

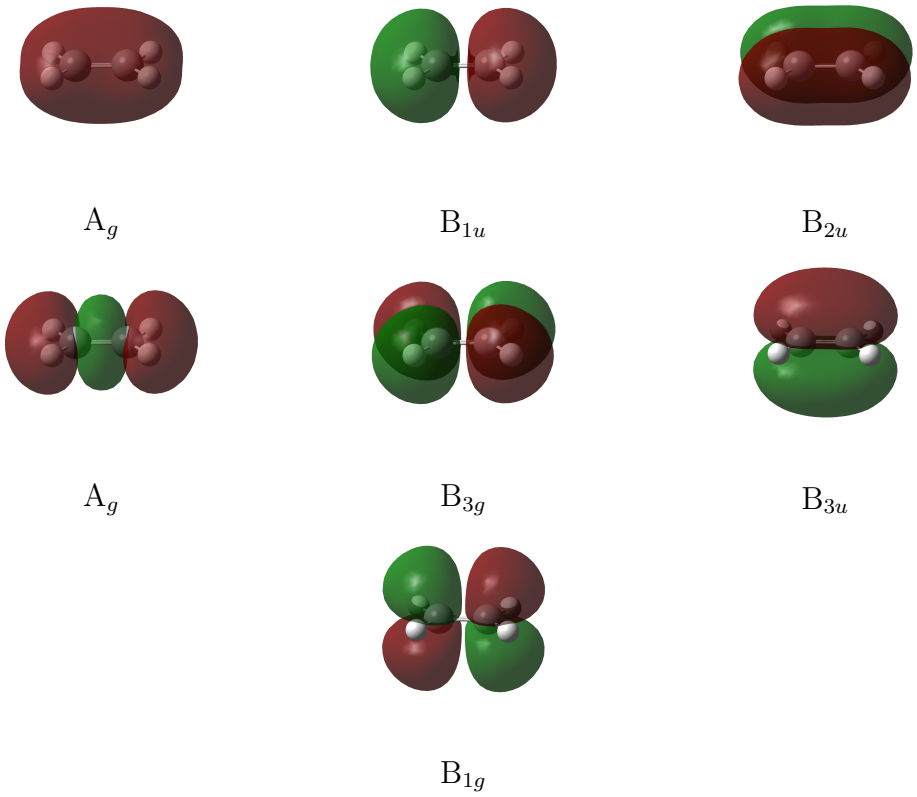

Fig. 5.16: CASSCF active space employed for the ethylene cation simulation defined at the FC geometry.

with positive coefficients at the initial geometry.

The nuclear wavefunction is represented as a linear combination of 25 GWP in a full shell around the neutral ground state S_0 FC point in momentum distribution using a Local Harmonic Approximation (LHA) expansion from a frequency calculation at B3LYP/6-31G* level of theory. The Runge-Kutta 5th order integrator is used and the wavefunction is propagated for a total simulation time of 50 *fs* with a time step of 0.01 *fs*.

The electric field of the pulse $E(t)$ used in the dynamics is defined by a gaussian function (see eq. 5.3) with the parameters given in Table 5.3 and is linearly polarized along the molecule axis (i.e. C=C double bond).

$$E(t) = E_0 \cdot \cos(\omega(t - t_0) + \gamma) \cdot \exp\left[-\left(\sqrt{\frac{2\ln(2)}{w^2}}(t - t_0)\right)^2\right] \tag{5.3}$$

5.4.3 Results

The dynamics is initialized on a superposition of pair of cationic states with a focus on the one relevant for the formation of hole in CH bonds. Thus, the results presented here are for a mixing of the $^2B_{3u}$, $^2B_{3g}$ and $^2B_{1u}$ states (at the FC point). The current work is focused mainly on comparing the difference in dynamics between the simulations with the presence of an IR pulse and without it. All NM are included in simulations. However, the attention is focused on the nuclear motions responsible for the CH bond stretching and couplings between electronic states. The symmetry notation is used to refer to the (initial) state mixing at the FC point and the cationic state labels D_x refer to the adiabatic state ordered by energy.

As introduced before, the short-term dynamics, in absence of pulse, is controlled by the initial gradient of the superpositions of states and the resulting CM producing instantaneous gradient. From the symmetry rules, we can determine the degrees of freedom that will contribute to the gradient but there is no information on the individual amplitude which can only be determined via an electronic structure calculation. As for the CM, we can determine the groups of localized holes related to each other under permutation representations which are the turning points of the electron dynamics.

Table 5.3: Parameters of the pulse included in ethylene cation dynamics.

Quantity	SI units	Atomic units
E_0	5 x 10^9 V/m	0.0098 a.u.
ω	3.7 x 10^{14} Hz	0.05625 a.u.
t_0	20 *fs*	826.8275 a.u.
γ	0	0
w	15 *fs*	620.1206 a.u.

Table 5.4: Irreducible representation in the D_{2h} point group of the symmetry products between two cationic states of ethylene with the symmetry label given in parenthesis.

	D_0 ($^2B_{3u}$)	D_1 ($^2B_{3g}$)	D_2 (^2A_g)	D_3 ($^2B_{2u}$)
D_0 $^2(B_{3u})$	A_g	A_u	B_{3u}	B_{1g}
D_1 ($^2B_{3g}$)	A_u	A_g	B_{3g}	B_{1u}
D_2 (^2A_g)	B_{3u}	B_{3g}	A_g	B_{2u}
D_3 ($^2B_{2u}$)	B_{1g}	B_{1u}	B_{2u}	A_g

From the resulting symmetry products in Table 5.4 and the irreducible characters of the NM given in Fig. 5.17, we can rationalize the initial nuclear dynamics observed in Fig. 5.18b and 5.18f. In both results, the nuclear wavepackets show substantial motion along NM 10 which corresponds to the symmetric CH stretching. Moreover, an oscillatory pattern with relatively small amplitudes for NM 4 (torsion, A_u) and 9 (asymmetric CH_2 stretching, B_{1u}) is observed for the $^2B_{3u}/^2B_{3g}$ and $^2B_{3g}/^2B_{1u}$ mixing, respectively. These two nuclear degrees of freedom of symmetry correspond to motion that can couple the states involved in their respective superpositions (see Table 5.4). Furthermore, these periodic changes in the value along NM 4 and 9 are caused by the electron dynamics as the change in the electronic state coefficients leads to a different weight for the individual term of the gradient. In both cases, the oscillatory motion lasts up to around 5 *fs*. Around that point, one can observed substantial asymmetry (i.e. a non-zero average value) slowly building up along NM that were initially inaccessible due to symmetry.

As for the electron dynamics, one can observe minor adiabatic state population transfers from the D_1 to D_2 when the simulation is initiated on a superposition of $^2B_{3u}/^2B_{3g}$ (see Fig. 5.18a). Moreover, almost no decay to the ground state is observed despite previous theoretical results identifying a fast decay mechanism through the torsional channel.[173] Whereas for dynamic initiated on the $^2B_{3g}/^2B_{1u}$ mix, rich electron dynamics can be observed in Fig. 5.18e with a fast population decay from the D_3 state to D_2 state in about 10 *fs*. Additionally, substantial population transfer to the D_0 can be seen at 30 *fs*.

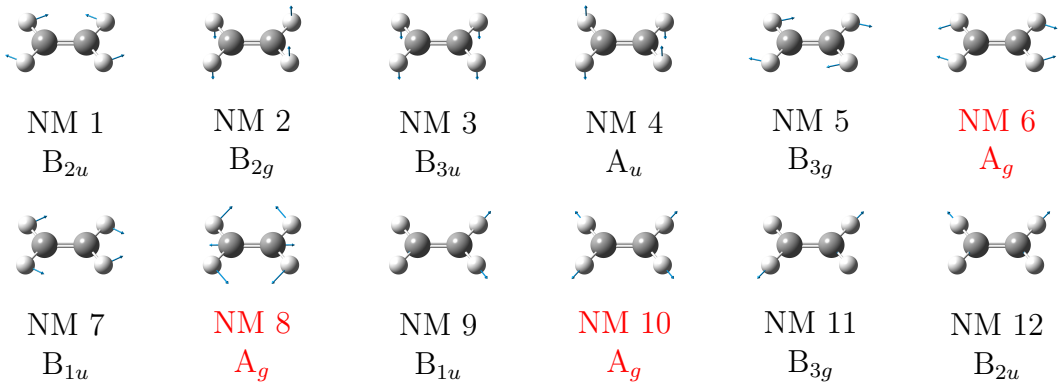

Fig. 5.17: NM basis obtained from a B3LYP/6-31G* frequency calculation at the optimized neutral ground state of ethylene. and their irreducible representations written below with the totally symmetric motion in red.

For the $^2B_{3u}/^2B_{3g}$ superposition of states (see Fig. 5.18d), upon inclusion of the pulse in the simulation, the displacement along NM 4 is greatly enhanced. As a consequence of motion along non-totally symmetric NM such as torsion, the symmetry point group of the molecule is lowered and thus, more nuclear degrees of freedom become symmetry allowed given rise to a Jahn-Teller like effect. Despite the large changes observed in the nuclear dynamics, the adiabatic state populations are barely affected by the presence of the pulse (see Fig. 5.18c). A slightly bigger difference can be observed at longer timescale. It appears that for a superposition of $^2B_{3u}/^2B_{3g}$ states the oscillating electric field does not provide substantial photo-excitation to a different electronic state and thus, the pulse seems to induce non-resonant changes in the molecular dynamics.

By including the pulse in the dynamics initiated on superposition of $^2B_{3g}/^2B_{1u}$ states, a greater decay to the D_2 followed by the D_1 state is observed (see Fig. 5.18g) and the associated nuclear motion shows a different behaviour for NM 9 (see Fig. 5.18h). By comparing the nuclear dynamics in Fig. 5.18f and 5.18h, one can observed a slight change initially along the other three NM for CH stretch and the difference grows bigger as the dynamics progress. In comparison to the superposition of $^2B_{3u}/^2B_{3g}$ states, the electron and nuclear dynamics of the $^2B_{3g}/^2B_{1u}$

demonstrate a greater difference with the inclusion of an oscillating electric field.

Whilst the current results show that the use of an IR pulse centred at 20 *fs* can affect the molecular dynamics, the coupled electron-nuclear dynamics seems to be relatively complex. However, an attempt at rationalizing the pulse can be done using group theory by evaluating the motion that will interact with the pulse based on its alignment. In other words, a motion along a specific NM is enhanced if the product of the individual irreducible character of the electronic states I and II , pulse direction E and NM Q_i yields the totally symmetric term which is A_g in the case of ethylene.

$$\alpha^{I} \otimes \alpha^{E} \otimes \alpha^{Q_i} \otimes \alpha^{II} = A_g \tag{5.4}$$

Thus, the pulse can yield an intra and interstate states and we can use symmetry product to determine the nuclear modes enhanced by applying an electric field in a specific direction. By orienting the oscillating electric field along the molecular axis, NM 7 and 9 spanned by B_{1u} will be changed due to the interaction of the electronic wavefunction and electric field along that direction for the intrastate effect. It is rather challenging to separate the 'natural' nonadiabatic events from the interference of the electron dynamics with the pulse. From the results, it seems that the pulse doesn't greatly affect the population transfer between electronic states and thus, a change is induced in the molecular dynamics with a non-resonant pulse (i.e. no visible photoexcitation).

The current preliminary work on ethylene cation only provides an insight into the effect of the pulse in dynamics. Further analysis of the electric field induced dynamics with symmetry will require simulation by aligning the pulse in different directions.

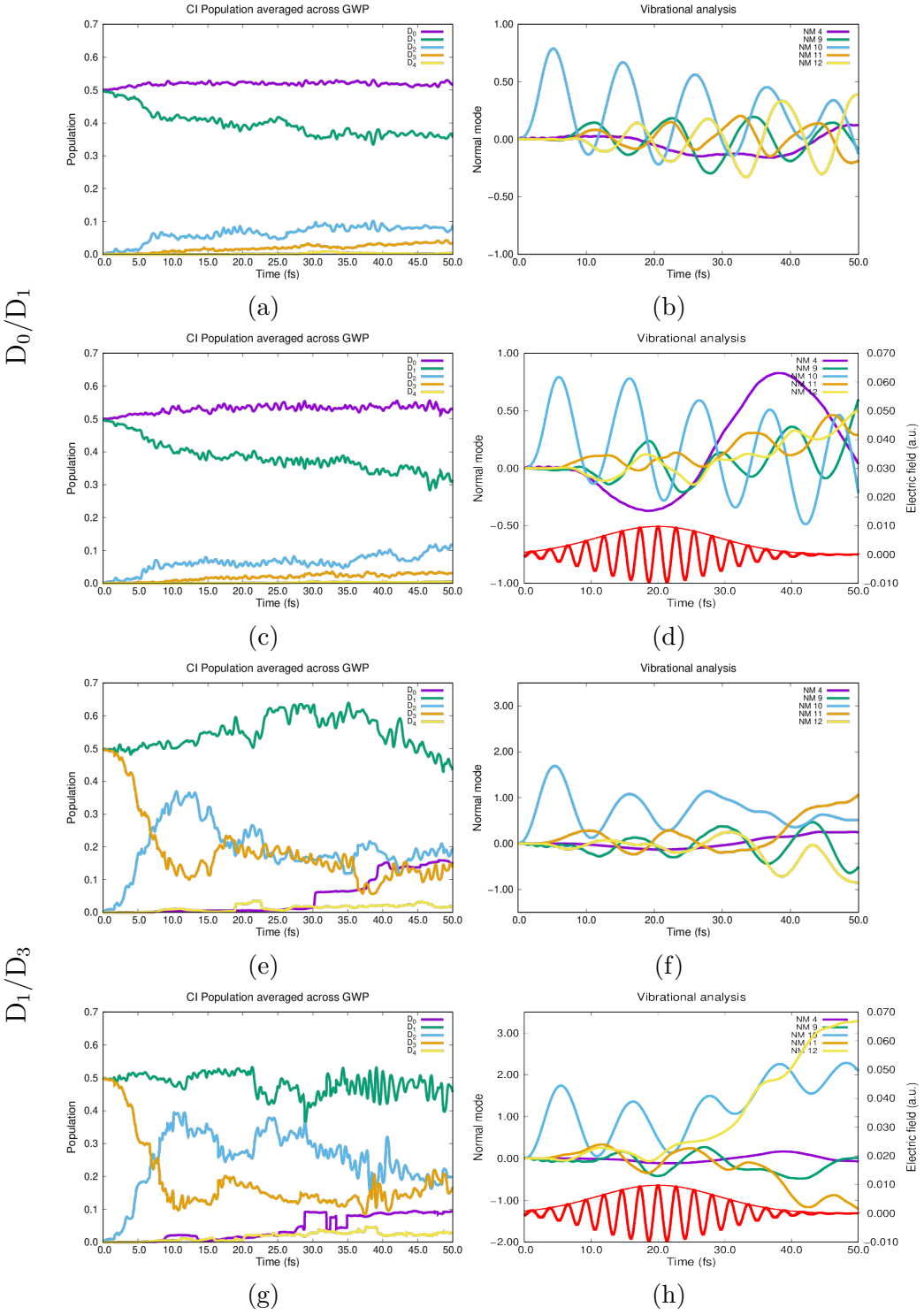

Fig. 5.18: Average adiabatic state populations and associated NM displacement for simulation initiated on a superposition of (top) $^2B_{3u}/^2B_{3g}$ and (bottom) $^2B_{3g}/^2B_{1u}$. The average is done over the 25 GWP with their GGP. The oscillating electric field of the pulse is shown in red (with electric field in atomic unit, right vertical axis)

5.5 Summary

The nonadiabatic dynamics of the cation of all-trans octa-3,5,6-trieniminium (rPSB4), benzene and ethylene has been simulated using the QuEh method for investigating the importance of CM for nuclear dynamics and its potential control with a laser pulse. From the results of rPSB, it is shown that the deactivation mechanism of the photoexcited species can be controlled by designing a coherent superposition of electronic eigenstates. The coupled electron-nuclear dynamics of the molecule is driven by two main factors: the initial gradient and the CM due to the non-staionary nature of the electronic wavefunction. The initial gradient is a linear composition of intra and inter-state gradients.

The results on benzene cation shown that the initial electron and nuclear dynamics can be explained using group theory by determining the symmetry allowed motion arising from a superposition of electronic states. In the case of an electronic eigenstate, the only possible direction of the nuclear gradient is along the totally symmetric NM. To determine the non-totally symmetric components of the initial gradient, we identify the nuclear degrees of freedom responsible for coupling the pair of states considered symmetry wise. Thus, by creating a coherent superposition of states, it possible to steer the nuclear dynamics in specific direction and the system will display CoIn like dynamics even outside of region of degeneracy as shown by the results on benzene cation.

By introducing a pulse in the simulation, one can induce change in the nuclear dynamics of the system. Furthermore, the effect of the pulse can be partially rationalized using symmetry arguments and thus, the alignment of electric field can play a role in the dynamics. However, from the results of ethylene cation, it can be seen that the coupled electron-nuclear dynamics is relatively complicated and further data is needed to provide a more complete description of the mechanism of the pulse in the simulation.

The short-term dynamics provide rich electron dynamics induced by superposition of states and it opens a possible path for possible coherent control. For a short propagation, the real quantum nuclear wavepackets can be well represented with a small basis but as the simulation progresses, the nuclear wavepackets spread further and further in configuration space and thus, a larger number of GWP is required to more accurately reproduce its evolution in time. However, with the numerical challenges of the method such as small integration steps and potential linear dependency of the GWP, the simulation can only provide qualitative results for the dynamics of the system.

Chapter 6

Conclusions

The aim of this thesis is to show how one can try to control chemical photoreactivity by rationalizing the results observed in attosecond spectroscopy. The experimental background and theoretical methods introduced in chapter 2 gives a framework for the investigation of Charge Migration (CM) using a fully quantum treatment starting from the time-dependent Schrödinger equation (TDSE). The CM is a purely electron correlation driven effect and the resulting dynamics originate from the non-stationary nature of the electronic wavefunction (i.e. superposition of eigenstates).

The full methodology and protocols are presented in chapter 3. The dynamics in the Direct Dynamics variational Multi-Configurational Gaussian (DD-vMCG) method can be seen as a set of coupled basis functions following quantum trajectories. The Equations-Of-Motion (EOM) are obtained by expanding the nuclear wavefunction as a linear combination of Gaussian Wavepackets (GWP) and by applying the Dirac-Frenkel variational principle. By taking the single-set formalism, the GWP evolves on a Potential Energy Surface (PES) that is a linear combination of diabatic states with time-dependent coefficients. This yields an Ehrenfest-like PES and by taking a further step into the construction of the electronic wavefunction with an Ehrenfest approach, the resulting method is Quantum-Ehrenfest (QuEh). The advantage of doing the full Ehrenfest approach within the electronic

structure is the lower computation cost for the evaluation of the time-dependent PES compared to evaluating the same quantities for N electronic states. However, it comes at the cost of evaluating the derivatives of the PES of a non-eigenstate of the electronic Hamiltonian which is more costly than for eigenstate (i.e. due to some terms being zero for an eigenstate). Furthermore, a Complete Active Space Configuration Interaction (CAS-CI) method is employed for the electronic structure method which means that the wavefunction is optimized with respect to the configuration interaction coefficients but only a single second order step is employed for the orbital optimization.

The QuEh method requires the use of very small time steps to allow stable and smooth integration due to the fast electron dynamics (e.g. a full cycle of electronic population oscillation within 1 femtosecond). As the small time step and integrator for the electron dynamics are within the electronic structure method (i.e. prevent the use of a database), there is a predictable number of evaluations of the PES at each time step and thus, optimal speed-up can be achieved with parallelization by performing the electronic structure calculation on multiple processes at the same time. To further enhance the preexisting parallel interface of DD-vMCG (done with Open Multi-Processing Interface (OpenMP)), an extra layer of parallelization is added with the Message Passing Interface (MPI). This allows an execution of the program on computing architecture without shared memory such as parallelization across computing nodes. To allow usage of DD-vMCG with both parallel interfaces and the various possible options such as use of a database and diabatization method, the code sections related to database handling are rewritten using Structured Query Language (SQL). Finally, the last development involves implementing a light pulse interaction in the QuEh method. This is done within the dipole approximation and the dipole-electric field term is added within the Fock matrix construction of the Complete Active Space Self-Consistent Field (CASSCF)

code in GAUSSIAN.

In chapter 5, the development version of QuEh which has a MPI parallelization layer (and SQL code) has been employed for various applications on molecular systems in the context of simulating photoionized induced dynamics. By carefully selecting the initial coherent superposition of electronic states the nuclear dynamics can be steered in a specific direction by tuning the weight of the individual states. It was first demonstrated by the example on retinal Protonated Schiff Base (rPSB) that the alternation of single and double bonds can be controlled by varying the initial conditions for the electronic wavefunction.

Furthermore, the resulting dynamics from a specific superposition of states can be predicted using symmetry rules. By applying the symmetry analysis for Conical Intersections (CoIn) between electronic states of specific character (i.e. irreducible representation), one can evaluate which nuclear degrees of freedom can be considered as active (responsible for nonadiabatic events) or as spectatory motion (i.e. bath vibrational mode). The same analysis can be done for a superposition of electronic states even away from region of degeneracy and a similar CoIn electron dynamics can be seen with fast population oscillation within a few femtoseconds. By using the benzene cation and its rich symmetry, short-term nuclear dynamics based on the initial gradient and CM with a period based on the energy gap between states can be predicted using symmetry rules.

Finally, the work on ethylene cation shows how one could control the coupled electron-nuclear dynamics with a subsequent probe/control laser pulse. The mechanism of the infrared (IR) laser on the dynamics is being explained in term of symmetry but further works are needed to investigate effects such as the orientation of the pulse and time delay on the molecular dynamics.

Using the QuEh method, it is possible to simulate coupled electron-nuclear dynamics for system initiated on a superposition of eigenstates. The nuclear dy-

namics with GWP following quantum trajectory provide us the ability to quickly converge to the ideal nuclear wavepackets dynamics using a relatively small number of basis functions. The symmetry of the initial molecular wavefunction based on its electronic composition offer us the possibility of predicting short-term dynamics where the molecular wavefunction still has its symmetry and coherence in term of totally and non-totally symmetric motion. Furthermore, the inclusion of the pulse in dynamics opens the door for the coherent control of molecules at a short timescale. However, the use of a truncated nuclear basis can lead to unconverged dynamics at longer timescales due to the need of more basis function to properly map the whole nuclear wavepacket. Starting the simulation with a larger number of basis functions can mitigate the poorer convergence at longer time but it can lead to linear dependency of the nuclear basis which can give rise to numerical instability during the propagation. Furthermore, the fast electron dynamics require the use of small time step size for the simulation and the evaluation of the time-dependent PES with a fast oscillation in the electronic coefficient can lead to unsmooth integration for the time evolution of the electronic wavefunction. Despite the computational effort gain of only calculating the derivatives for an effective single time-dependent state, the numerical instability in the evaluation of these nuclear gradients and Hessians can lead to a substantial error build-up over time. Thus, currently, the QuEh method can provide accurate insight in the molecular dynamics at short-time but the longer timescale dynamics is only qualitative.

Further development work on the QuEh method is required to expand its scope and reliability for simulation of charge-drive dynamics. Using different (adaptive) step size for electronic step or interpolation of the electronic population changes could provide a more robust propagation scheme and potentially solve the numerical instability encountered in the evaluation of the derivatives of the PES.

Future works on coherent control with QuEh will focus on how the parameters of the laser pulse such as the time delay, width and phase can affect differently the molecular dynamics . In the last case, multiple theoretical works can be found in the literature on how the Carrier-Envelope Phase (CEP) of short pulse (i.e. few cycles) can affect the coupled electron-nuclear dynamics close to the vicinity of a CoIn.[175,176]

Appendix A

Theory

A.1 Molecular dynamics

A.1.1 The Schrödringer Equation

The quantum mechanical study of molecular systems is done by solving the Schrödinger equation, named after Erwin Schrödinger for his work on the formalism on the description of atoms and molecules using a wave equation.[177] The equation has a time-independent and time-dependent formulation. The different states of a system with N nuclei and n electrons are obtained through the solution of the time-independent Schrödinger equation (TISE),

$$\hat{H}_{tot}(\boldsymbol{R}, \boldsymbol{r})\Psi_{tot}(\boldsymbol{R}, \boldsymbol{r}) = E_{tot}\Psi_{tot}(\boldsymbol{R}, \boldsymbol{r}) \tag{A.1}$$

where $\boldsymbol{R}$ and $\boldsymbol{r}$ are the coordinate variables of the nuclei and electrons, respectively. Ψ_{tot} is the wavefunction representing the full molecular system and E_{tot} is the total energy associated with it through the many-body Hamiltonian operator $\hat{H}$. The set of solutions for the TISE forms the eigenstates of the system and the associated energies are the eigenvalues.

The evolution of a molecular system in time is described using the time-dependent Schrödinger equation (TDSE)

$$i\frac{\partial}{\partial t}\Psi_{tot}(\boldsymbol{R}, \boldsymbol{r}, t) = \hat{H}_{tot}\Psi_{tot}(\boldsymbol{R}, \boldsymbol{r}, t) \tag{A.2}$$

where i is the imaginary number.

The molecular Hamiltonian formulated in terms of Coulombic interactions is given as

$$\hat{H}_{tot}(\boldsymbol{R}, \boldsymbol{r}) = \hat{T}_N(\boldsymbol{R}) + \hat{T}_n(\boldsymbol{r}) + \hat{V}_{NN}(\boldsymbol{R}) + \hat{V}_{ee}(\boldsymbol{r}) + \hat{V}_{Ne}(\boldsymbol{R}, \boldsymbol{r}) \tag{A.3}$$

where $\hat{T}_N$ and $\hat{T}_e$ are the kinetic energy operators for the nuclei and electrons, respectively.

$$\hat{T}_N(\boldsymbol{R}) = -\sum_{I}^{N} \left(\frac{1}{2M_I} \right) \nabla_I^2 \tag{A.4}$$

$$\hat{T}_e(\boldsymbol{r}) = -\frac{1}{2} \sum_{I}^{n} \nabla_i^2 \tag{A.5}$$

M corresponds to the mass of the nuclei and ∇^2 is the Laplacian operator which in Cartesian coordinates is written:

$$\nabla^2 = \frac{\partial^2}{\partial x^2} + \frac{\partial^2}{\partial y^2} + \frac{\partial^2}{\partial z^2}. \tag{A.6}$$

$\hat{V}_{NN}$ and $\hat{V}_{ee}$ are Coulombic repulsions between the nuclei and between the electrons, respectively. $\hat{V}_{Ne}$ is the attractive interaction between the nuclei and the electrons.

$$\hat{V}_{NN} = \frac{1}{2} \sum_{I=1}^{N-1} \sum_{J=I+1}^{N} \frac{Z_I Z_J}{|\boldsymbol{R}_I - \boldsymbol{R}_J|} \tag{A.7}$$

$$\hat{V}_{ee} = \frac{1}{2} \sum_{i=1}^{n-1} \sum_{j=i+1}^{n} \frac{1}{|\boldsymbol{r}_i - \boldsymbol{r}_j|} \tag{A.8}$$

$$\hat{V}_{Ne} = -\sum_{I=1}^{N} \sum_{i=1}^{n} \frac{Z_I}{|\boldsymbol{R}_I - \boldsymbol{r}_i|} \tag{A.9}$$

Z_I and Z_J are the atomic number of nuclei I and J.

A.1.2 The Born-Oppenheimer Approximation

The Schrödinger equation can only be solved exactly for a 2-particle system. In bigger systems, the number of degrees of freedom scales with $3N$ spatial coordinates for the nuclei and $3n$ for the electrons. The use of an approximation is required for these calculations to be affordable. One common approach is the

Born-Oppenheimer approximation (BOA)[178] where the nuclear frame is considered stationary with respect to the electrons. The rational for this approximation is that electrons are much lighter than nuclei (there is a ratio of 1836 between the mass of an electron and a proton) and thus, the motion of the electrons is much quicker compared to the nuclei. Additionally, it is considered that electron rearrangement is instantaneous with respect to the motion of nuclei. Thus, the total wavefunction can be written as a product of a nuclear wavefunction χ and an electronic wavefunction ψ.

$$\Psi_{tot}(\boldsymbol{R}, \boldsymbol{r}) = \chi(\boldsymbol{R})\psi(\boldsymbol{r}; \boldsymbol{R}) \tag{A.10}$$

The electronic wavefunction is obtained by solving the electronic Schrödinger equation

$$\hat{H}_{el}\psi_s(\boldsymbol{r}; \boldsymbol{R}) = E_s(\boldsymbol{R})\psi_s(\boldsymbol{r}; \boldsymbol{R}) \tag{A.11}$$

where the electronic Hamiltonian $\hat{H}_{el}$ contains the electronic kinetic operator and all Coulombic interations.

$$\hat{H}_{el} = \hat{T}_e + \hat{V}_{NN} + \hat{V}_{ee} + \hat{V}_{Ne} \tag{A.12}$$

The nuclear wavefunction is obtained by solving the rewritten Schrödinger equation in the BOA

$$\hat{H}_N\chi(\boldsymbol{R}) = E_N\chi(\boldsymbol{R}) \tag{A.13}$$

where $\hat{H}_N$ is the nuclear Hamiltonian

$$\hat{H}_N = \hat{T}_N + \hat{V} \tag{A.14}$$

where $\hat{V}$ is the potential energy operator and E_N is the molecular energy associated to the different nuclear eigenstates. In the BOA, the full wavefunction is obtained by first solving the electronic equation with a given set of position $\boldsymbol{R}$ for the nuclei and then, the nuclear eigenstates are obtained for a potential energy surface

(PES) described by the electronic energy E_s explicitely dependent on $\boldsymbol{R}$. The PES describes the energy of the system for a given electronic state as a function of the nuclear coordinates and it corresponds to a hypersurface with a dimension of $3N$-6 where the degrees of freedom related to translation and rotation of the nuclear frame are removed (3 for each). In a case of linear molecules, the dimension of the hypersurface is $3N$-5.

For a propagation in time of the nuclear wavefunction using the TDSE,

$$\left(\hat{T}_N + \hat{V}\right) \chi(\boldsymbol{R}) = i\frac{\partial \chi(\boldsymbol{R})}{\partial t} \tag{A.15}$$

the nuclei evolve on a PES described by the electronic energy dependent only on the parameter $\boldsymbol{R}$ and it is considered independent of time (due to instantaneous rearrangement of electrons around the nuclei). This type of dynamics is known as Born-Oppenheimer dynamics. In that representation, the motion of electrons and nuclei are said to be decoupled.

In the BOA, the solutions of the eigenvalue problem for the electronic Hamiltonian are often termed then adiabatic representation where a surface is associated to each electronic state (*i.e.* eigenvalue), ordered in energy. The dynamics occurring on such surface is called adiabatic dynamics.

The lowest eletronic state (called the ground state) is often the most relevant for many applications and studies such as chemical reactions or molecular spectroscopy. The pathway for a chemical reactions can be followed along a reaction coordinate by finding the stationary points on the PES with 2 minima corresponding to the product and the reactant linked together through one or multiple maxima (*i.e.* transition states).

A.1.3 Beyond the Born-Oppenheimer Approximation

The BOA is not suitable for treating cases where the coupling between electronic and nuclear motions is not negligible.[179–185] The dynamics involving electronic

excited states cannot be treated correctly within the adiabatic approximation due to the presence of these couplings.[186] These effects are stronger for molecular geometries where two or more electronic states are very close in energy. The regions of degeneracies are known as conical intersections and they form seams of crossing points on a hypersurface of $3N$-8 dimension (for a two state degeneracy).[187–191] Such couplings between the electronic states are called nonadiabatic couplings or derivative couplings and, mathematically, these terms arise from the application of the nuclear kinetic operator on the electronic wavefunctions that are not an eigenfunction of that operator. The coupling between the electronic and nuclear motion

$$F_{ji} = \langle \psi_j(\boldsymbol{R}, \boldsymbol{r}) | \nabla_R \psi_i(\boldsymbol{R}, \boldsymbol{r}) \rangle \tag{A.16}$$

corresponds to a mixing of different electronic states i and j due to nuclear motion (represented by the derivative with respect to the nuclear coordinate R). When the coupling becomes non-negligible, the BOA breaks down.[121,192–197]

An alternative picture for PES is the diabatic representation[198] where the resulting TDSE for the nuclear wavefunction is

$$(\hat{T}_N \boldsymbol{1} + \hat{W})\chi(\boldsymbol{R}) = i\frac{\partial \chi(\boldsymbol{R})}{\partial t} \tag{A.17}$$

Using this representation, the kinetic operator $\hat{T}_N$ is diagonal and $\hat{W}$ corresponds to the diabatic energy operator containing the electronic energy, in the diagonal and the coupling in the off-diagonal elements.

Another representation of the electronic PES is the Ehrenfest state[62] where only a single PES is considered. The single state is a weighted average of adiabatic electronic states based on the electronic population. The coefficients of the individual electronic states usually vary in time, thus making the Ehrenfest surface a time-dependent PES.

Appendix B

Development

B.1 QUANTICS structure and DD-vMCG algorithm

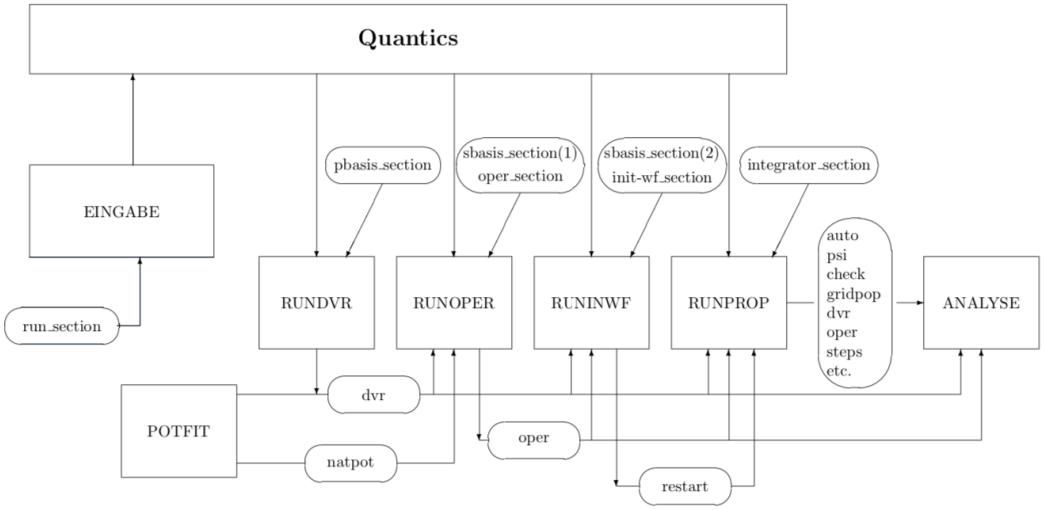

Fig. B.1: Structure of the main QUANTICS program with the individual modules represented by square boxes and input/output represented by ovals. Reproduced with permission from Ref. 199. Copyright 2019 Elsevier B.V.

Algorithm 1 Algorithm for the direct dynamics part of vMCG

```
1: procedure GETDDPES
2:     Allocate array xgp for coordinate of all GWP
3:     xgp ← Coordinate of centre of GWP
4:     if use db and dbnrec = 0 then:
5:         xgp0 ← Coordinate of the first GWP in xgp
6:         Allocate array for output of quantum chemistry calculation
7:         Call interface to quantum chemistry software
8:         ddv, ddder1, ddder2 ← diabatization of adv, adder1, adder2
9:         Write results to database
10:        Deallocate array for output of quantum chemistry calculation
11:    end if
12:    Allocate array lrddb for reading database
13:    for all GWP do:
14:        gwpdist ← distance between GWP and points in database
15:        if gwpdist < ddmindb then:
16:            lrddb ← true
17:        end if
18:    end for
19:    Allocate eex2 with number of GWP
20:    nex2 ← 0
21:    for all GWP do:                    ▷ Evaluate number of calculation to do
22:        if lrddb = false then:
23:            nex2 ← nex2 + 1
24:            Map which calculation to which GWP in eex2
25:        end if
26:    end for
27:    Allocate array for output of quantum chemistry
28:    Allocate array hopiparp ▷ Array containing the quantum chemistry option
29: OpenMP section start
30:    for e = 1,nex2 do:
31:        if method = CAS and dbnec! = 0 then:
32:            ddmoco ← MO guess from database
33:        end if
34:        Call interface to quantum chemistry
35:        ddv, ddder1, ddder2 ← diabatization of adv, adder1, adder2
36:        if lupdhes = true then:
37:            Evaluate ddder2, adder2 with Hessian update
38:        end if
39:    end for
40: OpenMP section end
41:    Write results to database
42:    Deallocate array for output of quantum chemistry
43: end procedure
```

B.2 MPI routine

The MPI_Barrier() routine is used to synchronize all the processes where the individual unit can only execute the next directive if all processes in the same communicator has reached that barrier. This routine is useful to ensure that all the parallel run of the program has reached the same place in the code such as after a block of communication to confirm that all of them have received all the necessary information to execute the next part of the algorithm.

The MPI_Bcast() routine is the main line employed for communication between processes in the same communicator. By using this command, the root process, specified by its mpirank, broadcast the data to all other processess which will fill the data variable from the value of the root process. This routine is used whenever similar data need to be exactly copied from one unit to all the others. In a case of partial data collection or sending such as matrix elements of a part of large array, a more efficient routine should be used since only a section of the array is actively used/evaluated. By using the scatter and gather routine of MPI, it is possible to reduce the amount of data sent to each process by splitting the whole array based on the number of MPI processor requested by the users.

In the MPI_Scatter() routine, the root process distributes the element from an array to the other process in the order of the rank (from lowest to highest). The main advantage is the reduction of information being effectively transmitted to each individual process.

The MPI_Gatherv() routine achieved the opposite effect of the scatter command. In this routine, the root process gathers the elements that has been evaluated on all the MPI processes in the same communicator (including the root itself) and concatenate all the data into an array in a sequential way based on the rank of the process sending the information.

In both the scatter and gatherv command, the handling of the array and its

size require some careful consideration. The splitting of the data is not managed automatically by the routine based on the number of data in the array and the number of MPI processes in the communicator. The use of these routines requires the number of elements sent/received by the root process as an argument. Thus, the exact same number of elements are send to/from all MPI processes. Arrays with number of elements divisible by the number of MPI processes are the easiest to handle with these two routines.

In the development of the MPI algorithm for DD-vMCG, the root process in all of the routine described above are the main process.

```
MPI_Barrier(
  MPI_Comm communicator,
  Int mpierror)
```

Fig. B.2: MPI_Barrier() routine with the arguments (and their type) required to execute it. The mpierror argument is optional.

```
MPI_Bcast(
  Void* data,
  Int count,
  MPI_Datatype datatype,
  Int root,
  MPI_Comm communicator,
  Int mpierror)
```

Fig. B.3: MPI_Bcast() routine with the arguments required to execute it. The "root" process transfer the array "data" with the size of "count" to all processes in the "communicator". The "mpierror" argument is optional

```
MPI_Scatter/Gatherv(
  Void* send_data,
  Int send_count,
  MPI_Datatype send_datatype,
  Void* recv_data
  Int recv_count
  MPI_Datatype recv_datatype
  Int root,
  MPI_Comm communicator,
  Int mpierror)
```

Fig. B.4: General form of the MPI_Scatter() and MPI_Gatherv() routines with the arguments required to execute it. The "root" process send/receive the array "data" with the size of "count" to all processes in the "communicator". The value to put for the relevant "data" and "count" depends on the number of elements dealt individually for each process and not the total number of data on the root process. The "mpierror" argument is optional.

Bibliography

[1] Hohenberg, P.; Kohn, W. Inhomogeneous electron gas. *Phys. Rev. B* **1964**, *136*, 864–871.

[2] Kohn, W.; Sham, L. J. Self-consistent equations including exchange and correlation effects. *Phys. Rev. A* **1965**, *140*, 1133–1138.

[3] Raghavachari, K.; Anderson, J. B. Electron Correlation and Effects in Molecules. *J. Phys. Chem.* **1996**, *100*, 12960–12973.

[4] Cederbaum, L. S.; Zobeley, J. Ultrafast charge migration by electron correlation. *Chem. Phys. Lett.* **1999**, *307*, 205–210.

[5] Kuleff, A. L.; Cederbaum, L. S. Ultrafast correlation-driven electron dynamics. *J. Phys. B* **2014**, *47*, 124002.

[6] Kling, M. F.; Vrakking, M. J. J. Attosecond Electron Dynamics. *Annu. Rev. Phys. Chem.* **2008**, *59*, 463–492.

[7] Ramasesha, K.; Leone, S. R.; Neumark, D. M. Real-Time Probing of Electron Dynamics Using Attosecond Time-Resolved Spectroscopy. *Annu. Rev. Phys. Chem.* **2016**, *67*, 41–63.

[8] Kraus, P. M.; Wörner, H. J. Perspectives of Attosecond Spectroscopy for the Understanding of Fundamental Electron Correlations. *Angew. Chem. Int. Ed.* **2018**, *57*, 5228–5247.

[9] Nisoli, M.; Decleva, P.; Calegari, F.; Palacios, A.; Martín, F. Attosecond Electron Dynamics in Molecules. *Chem. Rev.* **2017**, *117*, 10760–10825.

[10] Zewail, A. H. Femtochemistry: Atomic-Scale Dynamics of the Chemical Bond. *J. Phys. Chem. A* **2000**, *104*, 5660–5694.

[11] Lépine, F.; Sansone, G.; Vrakking, M. J. J. Molecular applications of attosecond laser pulses. *Chem. Phys. Lett.* **2013**, *578*, 1–14.

[12] Carley, R. E.; Heesel, E.; Fielding, H. H. Femtosecond lasers in gas phase chemistry. *Chem. Soc. Rev.* **2005**, *34*, 949–969.

[13] Krausz, F.; Ivanov, M. Attosecond physics. *Rev. Mod. Phys.* **2009**, *81*, 163–234.

[14] Smirnova, O.; Mairesse, Y.; Patchkovskii, S.; Dudovich, N.; Villeneuve, D.; Corkum, P.; Ivanov, M. Y. High harmonic interferometry of multi-electron dynamics in molecules. *Nat.* **2009**, *460*, 972–977.

[15] Paul, P. M.; Toma, E. S.; Breger, P.; Mullot, G.; Augé, F.; Balcou, P.; Muller, H. G.; Agostini, P. Observation of a train of attosecond pulses from high harmonic generation. *Science* **2001**, *292*, 1689–1692.

[16] McNeil, B. W. J.; Thompson, N. R. X-ray free-electron lasers. *Nat. Photonics* **2010**, *4*, 814–821.

[17] Corkum, P. B. Plasma perspective on strong field multiphoton ionization. *PRL* **1993**, *71*, 1994–1997.

[18] Chini, M.; Zhao, K.; Chang, Z. The generation, characterization and applicationsof broadband isolated attosecond pulses. *Nat. Photonics* **2014**, *8*, 178–186.

[19] Nisoli, M.; Sansone, G. New frontiers in attosecond science. *Prog. Quant. Electron.* **2009**, *33*, 17–59.

[20] Sansone, G.; Poletto, L.; Nisoli, M. High-energy attosecond light sources. *Nat. Photonics* **2011**, *5*, 655–663.

[21] Bonifacio, R.; Pellegrini, C.; Narducci, L. M. Collective instabilities and high-gain regime in a free electron laser. *Opt. Commun.* **1984**, *50*, 373–378.

[22] Emma, P.; Akre, R.; Arthur, J.; Bionta, R.; Bostedt, C.; Bozek, J.; Brachmann, A.; Bucksbaum, P.; Coffee, R.; Decker, F.-J.; Ding, Y.; Dowell, D.; Edstrom, S.; Fisher, A.; Frisch, J.; Gilevich, S.; Hastings, J.; Hays, G.; Hering, P.; Huang, Z.; Iverson, R.; Loos, H.; Messerschmidt, M.; Miahnahri, A.; Moeller, S.; Nuhn, H.-D.; Pile, G.; Ratner, D.; Rzepiela, J.; Schultz, D.; Smith, T.; Stefan, P.; Tompkins, H.; Turner, J.; Welch, J.; White, W.; Wu, J.; Yocky, G.; Galayda, J. First lasing and operation of an ångstrom-wavelength free-electron laser. *Nat. Photonics* **2010**, *4*, 641–647.

[23] Ackermann, W.; Asova, G.; Ayvazyan, V.; Azima, A.; Baboi, N.; Bähr, J.; Balandin, V.; Beutner, B.; Brandt, A.; Bolzmann, A.; Brinkmann, R.; Brovko, O. I.; Castellano, M.; Castro, P.; Catani, L.; Chiadroni, E.; Choroba, S.; Cianchi, A.; Costello, J. T.; Cubaynes, D.; Dardis, J.; Decking, W.; Delsim-Hashemi, H.; Delserieys, A.; Di Pirro, G.; Dohlus, M.; Düsterer, S.; Eckhardt, A.; Edwards, H. T.; Faatz, B.; Feldhaus, J.; Flöttmann, K.; Frisch, J.; Fröhlich, L.; Garvey, T.; Gensch, U.; Gerth, C.; Görler, M.; Golubeva, N.; Grabosch, H.-J.; Grecki, M.; Grimm, O.; Hacker, K.; Hahn, U.; Han, J. H.; Honkavaara, K.; Hott, T.; Hüning, M.; Ivanisenko, Y.; Jaeschke, E.; Jalmuzna, W.; Jezynski, T.; Kammering, R.; Katalev, V.; Kavanagh, K.; Kennedy, E. T.; Khodyachykh, S.; Klose, K.; Kocharyan, V.; Körfer, M.; Kollewe, M.; Koprek, W.; Korepanov, S.;

Kostin, D.; Krassilnikov, M.; Kube, G.; Kuhlmann, M.; Lewis, C. L. S.; Lilje, L.; Limberg, T.; Lipka, D.; Löhl, F.; Luna, H.; Luong, M.; Martins, M.; Meyer, M.; Michelato, P.; Miltchev, V.; Möller, W. D.; Monaco, L.; Müller, W. F. O.; Napieralski, O.; Napoly, O.; Nicolosi, P.; Nölle, D.; Nuñez, T.; Oppelt, A.; Pagani, C.; Paparella, R.; Pchalek, N.; Pedregosa-Gutierrez, J.; Petersen, B.; Petrosyan, B.; Petrosyan, G.; Petrosyan, L.; Pflüger, J.; Plönjes, E.; Poletto, L.; Pozniak, K.; Prat, E.; Proch, D.; Pucyk, P.; Radcliffe, P.; Redlin, H.; Rehlich, K.; Richter, M.; Roehrs, M.; Roensch, J.; Romaniuk, R.; Ross, M.; Rossbach, J.; Rybnikov, V.; Sachwitz, M.; Saldin, E. L.; Sandner, W.; Schlarb, H.; Schmidt, B.; Schmitz, M.; Schmüser, P.; Schneider, J. R.; Schneidmiller, E. A.; Schnepp, S.; Schreiber, S.; Seidel, M.; Sertore, D.; A. Shabunov, V.; Simon, C.; Simrock, S.; Sombrowski, E.; Sorokin, A. A.; Spanknebel, P.; Spesyvtsev, R.; Staykov, L.; Steffen, B.; Stephan, F.; Stulle, F.; Thom, H.; Tiedtke, K.; Tischer, M.; Toleikis, S.; Treusch, R.; Trines, D.; Tsakov, I.; Vogel, E.; Weiland, T.; Weise, H.; Wellhöfer, M.; Wendt, M.; Will, I.; Winter, A.; Wittenburg, K.; Wurth, W.; Yeates, P.; Yurkov, M. V.; Zagorodnov, I.; Zapfe, K. Operation of a free-electron laser from the extreme ultraviolet to the water window. *Nat. Photonics* **2007**, *1*, 336–342.

[24] Duris, J.; Li, S.; Driver, T.; Champenois, E. G.; MacArthur, J. P.; Lutman, A. A.; Zhang, Z.; Rosenberger, P.; Aldrich, J. W.; Coffee, R.; Coslovich, G.; Decker, F.-J.; Glownia, J. M.; Hartmann, G.; Helml, W.; Kamalov, A.; Knurr, J.; Krzywinski, J.; Lin, M.-F.; Marangos, J. P.; Nantel, M.; Natan, A.; O'Neal, J. T.; Shivaram, N.; Walter, P.; Wang, A. L.; Welch, J. J.; Wolf, T. J. A.; Xu, J. Z.; Kling, M.-F.; Bucksbaum, P. H.; Zholents, A.; Huang, Z.; Cryan, J. P.; Marinelli, A. Tunable isolated attosecond X-ray pulses with gigawatt peak power from a free-electron laser.

Nat. Photonics **2020**, *14*, 30–36.

[25] Spinlove, K. E.; Vacher, M.; Bearpark, M.; Robb, M. A.; Worth, G. A. Using quantum dynamics simulations to follow the competition between charge migration and charge transfer in polyatomic molecules. *Chem. Phys.* **2017**, *482*, 52–63.

[26] Remacle, F.; Levine, R. D. An electronic time scale in chemistry. *PNAS* **2006**, *103*, 6793–6798.

[27] Wörner, H. J.; Arrell, C. A.; Banerji, N.; Cannizzo, A.; Chergui, M.; Das, A. K.; Hamm, P.; Keller, U.; Kraus, P. M.; Liberatore, E.; Lopez-Tarifa, P.; Lucchini, M.; Meuwly, M.; Milne, C.; Moser, J.-E.; Rothlisberger, U.; Smolentsev, G.; Teuscher, J.; van Bokhoven, J. A.; Wenger, O. Charge migration and charge transfer in molecular systems. *Struct. Dyn.* **2017**, *4*, 061508.

[28] Lünnemann, S.; Kuleff, A. I.; Cederbaum, L. S. Ultrafast charge migration in 2-phenylethyl-N,N-dimethylamine. *Chem. Phys. Lett.* **2008**, *450*, 232–235.

[29] Kuleff, A. L.; Lünnemann, S.; Cederbaum, L. S. Electron-correlation-driven charge migration in oligopeptides. *Chem. Phys.* **2013**, *414*, 100–105.

[30] Weinkauf, R.; Schanen, P.; Yang, D.; Soukara, S.; Schlag, E. W. Elementary Processes in Peptides: Electron Mobility and Dissociation in Peptide Cations in the Gas Phase. *J. Phys. Chem.* **1995**, *99*, 11255–11265.

[31] Weinkauf, R.; Schanen, P.; Metsala, A.; Schlag, E. W.; Bürgle, M.; Kessler, H. Highly Efficient Charge Transfer in Peptide Cations in the Gas Phase: Threshold Effects and Mechanism. *J. Phys. Chem.* **1996**, *3654*, 18567–18585.

[32] Sansone, G.; Kelkensberg, F.; Pérez-Torres, J. F.; Morales, F.; Kling, M. F.; Siu, W.; Ghafur, O.; Johnsson, P.; Swoboda, M.; Benedetti, E.; Ferrari, F.; Lépine, F. and Sanz-Vicario, J. L. and Zherebtsov, S. and Znakovskaya, I. and L'Huillier, A. and Ivanov, M. Y. and Nisoli, M. and Martí, F. and Vrakking, M. J. J., Electron localization following attosecond molecular photoionization. *Nature* **2010**, *465*, 763–766.

[33] Jiang, Y. H.; Rudenko, A.; Pérez-Torres, J. F.; Herrwerth, O.; Foucar, L.; Kurka, M.; Kühnel, K. U.; Toppin, M.; Plésiat, E.; Morales, F.; Martín, F.; Lezius, M.; Kling, M. F.; Jahnke, T.; Dörner, R.; Sanz-Vicario, J. L.; van Tilborg, J.; Belkacem, A.; Schulz, M.; Ueda, K.; Zouros, T. J. M.; D¨sterer, S.; Treusch, R.; Schröter, C. D.; Moshammer, R.; Ullrich, J. Investigating two-photon double ionization of D2 by XUV-pump-XUV-probe experiments. *Phys. Rev. A* **2010**, *81*, 051402.

[34] Jiang, Y. H.; Rudenko, A.; Plésiat, E.; Foucar, L.; Kurka, M.; Kühnel, K. U.; Ergler, T.; Pérez-Torres, J. F.; Martín, F.; Herrwerth, O.; Lezius, M.; Kling, M. F.; Titze, J.; Jahnke, T.; Dörner, R.; Sanz-Vicario, J. L.; Schöffler, M.; van Tilborg, J.; Belkacem, A.; Ueda, K.; Zouros, T. J. M.; D¨sterer, S.; Treusch, R.; Schröter, C. D.; Moshammer, R.; Ullrich, J. Tracing direct and sequential two-photon double ionization of D2 in femtosecondextreme-ultraviolet laser pulses. *Phys. Rev. A* **2010**, *81*, 021401.

[35] Meyer, H.-D.; Manthe, U.; Cederbaum, L. S. The Multi-Configurational Time-Dependent Hartree Approach. *Chem. Phys. Lett.* **1990**, *165*, 73–78.

[36] Beck, M. H.; Jäckle, A.; Worth, G. A.; Meyer, H.-D. The multiconfiguration time-dependent Hartree method: A highly efficient algorithm for propagating wavepackets. *Phys. Rep.* **2000**, *324*, 1–105.

[37] Meyer, H.-D.; Gatti, F.; Worth, G. A. *Multidimens. Quantum Dyn. MCTDH Theory Appl.*; Wiley-VCH: Weinheim, Germany, 2009.

[38] Vacher, M.; Bearpark, M. J.; Robb, M. A. Direct methods for non-adiabatic dynamics: connecting the single-set variational multi-configuration Gaussian (vMCG) and Ehrenfest perspectives. *Theor. Chem. Acc.* **2016**, *135*, 187–11.

[39] Agostini, F.; Curchod, B. F. E. Different flavors of nonadiabatic molecular dynamics. *WIREs Comput. Mol. Sci.* **2019**, *9*, e1417.

[40] Ibele, L. M.; Curchod, B. F. E.; Agostini, F. A Photochemical Reaction in Different Theoretical Representations. *J. Phys. Chem. A* **2022**, *126*, 1263–1281.

[41] Born, M.; Huang, K. *The Dynamical Theory of Crystal Lattices*; Oxford University Press: Oxford, U.K., 1954.

[42] Burghardt, I.; Meyer, H.-D.; Cederbaum, L. S. Approaches to the approximate treatment of complex molecular systems by the multiconfiguration time-dependent Hartree method. *J. Chem. Phys.* **1999**, *111*, 2927–2938.

[43] Worth, G. A.; Burghardt, I. Full quantum mechanical molecular dynamics using Gaussian wavepackets. *Chem. Phys. Lett.* **2003**, *368*, 502–508.

[44] Worth, G. A.; Robb, M. A.; Lasorne, B. L. Solving the time-dependent Schrödinger equation for nuclear motion in one step: Direct dynamics of non-adiabatic systems. *Mol. Phys.* **2008**, *106*, 2077–2091.

[45] Mendive-Tapia, D.; Lasorne, B.; Worth, G. A.; Robb, M. A.; Bearpark, M. J. Towards converging non-adiabatic direct dynamics calculations using frozen-width variational Gaussian product basis functions. *J. Chem. Phys.* **2012**, *548*, 22A548–10.

[46] Richings, G. W.; Polyak, I.; Spinlove, K. E.; Worth, G. A.; Burghardt, I.; Lasorne, B. Quantum dynamics simulations using Gaussian wavepackets: the vMCG method. *Int. Rev. Phys. Chem.* **2015**, *34*, 269–308.

[47] Martínez, T. J.; Ben-Nun, M.; Levine, R. D. Multi-Electronic-State Molecular Dynamics: A Wave Function Approach with Applications. *J. Phys. Chem.* **1996**, *100*, 7884–7895.

[48] Ben-Nun, M.; Martínez, T. J. A multiple spawning approach to tunneling dynamics. *J. Chem. Phys.* **2000**, *112*, 6113–6121.

[49] Tully, J. C.; Preston, R. K. Trajectory Surface Approach to Nonadiabatic Molecular Collisions: The Reaction of H^+ with D_2. *J. Chem. Phys.* **1971**, *55*, 562–572.

[50] Abedi, A.; Maitra, N. T.; Gross, E. K. U. Exact Factorization of the Time-Dependent Electron-Nuclear Wave Function. *Phys. Rev. Lett.* **2010**, *105*, 123002.

[51] Min, S. K.; Agostini, F.; Gross, E. K. U. Coupled-Trajectory Quantum-Classical Approach to Electronic Decoherence in Nonadiabatic Processes. *Phys. Rev. Lett.* **2015**, *115*, 073001–5.

[52] Min, S. K.; Agostini, F.; Tavernelli, I.; Gross, E. K. U. Ab Initio Nonadiabatic Dynamics with Coupled Trajectories: A Rigorous Approach to Quantum (De)Coherence. *J. Phys. Chem. Lett.* **2017**, *8*, 3048–3055.

[53] Curchod, B. F. E.; Agostini, F.; Tavernelli, I. CT-MQC - a coupled-trajectory mixed quantum/classical method including nonadiabatic quantum coherence effects. *Eur. Phys. J. B* **2018**, *91*, 168.

[54] Gossel, G. H.; Agostini, F.; Maitra, N. T. Coupled-Trajectory Mixed

Quantum-Classical Algorithm: A Deconstruction. *J. Chem. Theory Comput.* **2018**, *14*, 4513–4529.

[55] Pieroni, C.; Agostini, F. Nonadiabatic Dynamics with Coupled Trajectories. *J. Chem. Theory Comput.* **2021**, *17*, 5969–5991.

[56] Jenkins, A. J.; Spinlove, K. E.; Vacher, M.; Worth, G. A.; Robb, M. A. The Ehrenfest method with fully quantum nuclear motion (Qu-Eh): Application to charge migration in radical cations. *J. Chem. Phys.* **2018**, *149*, 094108.

[57] Vacher, M.; Bearpark, M. J.; Robb, M. A.; Malhado, J. P. Electron Dynamics upon Ionization of Polyatomic Molecules: Coupling to Quantum Nuclear Motion and Decoherence. *Phys. Rev. Lett.* **2017**, *118*, 083001.

[58] Shalashilin, D. V.; Child, M. S. The phase space CCS approach to quantum and semiclassical molecular dynamics for high-dimensional systems. *Chem. Phys.* **2004**, *304*, 103–120.

[59] Shalashilin, D. V. Quantum mechanics with the basis set guided by Ehrenfest trajectories: theory and application to spin-boson model. *J. Chem. Phys.* **2009**, *130*, 244101–244111.

[60] Shalashilin, D. V. Nonadiabatic dynamics with the help of multiconfigurational Ehrenfest method: Improved theory and fully quantum 24D simulation of pyrazine. *J. Chem. Phys.* **2010**, *132*, 244111.

[61] Saita, K.; Shalashilin, D. V. On-the-fly ab initio molecular dynamics with multiconfigurational Ehrenfest method. *J. Chem. Phys.* **2012**, *137*, 22A506–8.

[62] Ehrenfest, P. Bemerkung über die angenäherte Gültigkeit der klassischen Mechanik innerhalb der Quantenmechanik. *Z. Phys.* **1927**, *45*, 455.

[63] Delos, J. B.; Thorson, W. R.; Knudson, S. K. Semiclassical Theory of Inelastic Collisions. I. Classical Picture and Semiclassical Formulation. *Phys. Rev. A* **1972**, *6*, 709–720.

[64] Delos, J. B.; Thorson, W. R. Semiclassical Theory of Inelastic Collisions. II. Momentum-Space Formulation. *Phys. Rev. A* **1972**, *6*, 720–727.

[65] Wahnström, G.; Carmeli, B.; Metiu, H. The calculation of the thermal rate coefficient by a method combining classical and quantum mechanics. *J. Chem. Phys.* **1988**, *88*, 2478.

[66] Amarouche, M.; Gadea, F. X.; Durup, J. A proposal for the theoretical treatment of multi-electronic-state molecular dynamics with the whole DIM basis (HWD). A test on the evolution of excited Ar_3^+ cluster ions. *Chem. Phys.* **1989**, *130*, 145–157.

[67] Avagliano, D.; Lorini, E.; González, L. Sampling effects in quantum mechanical/molecular mechanics trajectory surface hopping non-adiabatic dynamics. *Phil. Trans. R. Soc. A* **2022**, *380*, 20200381.

[68] Makhov, D. V.; Shalashilin, D. V. Floque Hamiltonian for incorporating electronic excitation by a laser pulse into simulations of non-adiabatic dynamics. *Chem. Phys.* **2018**, *515*, 46–51.

[69] Shirley, J. H. Solution of the Schrödinger Equation with a Hamiltonian Periodic in Time. *Phys. Rev.* **1965**, *138*, b979–987.

[70] Schirò, M.; Eich, F. G.; Agostini, F. Quantum-classical nonadiabatic dynamics of Floquet driven systems. *J. Chem. Phys.* **2021**, *154*, 114101.

[71] Penfold, T. J.; Pápai, M.; Møller, K. B.; Worth, G. A. Excited state dynamics initiated by an electromagnetic field within the Variational Multi-

Configurational Gaussian (vMCG) method. *Comput. Theo. Chem.* **2019**, *1160*, 24–30.

[72] Chen, L.; Sun, K.; Shalashilin, D. V.; Gelin, M. F.; Zhao, Y. Efficient simulation of time- and frequency-resolved four-wave-mixing signals with a multiconfigurational Ehrenfest approach. *J. Chem. Phys.* **2021**, *154*, 054105.

[73] Chang, B. Y.; Shin, S.; Malinovsky, V. S.; Sola, I. R. Grid-Based Ehrenfest Model To Study Electron-Nuclear Processes. *J. Phys. Chem. A* **2019**, *123*, 7171–7176.

[74] Hartree, D. R.; Hartree, W. Self-consistent field, with exchange, for beryllium. *Proc. R. Soc. Lond. A* **1935**, *150*, 9–33.

[75] Slater, J. C. The theory of complex spectra. *Phys. Rev.* **1929**, *34*, 1293–1322.

[76] Roothaan, C. C. J. New Developments in Molecular Orbital Theory. *Rev. Mod. Phys.* **1951**, *23*, 69–89.

[77] Hehre, W. J.; Ditchfield, R.; Pople, J. A. Self—Consistent Molecular Orbital Methods. XII. Further Extensions of Gaussian—Type Basis Sets for Use in Molecular Orbital Studies of Organic Molecules. *J. Chem. Phys.* **1972**, *56*, 2257–2261.

[78] Del Bene, J. E.; Ditchfield, R.; Pople, J. A. Self-Consistent Molecular Orbital Methods. X. Molecular Orbital Studies of Excited States with Minimal and Extended Basis Sets. *J. Chem. Phys.* **1971**, *55*, 2236–2241.

[79] Binkley, J. S.; Pople, J. A.; Hehre, W. J. Self-Consistent Molecular-Orbital Methods. 21. Small Split-Valence Basis-Sets for 1st-Row Elements. *J. Am. Chem. Soc.* **1980**, *102*, 939–947.

[80] Davidson, E. R.; Feller, D. Basis set selection for molecular calculations. *Chem. Rev.* **1986**, *86*, 681–696.

[81] Jensen, F. Atomic orbital basis sets. *WIREs Comput. Mol. Sci.* **2013**, *3*, 273–295.

[82] Helgaker, T.; Jørgensen, P.; Olsen, J. *Molecular Electronic-Structure Theory*; John Wiley and Sons, Ltd, 2000.

[83] González, L., Lindh, R., Eds. *Quantum Chemistry and Dynamics of Excited States: Method and Applications*; John Wiley and Sons, Ltd, 2021.

[84] Hartree, D. R. The Wave Mechanics of an Atom with a non-Coulomb Central Field. Part II. Some Results and Discussion. *Math. Proc. Cam. Phil. Soc.* **1928**, *24*, 111–132.

[85] Fock, V. Näherungsmethode zur Lösung des quantenmechanischen Mehrkörperproblems. *Zeitschrift für Physik* **1930**, *61*, 126–148.

[86] Löwdin, P.-O. Quantum Theory of Many-Particle Systems. III. Extension of the Hartree-Fock Scheme to Include Degenerate Systems and Correlation Effects. *Phys. Rev.* **1955**, *97*, 1509–1520.

[87] González, L.; Escudero, D.; Serrano-Andrés, L. Progress and Challenges and in the Calculation and of Electronic and Excited States. *ChemPhysChem* **2012**, *13*, 28–51.

[88] Tran, T.; Segarra-Martí, J.; Bearpark, M. J.; Robb, M. A. Molecular Vertical Excitation Energies Studied with First-Order RASSCF (RAS[1,1]): Balancing Covalent and Ionic Excited States. *J. Phys. Chem. A* **2019**, *123*, 5223–5230.

[89] Runge, E.; Gross, E. K. U. Density-Functional Theory for Time-Dependent Systems. *Phys. Rev. Lett.* **1984**, *52*, 997–1000.

[90] Levine, B. G.; Ko, C.; Quenneville, J.; Martínez, T. J. Conical intersections and double excitations in time-dependent density functional theory. *Mol. Phys.* **2006**, *106*, 1039–1051.

[91] Szalay, P. G.; Müller, T.; Gidofalvi, G.; Lischka, H.; Shepard, R. Multiconfiguration self-consistent field and multireference configuration interaction methods and applications. *Chem. Rev.* **2012**, *112*, 108–181.

[92] Sherrill, C. D.; Schaefer, H. F. The Configuration Interaction Method: Advances in Highly Correlated Approaches. *Adv. Quantum Chem.* **1999**, *34*, 143–269.

[93] Raghavachari, K.; Pople, J. A. Calculation of one-electron properties using limited configuration interaction techniques. *Int. J. Quantum Chem.* **1981**, *20*, 1067–1071.

[94] Pople, J. A.; Seeger, R.; Krishnan, R. Variational configuration interaction methods and comparison with perturbation theory. *Int. J. Quantum Chem.* **1977**, *11*, 149–163.

[95] Levy, B.; Berthier, G. Generalized Brillouin Theorem for Multiconfigurational SCF Theories. *Int. J. Quant. Chem.* **1968**, *11*, 307–319.

[96] Levy, B. Molecular MC-SCF Calculations. *Int. J. Quantum Chem.* **1970**, *4*, 297–313.

[97] Hinze, J. MC-SCF. I. The multi-configuration self-consistent-field method. *J. Chem. Phys.* **1973**, *59*, 6424.

[98] Dalgaard, E.; Jargensen, P. Optimization of orbitals for multiconfigurational reference states. *J. Chem. Phys.* **1978**, *69*, 3833–3844.

[99] Roothaan, C. C. J.; Detrich, J.; Hopper, D. G. An improved MCSCF method. *Int. J. Quant. Chem.* **1979**, *13*, 93–101.

[100] Roos, B. O.; Taylor, P. R.; Siegbahn, P. E. M. A complete active space SCF method (CASSCF) using a density matrix formulated super-CI approach. *Chem. Phys.* **1980**, *48*, 157–173.

[101] Shavitt, I. Graph theoretical concepts for the unitary group approach to the many-electron correlation problem. *Int. J. Quantum Chem.* **1977**, *12*, 131–148.

[102] Shavitt, I. The graphical unitary group approach and its application to direct configuration interaction calculations. The Unitary Group for the Evaluation of Electronic Energy Matrix Elements. Berlin, Heidelberg, 1981; pp 51–99.

[103] Jenkins, A. J.; Robb, M. A. The damped Ehrenfest (D-Eh) method: Application to non-adiabatic reaction paths. *Comput. Theor. Chem.* **2019**, *1152*, 53–61.

[104] Knowles, P. J.; Werner, H.-J. An Efficient Second Order MCSCF Method for Long Configuration Expansions. *Chem. Phys. Lett.* **1985**, *115*, 259–267.

[105] Werner, H.-J.; Meyer, W. A quadratically convergent MCSCF method for the simultaneous optimisation of several states. *J. Chem. Phys.* **1981**, *74*, 5794–5801.

[106] Olsen, J.; Roos, B. O.; Jorgensen, P.; Jensen, H. J. A. Determinant based configuration interaction algorithms for complete and restricted configuration interaction spaces. *J. Chem. Phys.* **1988**, *89*, 2185.

[107] Klene, M.; Robb, M. A.; Blancafort, L.; Frisch, M. J. A new efficient approach to the direct restricted active space self-consistent field method. *J. Chem. Phys.* **2003**, *119*, 713.

[108] Anderson, K.; Malmqvist, P.-Å.; Roos, B. O.; Sadlej, A. J.; Wolinski, K. Second-Order Perturbation Theory with a CASSCF Reference Function. *J. Phys. Chem.* **1990**, *94*, 5483–5488.

[109] Andersson, K.; Malmqvist, P.-Å.; Roos, B. O. Second-order perturbation theory with a complete active space self-consistent field reference function. *J. Chem. Phys.* **1992**, *96*, 1218–1226.

[110] Finley, J.; Malmqvist, P.-A.; Roos, B. O.; Serrano-andrés, L. The multi-state CASPT2 method. *Chem. Phys. Lett.* **1998**, *288*, 299–306.

[111] Worth, G. A.; Robb, M. A.; Burghardt, I. A novel algorithm for non-adiabatic direct dynamics using variational Gaussian wavepackets. *Faraday Discuss.* **2004**, *127*, 307–323.

[112] Lasorne, B.; Bearpark, M. J.; Robb, M. A.; Worth, G. A. Direct quantum dynamics using variational multi-configuration Gaussian wavepackets. *Chem. Phys. Lett.* **2006**, *432*, 604–609.

[113] Lasorne, B.; Robb, M. A.; Worth, G. A. Direct quantum dynamics using variational multi-configuration Gaussian wavepackets. Implementation details and test case. *Phys. Chem. Chem. Phys.* **2007**, *9*, 3210–3227.

[114] Dirac, P. A. M. Note on exchange phenomena in the Thomas atom. *Proc. Cambridge Philos. Soc.* **1930**, *26*, 376–385.

[115] Frenkel, J. *Wave Mechanics*; Clarendon Press: Oxford, U.K., 1934.

[116] Meisner, J.; Vacher, M.; Bearpark, M. J.; Robb, M. A. Geometric Rotation of the Nuclear Gradient at a Conical Intersection: Extension to Complex Rotation of Diabatic States. *J. Chem. Theory Comput.* **2015**, *11*, 3115–3122.

[117] Mulliken, R. S. Electronic Population Analysis on LCAO–MO Molecular Wave Functions. I. *J. Chem. Phys.* **1955**, *23*, 1833–1840.

[118] Coe, J. D.; Ong, M. T.; Levine, B. G.; Martínez, T. J. On the Extent and Connectivity of Conical Intersection Seams and the Effects of Three-State Intersections. *J. Phys. Chem. A* **2008**, *112*, 12559–12567.

[119] Allan, C. S. M.; Lasorne, B.; Worth, G. A.; Robb, M. A. A straightforward method of analysis for direct quantum dynamics: Application to the photochemistry of a model cyanine. *J. Phys. Chem. A* **2010**, *114*, 8713–8729.

[120] Plasser, F.; Gómez, S.; Menger, M. F. S. J.; Mai, S.; González, L. Highly efficient surface hopping dynamics using a linear vibronic coupling model. *Phys. Chem. Chem. Phys.* **2019**, *21*, 57–69.

[121] Worth, G. A.; Cederbaum, L. S. Beyond Born-Oppenheimer: Conical intersections and their impact on molecular dynamics. *Ann. Rev. Phys. Chem.* **2004**, *55*, 127–158.

[122] Polyak, I.; Bearpark, M. J.; Robb, M. A. Application of the unitary group approach to evaluate spin density for configuration interaction calculations in a basis of S^2 eigenfunctions. *Int. J. Quantum Chem.* **2018**, *118*, e25559.

[123] Worth, G. A.; Giri, K.; Richings, G. W.; Beck, M. H.; Jäckle, A.; Meyer, H.-D. Quantics package, Version 1.1. 2015.

[124] Tran, T.; Jenkins, A. J.; Worth, G. A.; Robb, M. A. The quantum-Ehrenfest method with the inclusion of an IR pulse: Application to electron dynamics of the allene radical cation. *J. Chem. Phys.* **2020**, *153*, 031102–8.

[125] Jeffers, J.; Reinders, J.; Sodani, A. *Intel Xeon Phi Processor High Performance Programming*, 2nd ed.; Morgan Kaufmann: Boston, 2016; pp 3–13.

[126] Alessandrini, V. In *Shared Memory Application Programming*; Kaufmann, M., Ed.; 2015; pp 307–309.

[127] Kirk, D.; Hwu, W.-M. W. In *Programming Massively Parallel Processors*, 3rd ed.; Kaufmann, M., Ed.; 2016; pp 1–18.

[128] Markus, A. *Modern Fortran in Practice*; Cambridge University Press, 2012; pp 196–220.

[129] Frankcombe, T. J.; Collins, M. A.; Worth, G. A. Converged quantum dynamics with modified Shepard interpolation and Gaussian wave packets. *Chem. Phys. Lett.* **2010**, *489*, 242–247.

[130] Markus, A. *Modern Fortran in Practice*; Cambridge University Press, 2012; pp 76–91.

[131] Li, X.; Smith, S. M.; Markevitch, A. N.; Romanov, D. A.; Levis, R. J.; Schlegel, H. B. A time-dependent Hartree-Fock approach for studying the electronic optical response of molecules in intense fields. *Phys. Chem. Chem. Phys.* **2005**, *7*, 233–239.

[132] Harumiya, K.; Kono, H.; Fujimura, Y.; Kawata, I.; Bandrauk, A. D. Intense laser-field ionization of H_2 enhanced by two-electron dynamics Kenji. *Phys. Rev. A* **2002**,

[133] Lein, M.; Kreibich, T.; Gross, E. K. U.; Engel, V. Strong-field ionization dynamics of a model H_2 molecule. *Phys. Rev. A* **2002**, *65*, 033403.

[134] Agostini, F.; Min, S. K.; Abedi, A.; Gross, E. K. U. Quantum-Classical

Nonadiabatic Dynamics: Coupled- vs Independent-Trajectory Methods. *J. Chem. Theory Comput.* **2016**, *12*, 2127–2143.

[135] Abedi, A.; Maitra, N. T.; Gross, E. K. U. Correlated electron-nuclear dynamics: Exact factorization of the molecular wavefunction. *J. Chem. Phys.* **2012**, *137*, 22A530.

[136] Sussman, B. J.; Townsend, D.; Ivanov, M. Y.; Stolow, A. Dynamic Stark Control of Photochemical Processes. *Science* **2006**, *314*, 278–281.

[137] Markmann, A.; Worth, G. A.; Cederbaum, L. S. Allene and pentatetraene cations as models for intramolecular charge transfer: vibronic coupling Hamiltonian and conical intersections. *J. Chem. Phys.* **2005**, *122*, 144320.

[138] Shalashilin, D. V. Multiconfigurational Ehrenfest approach to quantum coherent dynamics in large molecular systems. *Farad. Discuss.* **2011**, *153*, 105–116.

[139] Gómez, S.; Heindl, M.; Szabadi, A.; Gonzó, From Surface Hopping to Quantum Dynamics and Back. Finding Essential Electronic and Nuclear Degrees of Freedom and Optimal Surface Hopping Parameters. *J. Phys. Chem. A* **2019**, *123*, 8321–8332.

[140] Olivucci, M.; Tran, T.; Worth, G. A.; Robb, M. A. Unlocking the Double Bond in Protonated Schiff Bases by Coherent Superposition of S_1 and S_2. *J. Phys. Chem. Lett.* **2021**, *12*, 5639–5643.

[141] Tran, T.; Worth, G. A.; Robb, M. A. Control of nuclear dynamics in the benzene cation by electronic wavepacket composition. *Commun. Chem.* **2021**, *4*, 48.

[142] Gozem, S.; Luk, H. L.; Schapiro, I.; Olivucci, M. Theory and Simulation of

the Ultrafast Double-Bond isomerization of Biological Chromophores. *Chem. Rev.* **2017**, *117*, 13502–13565.

[143] Frutos, L. M.; Andruniów, T.; Santoro, F.; Ferré, N.; Olivucci, M. Tracking the excited-state time evolution of the visual pigment with multiconfigurational quantum chemistry. *PNAS* **2007**, *104*, 7764–7769.

[144] Ernst, O. P.; Lodowski, D. T.; Elstner, M.; Hegemann, P.; Brown, L. S.; Kandori, H. Microbial and Animal Rhodopsins: Structures, Functions, and Molecular Mechanisms. *Chem. Rev.* **2014**, *114*, 126–163.

[145] Kukura, P.; McCamant, D. W.; Yoon, S.; Wandschneider, D. B.; Mathies, R. A. Structural observation of the primary isomerization in vision with femtosecond-stimulated Raman. *Science* **2005**, *310*, 1006–1009.

[146] Stehle, J.; Silvers, R.; Werner, K.; Chatterjee, D.; Gande, S.; Scholz, F.; Dutta, A.; Wachtveitl, J.; Klein-Seetharaman, J.; Schwalbe, H. Characterization of the Simultaneous Decay Kinetics of Metarhodopsin State II and III in Rhodopsin by Solution-state NMR Spectroscopy. *Angew. Chem. Int. Ed.* **2014**, *53*, 2078–2084.

[147] Bibikov, S. I.; Grishanin, R. N.; Kaulen, A. D.; Marwan, W.; Oesterhelt, D.; Skulachev, V. P. Bacteriorhodopsin is involved in halobacterial photoreception. *PNAS* **1993**, *90*, 9446–9450.

[148] Mathies, R. A. Photochemistry: A coherent picture of vision. *Nat. Chem.* **2015**, *7*, 945–947.

[149] Wang, Q.; Schoenlein, R.; Peteanu, L.; Mathies, R. A.; Shank, C. V. Vibrationally Coherent Photochemistry in the Femtosecond Primanry Event of Vision. *Science* **1994**, *266*, 422–424.

[150] Johnson, P. J. M.; Halpin, A.; Morizumi, T.; Prokhorenko, V. I.; Ernst, O. P.; Miller, R. J. D. Local vibrational coherences drive the primary photochemistry of vision. *Nat. Chem.* **2015**, *7*, 980–986.

[151] Schapiro, I.; Ryazantsev, M. N.; Frutos, L. M.; Ferré, N.; Lindh, R.; Olivucci, M. The Ultrafast Photoisomerizations of Rhodopsin and Bathorhodopsin are modulated by bond alternation and HOOP driven electronic effects. *J. Am. Chem. Soc.* **2011**, *133*, 3354–3364.

[152] Celani, P.; Garavelli, M.; Ottani, S.; Bernardi, F.; Robb, M. A.; Olivucci, M. Molecular "Trigger" for the Radiationless Deactivation of Photoexcited Conjugated Hydrocarbons. *J. Am. Chem. Soc.* **1995**, *117*, 11584–11585.

[153] Gozem, S.; Johnson, P. J. M.; Halpin, A.; Luk, H. L.; Morizumi, T.; Prokhorenko, V. I.; Ernst, O. P.; Olivucci, M.; Miller, R. J. D. Excited-State Vibronic Dynamics of Bacteriorhodopsin from Two-Dimensional Electronic Photon Echo Spectroscopy and Multiconfigurational Quantum Chemistry. *J. Phys. Chem. Lett.* **2020**, *11*, 3889–3896.

[154] Manathunga, M.; Yang, X. C.; Orozco-Gonzalez, Y.; Olivucci, M. Impact of Electronic State Mixing on the Photoisomerization Time Scale of the Retinal Chromophore. *J. Phys. Chem. Lett.* **2017**, *8*, 5222–5227.

[155] Manathunga, M.; Yang, X. C.; Olivucci, M. Electronic State Mixing Controls the Photoreactivity of a Rhodopsin with all-trans Chromophore Analogues. *J. Phys. Chem. Lett.* **2018**, *9*, 6350–6355.

[156] Marín, M. d. C.; Agathangelou, D.; Orozco-Gonzalez, Y.; Valentini, A.; Kato, Y.; Abe-Yoshizumi, R.; Kandori, H.; Choi, A.; Jung, K.-H.; Haacke, S.; Olivucci, M. Fluorescence Enhancement of a Microbial Rhodopsin via Electronic Reprogramming. *J. Am. Chem. Soc* **2019**, *141*, 262–271.

[157] Luk, H. L.; Melaccio, F.; Rinaldi, S.; Gozem, S.; Olivucci, M. Molecular bases for the selection of the chromophore of animal rhodopsins. *PNAS* **2015**, *112*, 15297–15302.

[158] Garavelli, M.; Celani, P.; Bernardi, F.; Robb, M. A.; Olivucci, M. The $C_5H_6NH_2^+$ protonated Shiff base: An *ab initio* minimal model for retinal photoisomerization. *J. Am. Chem. Soc.* **1997**, *119*, 6891–6901.

[159] Rinaldi, S.; Melaccio, F.; Gozem, S.; Fanelli, F.; Olivucci, M. Comparison of the isomerization mechanisms of human melanopsin and invertebrate and vertebrate rhodopsins. *PNAS* **2014**, *111*, 1714–1719.

[160] Mališ, M.; Novak, J.; Zgrablić, G.; Parmigiani, F.; Došlić, N. Mechanism of ultrafast non-reactive deactivation of the retinal chromophore in non-polar solvents. *Phys. Chem. Chem. Phys.* **2017**, *19*, 25970–25978.

[161] Gai, F.; Hasson, K. C.; McDonald, J. C.; Anfinrud, P. A. Chemical Dynamics in Proteins: The Photoisomerization of Retinal in Bacteriorhodopsin. *Science* **1998**, *279*, 1886–1891.

[162] Galbraith, M. C. E.; Scheit, S.; Golubev, N. V.; Reitsma, G.; Zhavoronkov, N.; Despré, V.; Lépine, F.; Kuleff, A. I.; Vrakking, M. J. J.; Kornilov, O.; Köppel, H.; Mikosch, J. Few-femtosecond passage of conical intersections in the benzene cation. *Nat. Comm.* **2017**, *8*, 1018–7.

[163] Kuleff, A. I.; Breidbach, J.; Cederbaum, L. S. Multielectron wave-packet propagation: General theory and application. *J. Chem. Phys.* **2005**, *123*, 044111.

[164] Breidbach, J.; Cederbaum, L. S. Universal attosecond response to the removal of an electron. *Phys. Rev. Lett.* **2005**, *94*, 33901–33904.

[165] Mignolet, B.; Gijsbertsen, A.; Vrakking, M. J. J.; Levine, R. D.; Remacle, F. Stereocontrol of attosecond time-scale electron dynamics in ABCU using ultrafast laser pulses: a computational study. *Phys. Chem. Chem. Phys.* **2011**, *13*, 8331–8344.

[166] Jenkins, A. J.; Vacher, M.; Bearpark, M. J.; Robb, M. A. Nuclear spatial delocalization silences electron density oscillations in 2-phenyl-ethyl-amine (PEA) and 2-phenylethyl-N,N-dimethylamine (PENNA) cations. *The Journal of Chemical Physics* **2016**, *144*, 104110.

[167] Robb, M. A.; Jenkins, A. J.; Vacher, M. In *Attosecond Molecular Dynamics*; Vrakking, M. J. J., Lepine, F., Eds.; The Royal Society of Chemistry, 2018; pp 275–307.

[168] Döscher, M.; Köppel, H.; Szalay, P. G. Multistate vibronic interactions in the benzene radical cation. I. Electronic structure calculations. *J. Chem. Phys.* **2002**, *117*, 2645–2656.

[169] Köppel, H.; Döscher, M.; Baldea, I.; Meyer, H.-D.; Szalay, P. G. Multistate vibronic interactions in the benzene radical cation. II. Quantum dynamical simulations. *J. Chem. Phys.* **2002**, *117*, 2657–2671.

[170] Merritt, I. C. D.; Jacquemin, D.; Vacher, M. Attochemistry: Is Controlling Electrons the Future of Photochemistry? *J. Phys. Chem. Lett.* **2021**, *12*, 8404–8415.

[171] Blancafort, L.; Lasorne, B.; Bearpark, M. J.; Worth, G. A.; Robb, M. A. In *Jahn-Teller Eff. Advances Perspectives*; Köppel, H., Yarkony, D. R., Barentzen, H., Eds.; Springer: Heidelberg, Germany, 2009; pp 169–200.

[172] Ludwig, A.; Liberatore, E.; Herrmann, J.; Kasmi, L.; López-Tarifa, P. and Gallmann, L. and Rothlisberger, U. and Keller, U. and Lucchini, M., Ul-

trafast Relaxation Dynamics of the Ethylene Cation $C_2H_4^+$. *J. Phys. Chem. Lett.* **2016**, *7*, 1901–1906.

[173] Joalland, B.; Mori, T.; Martínez, T. J.; Suits, A. G. Photochemical Dynamics of Ethylene Cation $C_2H_4^+$. *J. Phys. Chem. Lett.* **2014**, *5*, 1467–1471.

[174] Lucchini, M.; Murari, M.; Lucarelli, G. D.; Frassetto, F.; Poletto, L.; Nisoli, M. Ultrafast mapping of relaxation dynamics of ethylene cation. *EPJ Web Conf.* **2019**, *205*, 06002.

[175] Schnappinger, T.; de Vivie-Riedle, R. Coupled nuclear and electron dynamics in the vicinity of a conical intersection. *J. Chem. Phys.* **2021**, *154*, 134306.

[176] Schüppel, F.; Schnappinger, T.; Bäum, L.; de Vivie-Riedle, W. Waveform control of molecular dynamics close to a conical intersection. *J. Chem. Phys.* **2020**, *153*, 224307.

[177] Schrödinger, E. An undulatory theory of the mechanics of atoms and molecules. *Phys. Rev.* **1926**, *28*, 1049–1070.

[178] Born, M.; Oppenheimer, R. Zur Quantentheorie der Molekeln. *Ann. Phys.* **1927**, *84*, 457–484.

[179] Mead, C. A.; Truhlar, D. G. On the determination of Born–Oppenheimer nuclear motion wave functions including complications due to conical intersections and identical nuclei. *J. Chem. Phys.* **1979**, *70*, 2284–2296.

[180] Mead, C. A. Superposition of reactive and nonreactive scattering amplitudes in the presence of a conical intersection. *J. Chem. Phys.* **1980**, 3839.

[181] Yarkony, D. R. Diabolical conical intersections. *Rev. Mod. Phys.* **1996**, *68*, 985–1013.

[182] Yarkony, D. R. Conical intersections: diabolical and often misunderstood. *Acc. Chem. Res.* **1998**, *31*, 511–518.

[183] Kutzelnigg, W. The adiabatic approximation I. The physical background of the Born-Handy ansatz. *Mol. Phys.* **1997**, 909–916.

[184] Baer, M. Introduction to the theory of electronic non-adiabatic coupling terms in molecular systems. *Phys. Rep.* **2002**, *358*, 75–142.

[185] Kendrick, B. K.; Mead, C. A.; Truhlar, D. G. Properties of nonadiabatic couplings and the generalized Born-Oppenheimer approximation. *Chem. Phys.* **2002**, *277*, 31–41.

[186] Lasorne, B.; Worth, G. A.; Robb, M. A. In *Wiley Interdiscip. Rev. Comput. Mol. Sci.*; Schreiner, P. R., Allen, W. D., Orozco, M., Thiel, W., Willett, P., Eds.; John Wiley: New York, 2011; Vol. 1; pp 460–475.

[187] Atchity, G. J.; Xantheas, S. S.; Ruedenberg, K. Potential energy surfaces near intersections. *J. Chem. Phys.* **1991**, *95*, 1862–1876.

[188] Blancafort, L. Photochemistry and Photophysics at Extended Seams of Conical Intersection. *ChemPhysChem* **2014**, *15*, 3166–3181.

[189] Paterson, M. J.; Bearpark, M. J.; Robb, M. A.; Blancafort, L. The curvature of the conical intersection seam: An approximate second-order analysis. *J. Chem. Phys.* **2004**, *121*, 11562–11571.

[190] Ragazos, I. N.; Robb, M. A.; Bernardi, F.; Olivucci, M. Optimization and charaterization of the lowest energy point on a conical intersection using an MC-SCF Lagrangian. *Chem. Phys. Lett.* **1992**, *197*, 217–223.

[191] Yarkony, D. R. Conical Intersections: The New Conventional Wisdom. *J. Phys. Chem. A* **2001**, 6277–6293.

[192] Domcke, W., Yarkony, D. R., Köppel, H., Eds. *Conical intersections: Electronic structure, dynamics and spectroscopy.*; World Scientific: Singapore, 2004.

[193] Robb, M. A. In *Advances in Physical Organic Chemistry*; Williams, I. H., Ed.; 2014; Vol. 48; pp 189–228.

[194] Robb, M. A. In *Conical Intersections, Theory, Computation and Experiment*; Domcke, W., Yarkony, D. R., Kopple, H., Eds.; World Scientific Singapore, 2011; pp 3–50.

[195] Levine, B. G.; Martínez, T. J. Isomerization Through Conical Intersections. *Annu. Rev. Phys. Chem.* **2007**, *58*, 613–634.

[196] Domcke, W.; Yarkony, D. R. Role of conical intersections in molecular spectroscopy and photoinduced chemical dynamics. *Ann. Rev. Phys. Chem.* **2012**, *63*, 325–352.

[197] Matsika, S.; Krause, P. Nonadiabatic Events and Conical Intersections. *Annu. Rev. Phys. Chem.* **2011**, *62*, 621–643.

[198] Smith, F. T. Diabatic and adiabatic representations for atomic collision problems. *Phys. Rev.* **1969**, *179*, 111–123.

[199] Worth, G. A. Quantics: A general purpose package for Quantum molecular dynamics simulations. *Comput. Phys. Commun.* **2020**, *248*, 107040.